Coordinated Active Power Reduction Strategy for Voltage Rise Mitigation in LV Distribution Network

By:
Priye Kenneth Ainah

Thesis Submitted for the Degree of

Doctor of Philosophy

In the Department of Electrical Engineering
Faculty of Engineering and the Built Environment
University of Cape Town

Supervisor: Professor Komla Agbenyo Folly

October 2018

Declaration

I, Priye Kenneth Ainah hereby declared that the thesis titled "*Coordinated Active Power Reduction Strategy for Voltage Rise Mitigation in LV Distribution Network*" is my original work. No parts or whole had earlier been submitted to any other University.

Signature…….

Date…….

Acknowledgements

I gratefully acknowledge and appreciated my supervisor Professor Komla A. Folly, whose incomparable support, patience, guidance and encouragement from the beginning of the Ph.D. journey to its final stage assisted me in the completion of this Ph.D. thesis. It is a great privilege for me to work under your supervision and develop my skill in research and presentation.

I wish to also express my thanks to the members of the intelligent power and energy group for their love and encouragement throughout my doctoral research and I would also like to thank also Subhransu Padhee for his support.

I would like to express my sincere gratitude to my parents, brothers, sisters, and mother –in law, Engr. Ebipaudo Sapre-obi, Engr. J. T. Afa, Pastor Joseph and Pastor James for their prayers, encouragement, support, and love in my academic pursuit.

I would like to express my deepest gratitude to my wife and best friend for her understanding, encouragement, prayers, love, and patience throughout my Ph.D. study.

Finally, I would like to thank the Almighty God and his precious son JESUS for his unimaginable love and protection throughout my Life.

Abstract

Integration of renewable energy systems by the utility, customers, and the third party into the electric power system, most especially in the MV and LV distribution networks grew over the last decade due to the liberalization of the electricity market, rising energy demand, and increasing environmental concern.

The distributed rooftop PV system contributes to relieve the overall load, reduce losses, avoid conventional generation upgrade, and better matching of demand on the LV distribution network. Originally, the LV distribution network is designed for unidirectional current flow, that is from the substation to customers. However, a high penetration of rooftop solar PVs (with power levels typically ranging from 1 – 10 kW) may lead to the current flowing in the reverse direction and this could result in a sudden voltage rise. These negative impacts on the network have discouraged the distribution network operators (DNOs) to allow increased PV penetration in the LV distribution network because some customers load, and equipment are sensitive to voltage perturbation.

Presently, the most applied voltage rise mitigation strategy for high rooftop solar PV penetration is the total disconnect from the LV distribution network when the voltage at the point of common coupling (PCC) goes above statutory voltage limits. However, the sudden disconnection of the PV system from the grid can cause network perturbation and affect the security of the network. This action may also cause voltage instability in the network and can reduce the lifetime of grid equipment such as voltage regulators, air conditioner etc.

Due to this negative impact, different voltage rise mitigation strategies such as the active transformer with on load tap changers (OLTC), distributed battery energy storage system and reactive power support (D-STATCOM, etc.) have been used to curtail voltage rise in the distribution network. However, the implementation of D-STATCOM device on a radial LV

distribution network results in high line current and losses. This may be detrimental to the distribution network.

Therefore, in this thesis, a coordinated active power reduction (CAPR) strategy is proposed using a modified PWM PI current control strategy to ramp down the output power and voltage of a grid-tied voltage source inverter (VSI). In the proposed strategy, a reactive reference is generated based on the measured voltage level at the PCC using a threshold voltage algorithm to regulate the amplitude of the modulating signal to increase the off time of the high frequency signal which shut down the PV array momentary in an extremely short time and allow the VSI to absorb some reactive power through the freewheeling diode and reduce voltage. The proposed CAPR strategy was designed and simulated on a scaled down simple radial LV distribution network in MATLAB®/Simulink® software. The results show that the CAPR can ramp down the PV output power, reduce reverse power flow and reduce the sudden voltage rise at the point of common coupling (PCC) within ±5% of the standard voltage limit.

The study also compares the performance of the proposed CAPR strategy to that of the distributed static compensator (D-STATCOM) and battery energy storage system (BESS) with respect to response time to curtail sudden voltage rise, losses and reverse power flow. The investigation shows that the D-STATCOM has the faster response time to curtail voltage rise. However, the voltage rise reduction is accompanied by high current, losses and reverse active power flow. The introduction of the BESS demonstrates better performance than the D-STATCOM device in terms of reverse power flow and losses. The CAPR strategy performs better than both D-STATCOM and BESS in terms of line losses and reverse power flow reduction.

Table of Contents

List of Figures

List of Tables

List of Abbreviations

Abbreviation	Definition
AEP	America Electric Power
AC	Alternating Current
APC	Active Power Curtailment
AVR	Automatic Voltage Regulator
BESS	Battery Energy Storage System
CAES	Compressed Air Energy Management System
CAPR	Coordinated Active Power Reduction
CSI	Current Source Inverter
CT	Current Transformer
DC	Direct Current
DER	Distributed Energy Resources
DG	Distributed Generation
DNO	Distribution Network Operator
DSM	Demand Side Management
ESS	Energy Storage System
D-STATCOM	Distributed Static Compensator
FIT	Feed-in Tariff
GRI	Gas Research Institute
ICT	Information Communication Technology
IEEE	Institute of Electrical Electronic Engineering
IGBT	Insulated-Gate Bipolar Transistor
LCL	Inductor Capacitor Inductor
LTC	Load Tap Changer
LV	Low Voltage
MCEMS	Multi Community Energy Management System
MG	Micro-Grid

MI	Modulation Index
MOSFET	Metal Oxide Semi-Conductor Field Effect Transistor
MV	Medium Voltage
OLTC	On-Load Tap Changer
OPL	Optimal Power Loss
PCC	Point of Common Coupling
PLL	Phase Lock Loop
PVU	Percentage Voltage Unbalance
RPI	Reactive Power Injection
SCE	Southern California Edison
SOC	State OF Charge
SRF-PLL	Synchronous Reference Frame- Phase Lock Loop
STATCOM	Static Compensator
SVC	Static Var Compensator
SWER	Single Wire Earth Return
TCR	Thyristor Controlled Reactor
THD	Total Harmonic Distortion
TSC	Thyristor switch Capacitor
UK	United Kingdom
UL	Underwriters Laboratories
UPFC	Unified Power Flow Controller
VSI	Voltage Source Inverter
VUF	Voltage Unbalance Factor
V_{PCC}	Voltage at the point of common coupling

List of Symbols

Symbol	Definition
$\Delta\vec{V}$	Controlled voltage
h	Hysteresis
f_{sw}	Switching frequency
L_f	Interface inductance
R_f	Filter resistance
I_{fact}	Actual filter current
V_{mpp}	Voltage at maximum power point
V_{oc}	Open circuit voltage
VCO	Voltage controlled oscillator
a	Normalization factor
G_{OL}	Open loop transfer function
G_{CL}	Close loop transfer function
G_{LCL}	LCL Filter transfer function
ω_c	Crossover frequency
K_p	Proportional gain
Ki	Integral gain
$V_{CE\text{-}rated}$	Collector to emitter rated voltage
Lg	Grid side inductance
Li	Inverter side inductance
PL	Penetration level
F_g	Grid frequency
C_f	Filter Capacitor
I_{max}	Maximum current rating
P_n	Inverter nominal power
Z_b	Base impedance
F_{res}	Resonance frequency

Chapter 1

Introduction

1.1 Background and Project Motivation

In the last decade or so, there has been a significant growth in the penetration of residential and commercial solar PV systems into the LV and MV distribution networks due to the global concern about climate change and increase in electrical energy demand. Renewable energy technologies (such as Photovoltaic system (PV), wind turbine, etc.) and their applications into the electric power system are a viable solution to reduce CO_2 emission.

The solar PV system is the most promising renewable energy technology because its primary resources are readily available and enormous in varying intensity globally. Embedded generation popularly known as distributed generation (DG) is the integration of renewable technologies like PV system and a wind turbine into the MV and LV power distribution networks. The application of solar PV system as DG is gaining popularity globally, most especially in countries like the United States (US), PR China, Germany, Spain, Netherland, Italy, Japan, Australia, South Africa, Kenya, etc. In recent years, some power system grids around the world are experiencing increasing installation of solar PV system in the LV and MV distribution network. These power grids will experience more penetration by residential, commercial and utility companies in the near future due to the falling price of solar PV modules, government subsidies, and policy incentives. The government incentive scheme is one of the driving forces to the increasing use and development of PV technology worldwide. The most commonly used incentive mechanisms in Europe are feed-in tariff (FIT) and quota system.

The FIT scheme has been practiced in over 45 countries in the last two-decades [1], and it has increased the integration of PV system in the LV distribution network around the world. As of 2016, Italy recorded about 369MW of newly installed PV capacity, which represents a 22% growth over the last year and most of the installed PVs, registered in the previous year are installed in the LV distribution network (Residential and Commercial) [2]. In 2016, the UK recorded a large installation of solar PV (about 10.4 TWh), which is due to both smaller solar PV installations in the LV distribution network supported by the FIT scheme and large scheme supported by renewable obligation [3]. In 2010, the Southern California Edison (SCE) was well into a five-year project to install a total of 500MW of distributed PV energy within its service territory. The typical installation of rooftop PV systems in the recent past in California is about 1-3 MW that interconnects with MV distribution network [4]. Japan has also taken a bold step by proposing a national target of installing about 53GW of PV capacity by 2030 under the J-recovery plan [5]. Due to the re-introduction of load shedding in early 2015, the South African energy giant (Eskom) is excited about grid-tied PV systems and have dedicated a research team to carry out investigations on grid-tied PV systems with possible solutions to mitigate negative impacts on the LV distribution network. [6]. Furthermore, South Africa has experienced hundreds of grid-tied PV system already and is expected to integrate more PV systems in the near future.

The widespread proliferation of PV systems in LV distribution networks has caused power system perturbation such as voltage rise, overcurrent, and overvoltage protection issues, increase network losses, voltage unbalance (a single-phase PV application), potential harmonic increase and reverse power flow in the distribution network [7]. The deployment of PV systems brings ample technology and environmental benefits of the LV distribution networks under the deregulated market structure [8] [9]. However, the negative impact of high PV integration tends to affect the operation, voltage profile level and security of the traditional LV distribution network. The uncontrolled penetration (high PV system) of single-phase PV inverter may cause voltage

unbalanced, which may result in an increased harmonic level in a three-phase system and this may violate the condition of equal magnitude of the phases [10].

The voltage rise issue which is accompanied by a reverse power flow has led to intensive research by academia, utility, and scientist and it has led to the development of different voltage rise mitigation strategies.

The thesis reviews the commonly used voltage rise mitigation techniques that have been developed by researchers and academia to curtail voltage rise issues during high PV penetration. The thesis also reviews the general drawbacks of these strategies. The developed voltage rise mitigation strategies over time are mainly on load tap changer (OLTC) scheme, energy storage system (ESS) application, Reactive power support, and active power curtailment (APC) scheme [11] [12] [13].

Among the voltage rise mitigation strategies, distribution network operators (DNOs) favor total disconnection of the PV system from the distribution network to curtail voltage rise issues during high PV penetration [14]. However, sudden disconnection of the PV system from the distribution network may result in instability which may impose severe challenges like voltage flicker and power quality issues. The total disconnection will deny small-scale PV operators return on investment and will also discourage the third parties from venturing into this new trend of business.

1.2 Thesis Motivation

The solar power radiated from the sun and received by earth's surface is about 86,000TW [15] and the use of such energy can be economically viable. This massive energy can solve the global energy need, most especially in the Sub-Saharan African region. According to the international energy agency (IEA) 2011, about 587 million people in Africa do not have access to electricity [16]. PV systems can play an important role in Sub-Saharan African energy crisis due to

the availability of high solar intensity in the region. It is expected that more customers can now participate in electricity generation by directly integrating PV systems into the existing electric power network especially in LV distribution network. Besides the benefits of integrating PV systems into the LV distribution network such as reducing CO_2 emission and satisfying energy demand, the new trend tends to undermine the stability and operation of the LV distribution network due to sudden voltage rise, reverse power flow, and overloading of the feeder transformer.

One of the key issues that have attracted increased attention is the sudden voltage rise issue, which usually occur at the end of the network with high PV penetration. These issues have been a major concern for DNOs and have limited the total installed PV system in the power system particularly in the LV distribution network. As a result, there is a need to develop and improve the existing voltage rise mitigation strategies.

1.3 Objectives

With the continuous increase of distributed PV system on the LV network and the sudden voltage rise issue due to the high penetration of distributed PV system on the customer's side, with changing interconnection requirements, there is a need to improve the existing voltage rise strategies.

The objectives of this thesis are to:

1. Investigate, and analyse the impact of high PV on the radial LV distribution network
2. Develop a voltage mitigation strategy for higher PV penetration
3. Compare the performance of the proposed voltage rise strategy with established strategies such as battery energy storage system (BESS) and a Distribution Static Compensator (D-STATCOM).

1.4 Thesis Contributions

Based on the voltage rise issues, the thesis presents, a new CAPR strategy using the inverter PWM capabilities to ramp down the active power and voltage profile at the PCC of the LV distribution network with higher PV penetration. The methodology of the proposed strategy is based on the manipulation of the high-frequency switching pattern to regulate the output parameters of the grid-tied VSI.

The strategy increases the off time of the high-frequency switching pattern, that is, the regulation of the modulating signal in the sinusoidal pulse width modulation (SPWM) scheme using a modified proportional-integral current control algorithm to ramp down the inverter output power. Increasing the off time of the high-frequency IGBT switch will force the inverter current to lag which makes the freewheeling diode in the inverter switch to absorb some of the reactive power and charge the DC link capacitor which forces the PV output voltage to move towards the open circuit and setting a lower maximum power point (MPP). This action ramps down the voltage at the PCC below the standard upper voltage limits. The strategy is intended to allow customers to stay connected to the LV network and get some return on investment, and to avoid disconnection of PV from the grid. This action also ramps down the maximum active power of the PV system.

D-STATCOM device and battery energy storage system (BESS) were also used to mitigate voltage rise issues with higher PV penetration on a scaled down radial LV distribution network and the results were compared with the proposed CAPR strategy.

1.5 Scope and Limitations

The scope of this thesis is to investigate, analyzed, and mitigate the impact of a sudden voltage rise due to higher PV penetration within the LV distribution network. The investigation is limited to a scaled down simple radial LV distribution network due to the inability of the SIMULINK® software environment to simulate and converge large LV distribution network with higher solar PV penetration with VSI, the inverter controller, and proposed CAPR strategy.

1.6 Structure of the Thesis

The thesis is organized into seven chapters as follows:

In Chapter 1, the research motivation, and impacts of higher PV penetration are defined. The objective and contribution of the thesis are listed. The chapter ends with the structure of the thesis.

Chapter 2 reviewed the FIT scheme and analyzed the impact of the high PV penetration on an LV distribution network. The literature review is carried out to identify the different voltage rise mitigation strategies so as to develop a voltage rise mitigation strategy. Some of the limitations of the different strategies were identified. The need for the combination of communication infrastructure with established voltage rise technique to form a smart grid was also reviewed.

Chapter 3 reviewed the idea of DG and functionalities of a grid-tied PWM VSI with the PI current controller scheme. The design equations of the key components such as the Inductor capacitor, inductor (LCL) filter and phase lock loop (PLL) were also reviewed so as to select and design components in our system.

In Chapter 4, two different investigations (i.e., Steady-state and dynamic studies) were carried out in a radial LV distribution network with higher PV penetration using DigSILENT power-factory® and MATLAB®/Simulink®. The negative impacts of higher penetration of PV in both cases were defined and discussed.

In Chapter 5, the methodology of the proposed CAPR strategy on grid-tied VSI for voltage rise mitigation is presented. The proposed CAPR/ramp down strategy is tested on a simple scaled down a radial LV distribution network with higher PV penetration (60%). The results of the simulation are presented in this Chapter.

In Chapter 6, the well-known D-STATCOM and BESS strategies were reviewed and used to curtail voltage rise in a radial LV distribution network with higher PV penetration. The results of the analysis are used to evaluate the performance of the proposed CAPR/ ramp down strategy. Comparison of both techniques CAPR, D-STATCOM and BESS are presented.

Finally, in Chapter 7, conclusions are drawn from the performance of the proposed CAPR, D-STATCOM and BESS strategies. The chapter also presented a recommendation for future work.

1.7. List of Publications

1. Ainah Priye Kenneth, Komla Folly, "Voltage Rise Issue with High Penetration of Grid Connected PV" IFAC Proceedings, Volume 47, Issue 3, 2014, pp 4959-4966
2. Ainah Priye Kenneth, Komla Folly "Investigation and Analysis of the Impact of "Shading" on Output Performance of Photovoltaic (PV) Array" Workshop on Renewable Energy, Smart Grid and Computational Intelligence Applied to Smart Grid, August 29-30, 2014, University of Cape Town, South Africa.
3. Ainah Priye Kenneth, Komla A. Folly, "Development of Micro-grid in Sub-Saharan Africa: An Overview" International Review of Electrical Engineering (IREE), Volume 10, No. 5, 2015, pp 633-645
4. Ainah Priye Kenneth, Komla A. Folly, Arnold F. Sagonda "Increasing PV Penetration with D-STATCOM in a Radial LV Distribution Feeder" Proceeding of the 26th Southern African Universities Power Engineering Conference (SAUPEC), 2018.

Chapter 2

Literature Review

Chapter 2 reviews the global PV installed capacity and the impact of the FIT scheme to increase PV usage. The chapter analyses the impact and conditions of voltage rise on a simple radial LV distribution network. The chapter also reviews the different voltage rise mitigation strategies that have been developed over the years to curtail the various impacts of higher PV penetration on the MV and LV distribution network. Chapter 2 further discusses the possibilities of a future smart grid with these strategies, that is, an active grid with communication infrastructure and intelligent systems to address some of the new challenges imposed on the distribution network by higher PV system penetration. Additionally, communication infrastructure-based voltage rise mitigation strategies were also reviewed.

2.1 Global Installed PV System Capacity

PV technology is becoming one of the fastest power generation technologies, expanding from standalone systems to grid-connected systems globally. Recently, PV installation is gaining momentum, with an impressive 38.7 GW global installed capacity in 2014, up from 37.6 GW in 2013. According to [16], a total of 75 GW PV systems was installed globally in 2016, with an impressive 50% growth from 2015 which brings the cumulative global capacity to be above 300 GW. As of 2016, PR China, the United States, Japan, Germany, and Italy account for 70% of the global cumulative PV installation (312 GW) as shown in Fig. 2.1.

Increased global PV installation has also led to increased production of PV cell globally. In March 2017, the average price for installation of residential PV system, without permission or

connection, cost about 1.56 USD/Wp (1.44 EUR/Wp) starting from 1.23 USD/Wp (1.14 EUR/Wp) in Europe and to 2.36 USD/Wp (2.18 EUR/Wp) in other cases [16]. In 2016, about 77 GW of PV cell was produced, with a 35% increase from the previous year. Fig. 2.2 shows the yearly production of PV cell from 2010 to 2017 around the globe with PR China and Taiwan leading the way [16]. Most of the installations are carried out on the MV and LV distribution networks due to subsidies from the government and the FIT scheme. The FIT scheme is discussed in section 2.2.

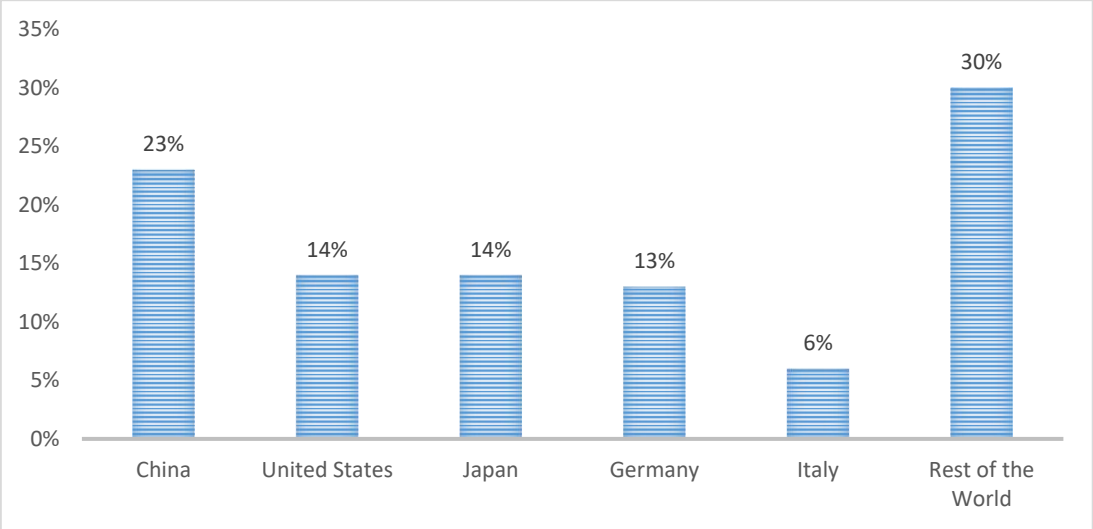

Fig. 2.1. Cumulative Global PV Installation 2016

Source: IHS

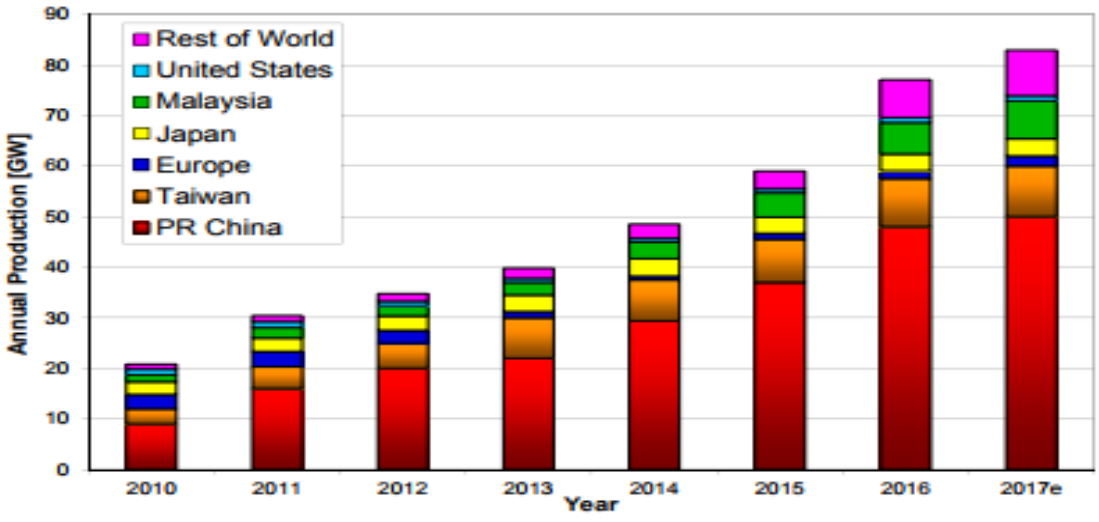

Fig. 2.2. Global PV cell Production from 2010 to 2017

2.2 Feed-In-Tariffs (FIT) Scheme

The push for renewable solar PV systems has resulted in fundamental changes in policies by government and utilities. This policy change has propagated large scale of small PV systems ranging from 1-10kW into the LV distribution network, and this has resulted in some negative impact [17] [18]. The solar PV system is seen as one of the most important strategies to reduce the impact of global warming, and one way of encouraging grid integrated PV system is through the FIT scheme.

The FIT scheme has been the most widely used support mechanism to encourage the growth of grid-connected renewable energy systems (most especially wind and PV technologies) by offering long-term contracts to renewable energy producers. As in 2015, the operational PV energy capacity between 1 - 10kW under the FIT scheme in Japan is about 0.86 GW [19]. It is also on record that the European Union installed more than 15GW of PV using the FIT scheme between 2000 and the end of 2009, and the FIT scheme amount to approximately 75% of the global PV deployment [20]. The FIT scheme guarantees renewable energy "projects a set payment for every kilowatt hour of energy produced – often a fixed rate above the brown power price to help overcome the high upfront capital costs of many renewable energy technologies" [21]. With the FIT program, developers and financiers of renewable energy projects can now set a known price for renewable energy systems in an attractive environment. Table 2.1 highlight on some of the key components and variables within the FIT Programs.

Table 2.1: Key Component and Variable in the FIT program [21]

Policy Variable	**Description**
Fixed price vs Premium price	"A fixed price FIT sets a constant rate, regardless of the wholesale market price. A premium FIT establishes a premium amount on top of wholesale prices so the overall rate fluctuates with the market"
Gross vs Net	"Consumers receive FIT for all electricity produced (gross) vs for the electricity fed back to the grid (net)"
Valued- based vs Cost based price	"The tariff rate can be set according to the generation cost plus a reasonable rate of return (cost based). An alternative is to value the tangible and intangible benefits of renewable energy technologies, such as a reduction in carbon and conventional pollution emission (value based)"
Eligible technologies and Differentiated payment levels	"FIT can include a variety of different renewable energy technologies, each of which will likely receive a separate rate (different size projects can also receive different rate) FIT rate can be set to vary for a specific technology, with project size. Resources quality (i.e. strength of wind, or specific location) (i.e., offshore vs onshore wind, ground or roof mounted solar)"
Contract duration	"The guaranteed timeframe of the contract differs by program. Typical FITs range from 15–20 years"
Price adjustment	"FITs can build in declining rate adjustment to account for reduced project installation cost overtime and advances in technological innovation. These altered rates apply to new contracts, not existing ones"
Project size cap	"Some FITs only apply to a specified range of sizes and can be capped to leave out large- scale projects"
Distribution cost	"FITs increase the cost of electricity. The cost is passed on to taxpayers in the form of taxes, to rate payers in the form of higher electricity bills or a combination of both."

The FIT scheme has been proven to be one of the most effective energy policies for promoting renewable energy, addressing cost barriers, supports investors security and making it economically viable. According to [22], a properly designed FIT scheme comes with a lot of benefits in the long run.

The FIT scheme can also provide more security for domestic energy supply, increased the drive for technological innovation, reduce CO_2 emissions, create jobs, enable fair market conditions

for renewable technologies and promote investment security. The FIT scheme has increased global installation of PV system, and this has led to extraordinary industry expansion with a new national market. The PV system markets are largely found in PR China, Germany, Italy, and Spain. Presently, the PV market is dominated by residential rooftop PV system, with low-rated power.

The FIT scheme application is gaining popularity globally due to the urgent need to reduce greenhouse gases. The scheme was first practiced in the United States of America in 1978 and began to expand to other nations since 1979. It was later adopted and implemented in Germany, Switzerland, and Italy by 1990, 1991 and 1992 respectively. Today, more than 45 countries have adopted and implemented the FIT scheme globally [23] [22]. Table 2.2 shows the global adoption and implementation of the FIT scheme by continent as of 2010.

Table 2.2: Global Adoption of Feed-in Tariff Scheme

Year	North/South America/Cities	Europe	Asia/Cities	Africa
1978	USA	-	-	-
1990	-	Germany	-	-
1991	-	Switzerland	-	-
1992	-	Italy	-	-
1993	-	Demark	India	-
1994	-	Spain, Greece	-	-
1997	-	-	Sri Lanka	
1998	-	Sweden	-	-
1999	-	Portugal, Norway, Slovenia	-	-
2000	-	-	Thailand	
2001		France, Latvia	-	-
2002	Brazil	Austria, Czech, Lithuania	Indonesia	Algeria
2003	-	Cyprus, Estonia, Hungry, Slovak Republic	South Korea, Maharashtra (India)	-
2004	Nicaragua, Prince Edward Island (Canada)	Israel	Andhra Pradesh, Madhya Pradesh (India)	-
2005	Ecuador Washington (US)	Turkey, Ireland	China, Karnataka, Uttaranchal, Uttar Pradesh (India)	-
2006	Argentina, Ontario (Canada)		Thailand	
2007	-	Albania, Bulgaria, Croatia, Macedonia	-	Uganda
2008	California (USA	Poland, Ukraine	Philippines, Gujarat, Maryana, Punjab, Rajasthan, Tamil, Nadu, West Bengal (India)	Kenya
2009	Gainesville, FL, Hawaii, Maine, Vermont (USA)	-	-	South Africa
2010	-	United Kingdom	-	-

With the introduction, adoption and the legal backing of the FIT scheme, utility, and energy companies are obliged to buy electricity from renewable energy producers at an affordable price per unit. The tariff rate is set by each government, depending on the cost of each renewable energy technology. The cooperation of grid owners to grant access to renewable energy producers most

especially PV systems to feed into the grid will create a synergy and secure investment for the investors, renewable producers, manufacturers, and suppliers.

The expansion of the FIT scheme and its impact on the electricity grid has made government and researchers, to develop grid codes that will secure the grid from some of the integration challenges. These grid codes have been developed by national governments and cities, that have adopted the FIT scheme due to the foreseen challenges (some technical and power quality issues) of higher PV penetration on the power system grid, most especially on the LV distribution network.

2.3 Electric Power Grid

An electric power system is an interconnection that consists of generating stations, substations, high voltage transmission lines, and distribution lines for delivery of electrical energy to end users (customers). Sometimes the power system stretches across international borders. The traditional organization of electrical power system dated from the 1950s followed a hierarchical structure with three different levels: generation, transmission, and distribution level as shown in Fig. 2.3 [24].

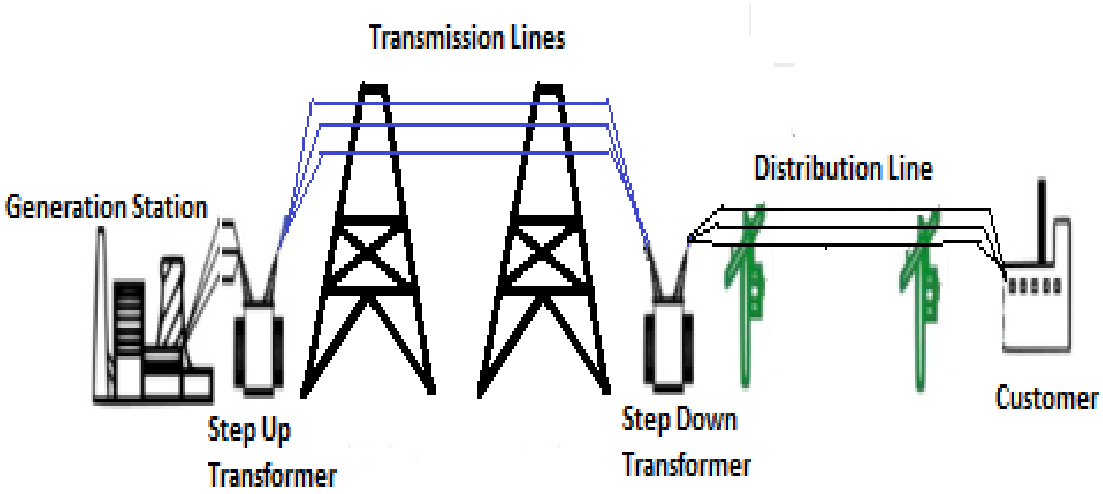

Fig. 2.3. A Simple Electrical Power System [25]

The distribution network is the final point of the power system linking the customers and the grid. The distribution level is made up of the MV and LV network. Traditionally, LV distribution networks are designed in a radial fashion and power flows from the high voltage sub-station to the LV customer loads. However, the high DG penetration will defile this order, as will be presented in this thesis. The LV distribution network is referred to as 230/240 or 110 Volts (Phase to neutral) and 400 /415 Volts or 440 Volts (Phase to phase). Voltage settings at the last controllable transformer before the customer's loads are often set at 5 – 10% higher than the nominal end-user voltage to accommodate line losses. The voltage levels and direction of the power flow is illustrated in Fig. 2.4. Section 2.4 helps us to understand the nature and dynamics of sudden voltage rise issue with DG penetration.

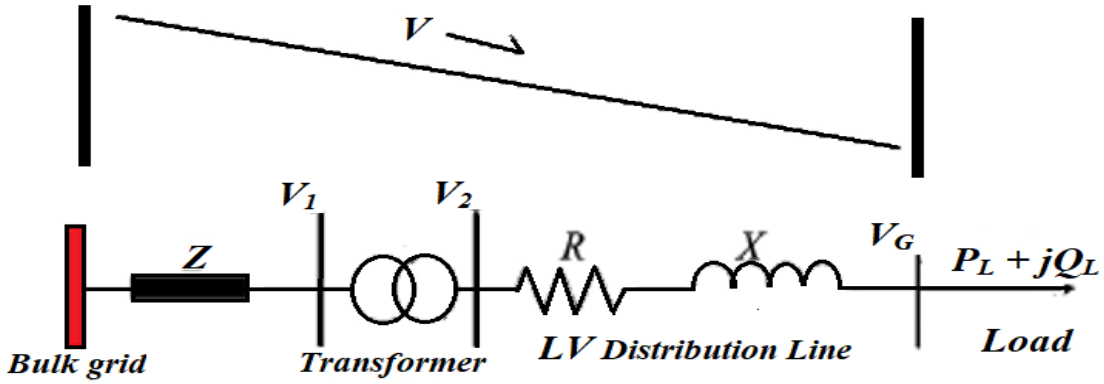

Fig. 2.4. A Simple Single Line LV Distribution Network

2.4. Analysis of the Impact of Higher PV Penetration on LV Distribution Network

The introduction of FIT has led to small power generation sources such as PV systems on the LV distribution grid. The high PV systems integration perturbs the dynamic of the LV distribution network because power flow can be in the reverse direction and overvoltage can occur. This means that the voltage at the load end may be greater than the network transformer supply voltage. Distribution networks are designed with the assumption that power will flow from the upstream high-voltage network to the downstream LV distribution network [26] but

the new trend of integrating PV systems on a radial LV distribution network can undermine the change in the behaviour of the traditional distribution network as shown in Fig. 2.5. And as shown in Fig. 2.6, the MV and LV distribution networks were not designed initially with anticipation of the integration of PV system which now is a major concern to the utility companies.

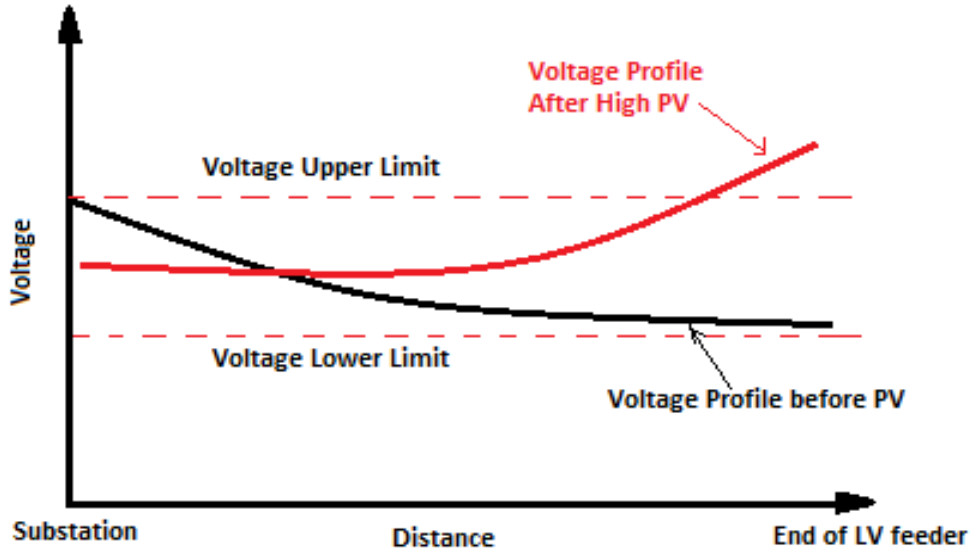

Fig. 2.5: Impact of Higher PV Penetration on LV Distribution Grid [27]

This change of voltage as shown in Fig. 2.5 illustrates the impact of high PV on the distribution network. As described in Fig. 2.6, power flow on a radial distribution network both real and reactive is from the substation (higher voltage) to the customer connection point (lower voltage) because, in the LV distribution network, the ratio of reactance to resistance $(\frac{X}{R})$ is less than equal to 0.5 as compared to transmission network with $(\frac{X}{R})$ value greater than equal to 10 [28]. This means that the resistance of the network is high and will lead to voltage drop along the line. Therefore, to effectively analyze the effect of voltage rise in an LV distribution network with high DG (PV, Wind turbine, etc.), the quantity of voltage drop on the distribution network should be understood.

To do this, we consider the system as shown in Fig. 2.7 which is used to evaluate the voltage profile of the LV distribution network with DG.

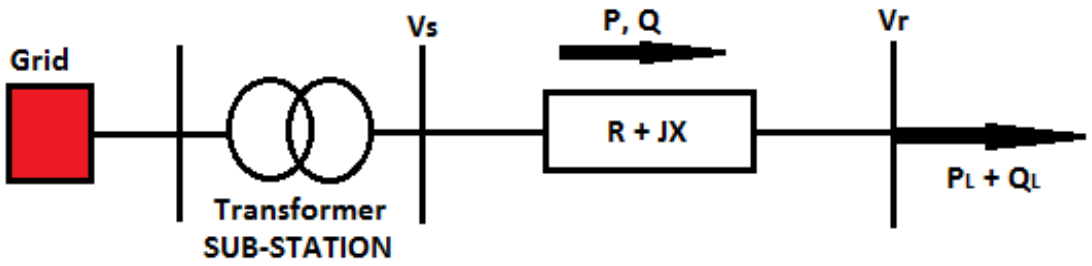

Fig. 2.6: A Simple Two Bus LV Distribution Network

2.4.1 Voltage Profile of the LV Distribution Network without DG (PV, etc.)

From Fig. 2.6, we consider the voltage V_s as the substation voltage:

$$\boldsymbol{V_s} = \boldsymbol{V_r} + \boldsymbol{I}\,(R + jX) \tag{2.1}$$

where $\boldsymbol{I}$ is the phasor current flowing through the distribution network and $\boldsymbol{V_r}$ is the voltage rise at the receiving end of the distribution network. For a radial network, the current flowing through the line is given as:

$$\boldsymbol{I} = \frac{P - jQ}{\boldsymbol{V_s}} \tag{2.2}$$

Therefore, substituting Eqn. (2.1) into Eqn. (2.2) and re-arranging gives the voltage drop of the radial distribution network without DG as:

$$\Delta V = \boldsymbol{V_s} - \boldsymbol{V_r} = \frac{RP + XQ}{V_s} + j\frac{XP - RQ}{V_s} \tag{2.3}$$

The voltage drop (ΔV) is very important at the customer's side because of the need for quality voltage supply to the load. Due to this fact, ΔV is guided by some technical regulation to maintain voltage within a certain voltage range which is determined by each country [28]. This

change in voltage on a radial distribution network gives us the insight to understand the dynamics of voltage rise due to the high penetration of DG (PV, Wind turbine, etc.), as described in subsection 2.4.2.

2.4.2. Voltage Rise on the LV Distribution Network with DG

Consider a DG in the radial LV distribution network as shown in Fig. 2.7 where V_s and Z are the equivalent substation voltage and impedance respectively. If the DG current is greater than the LV line current, the voltage at the PCC (V_{PCC}) will be greater than V_s and this may result in voltage rise.

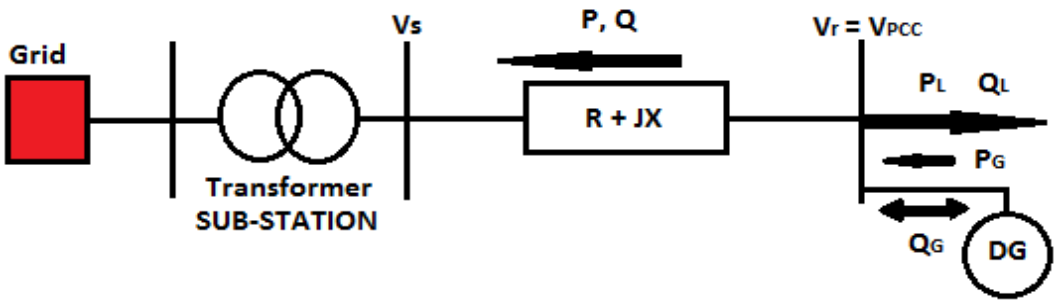

Fig. 2.7: Radial LV Distribution Network with PV Array

Therefore, we can say that the voltage at PCC is given as (neglecting the imaginary part of Eqn. (2.3)):

$$\boldsymbol{V_r = V_{PCC} \approx V_s + \frac{RP + XQ}{V_{pcc}}} \tag{2.4}$$

Then, the impact of the DG on the system will be the difference between the voltage at the PCC and the substation voltage, and the difference determines the effect of voltage rise as shown in Eqn. (2.5):

$$\Delta V = \boldsymbol{V_{PCC} - V_s \approx \frac{RP + XQ}{V_{pcc}}} \tag{2.5}$$

where $P = P_{DG} - P_L$, and $Q = \pm Q_{DG} - Q_L$.

If the standard voltage limit is assumed to be βV_S, then the voltage at the PCC should be lower than the upper limit voltage, that is, $V_{PCC} \leq \beta V_S$, where $\beta \leq 1.05$ in this case.

Therefore, if the $V_{PCC} \geq \beta V_S$, that is, if $\beta = 1.06$ for instance, then the $V_{PCC} = 1.06 V_S$.

Hence, the effect of voltage rise on the network is 0.06pu when the reference voltage (sub-station voltage), V_S is 1pu.

This determines the behaviour of voltage rise on the LV radial distribution network. If $\Delta V \leq 0$, the V_{PCC} is under the upper voltage limit, but if there is a high DG penetration during the off-peak period where $\Delta V \geq 0.05$, then voltage rise will occur because voltage rise is dependent on the penetration level of the DG (PV systems etc.).

According to [29], the penetration level (PL) is given as;

$$PL = \frac{Capacity\ factor * Installed\ DG\ Capacity}{Feeder\ Capacity} \tag{2.6}$$

where the installed capacity is known as the maximum output power of the individual DG or the total DG installed on the network while capacity factor is the ratio of the energy produced during a particular period to the energy that would have been produced if the DG would have functioned continuously at full power in the same period.

2.5 Review of Voltage Rise Mitigation Strategies

LV Distribution network supplies customers at voltages within specified voltage ranges that allow for efficient and economical operation of the customer's appliances [30]. However, the high PV penetration on the LV network has affected the standard voltage limits and the security of the network. According to [31], DNOs can adopt the strategy of limiting the total installed PV on the LV distribution network by using the grid data information such as grid

impedance, the number of customers and grid configuration to estimate the maximum possible installation of PV system on the distribution network that will prevent over-voltage. However, limiting the installation of PV systems in the LV distribution network is not a viable solution to mitigate voltage rise issues.

Therefore, to enable a massive deployment of distributed energy resources (DER), especially PV systems and cope with the challenges while simultaneously obtaining the potential benefits of these distributed PV systems, it is imperative to develop coordinated and efficient control strategies for the operation and management of these systems [24]. This section reviews and discusses the various voltage rise mitigation strategies that have been developed and investigated by different researchers. A summary of the commonly used voltage rise mitigation strategies and drawbacks are highlighted in Table 2.3.

Table 2.3: General Summary of the Drawbacks of the Reviewed Voltage Rise Mitigation Strategies.

Voltage rise Mitigation strategies	**Application Drawbacks**	**References**
Conventional control (OLTC)	- Not economically attractive with communication infrastructure (quite expensive) - The permissible voltage level is limited when located close to the load	[31] [32] - [33]
Disconnection of PV from grid	- Momentary oscillations in frequency - Causes significant increase in instability - Causes voltage flickers an power quality problems - Severe challenges on consumers equipment's - Customers not enjoying return on investment	[14], [34]- [35]
Energy Storage System	- High maintenance requirement - Environmental hazard - Cost of deep cycle solar batteries	[36], [37]- [38]
Reactive Power compensation and Inverter Var support	- FACTs devices such as STATCOM and SVC are quite expensive - Inverter Var support causes congestion in the network, increase losses and deteriorate power quality	[39], [40], [36] [41]- [42]
Active Power Curtailment	- Direct economic effect on owners of PV plants, but owners can still feed some quantity of power and still get some return on investment.	[43], [44], [14] [45], [42]- [46]

2.5.1 Conventional Voltage Control Strategy using OLTC

The system voltage of the distribution network is an essential parameter, and it is the responsibility of the DNOs to maintain the supplied voltage within an acceptable range on the load side of the network [32]. Traditionally, system voltage in the LV distribution network is controlled normally, through the use of a transformer OLTC at the MV substations using automatic voltage regulators (AVR) relay.

OLTC mechanism is a transformer component, controlled automatically by a relay, to increase or decrease voltage by altering the tap position of transformers [39]. The function of the automatic voltage regulator (AVR) is to measure the voltage and current through the voltage transformer (VT) and current transformer (CT) at the load side respectively, and then compare the measured voltage with the predetermined voltage (reference or setting voltage value) of the AVR (V_{ref}). The difference is then compared with the tolerance setting of the AVR, and if it exceeds the tolerance setting, a tap change is initiated to adjust the transformer voltage at the load side to a satisfactory level [47]. The AVR relay ensures that the voltage at a local or remote location is controlled within the set limits [48]. The application of active transformer with an efficient control of the OLTC has been recorded to be an effective solution for over-voltage prevention during higher PV penetration on the LV distribution network [31].

In reference [49], an OLTC-fitted transformer with the local voltage control approach was proposed and used to control voltage rise issue in an LV distribution network. It also suggested communication infrastructure with OLTC to increase PV penetration level on a long LV distribution network. In reference [50], the authors presented an overvoltage control method using an OLTC-fitted transformer and a voltage estimation technique to determine the minimum and maximum voltage values of an LV network during high PV penetration, so as to maintain the system voltage within the safe zone. The voltage control scheme was investigated

using a residential UK LV network and the results show the effectiveness of the technique to control the voltage within the safe zone. In reference [51], the authors proposed an overvoltage prevention strategy by coordinating the transformer OLTC with multi-community energy management systems (CEMSs) on an LV distribution network with higher PV penetration. The strategy adopts demand-side management (DSM) scheme to schedule each customer household load (that is, load that can be interrupted) so as to prevent over-voltage situation and relieve the OLTC. However, if the schedule load cannot prevent the overvoltage, the OLTC will kick in, by regulating its taps value downward to reduce the network voltage.

The major disadvantage of the OLTC on an LV grid is that when a load is situated close to the voltage regulator, the amount of permissible voltage increase will be limited [40]. OLTC is one of the best strategies to curtail sudden voltage rise, but it is not economically attractive (quite expensive) due to the cost of communication devices and the infrastructures, used for sending feedback signals from affected buses [52] [36] [43] [33].

2.5.2. Disconnection of PV System from Grid

The DNOs typically favours disconnection of PV systems from the LV distribution network as a means to prevent overvoltage at the PCC. According to [14], network distributors address the problem of overvoltage by using a maximum voltage protection scheme, embedded in the generation systems, which operate by shutting down the generation unit (On/Off) when the voltage at the PCC is close or at the statutory limit. The impacts of the disconnection from the distribution network recently gained increased attention from the DNOs and the PV inverter manufacturers, especially when a very high penetration of PV systems is coming into reality. In light of this thriving situation, typical anti-islanding disconnection may impose severe challenges on the whole power system, especially on end - user's equipment [34] [53].

For instance, an anti-islanding operation that results in the disconnection of PV systems may cause voltage flickers, power quality problems for the end-user equipment, and may lead to the loss of customer's income. According to [54] [35], sudden disconnection of PV systems from the distribution system can cause a significant increase in the instability of the system with momentary oscillations in the frequency, depending on the level of penetration in the distribution network. Total disconnection of the PV systems from the grid will be quite disturbing to the small-scale PV operators because of loss on the return of investment.

2.5.3. Energy Storage System (ESS)

Presently, BESS is undergoing different stages of development and deployment in various areas. There are a variety of technologies that can be used to store energy on the utility power system, such as lead-acid, nickel-electrode and sodium-sulphur modular batteries, zinc-bromine, vanadium redox, and polysulfide-bromide flow batteries, superconducting magnetic energy storage, flywheels, electrochemical capacitors (ultra-caps), and compressed air energy storage (CAES) [37]. ESS has been envisaged to play an important role in the advancement of grid-integrated PV systems and the future Smart Grid, particularly in the areas of high renewable energy penetration in the LV distribution network. Today, ESSs are applied in the distribution network with various control techniques to address some of the issues of high PV penetrations in different capacities. According to [55], widely deployed storage technologies in the power systems are pumped hydro and lead-acid batteries because they are technically and commercially mature. BESS can also be employed to regulate the power between the PV generation and utility grid to improve power quality and voltage profile at the PCC of the power system grid. According to [56], the implementation model of the battery energy system can be classified as decentralized storage systems with PVs in the LV network, a central storage system for whole LV network and the mix of both central and decentralized storage systems. Some of the battery control techniques used for application in the LV distribution networks are

highlighted in this section. In [36], the authors proposed a voltage rise mitigation approach using coordinated control of decentralized ESS with traditional voltage regulators, including the OLTC and step voltage regulators (SVR) to solve the voltage rise problem caused by the high photovoltaic (PV) penetration on the LV distribution network. The distributed ESS state of charge (SOC) controllers are used to relieve the tap changer operation stress, share the network peak load, and decrease the transmission and distribution resistive losses under high solar PV penetration. Through this coordinated control, the additional tap changing operations can minimize voltage rise. In reference [57], the author's proposed a preventive control technique using an adaptive control to store energy for voltage regulation in the distribution network. The voltage margins at the PCC is calculated by continuously measuring the voltage and current phasors to establish a real-time Théevenin equivalent, which is then used to determine the maximum and minimum power injections allowed at PCC. Based on this phenomenon, the ESS is controlled adaptively to prevent the occurrence of voltage violation. The proposed idea can identify possible voltage violation in advance and dispatch the right amount of power to prevent the voltage rise. In reference [58], the author's proposed a new charging/discharging control strategy to effectively utilize the distributed ESS with solar PV units in LV networks. In the approach, the SOC of the storage device is taken into consideration when designing the charging and discharging controller, so as to effectively utilize the available storage capacity of the battery. The proposed charging and discharging strategy mitigate sudden changes in PV output by operating the storage in a short-term discharge mode. The proposed strategy can also track the deviation in the actual SOC of the energy storage device at any given time instant and ensure a better utilization of the available storage capacity. The battery storage devices consume the surplus power from solar PV units during charging operation and reduce the amount of active power injected into the grid which mitigates the voltage rise.

In reference [59], the authors proposed an algorithm to coordinate an SVR, BESS, and smart PV inverter functionalities to curtail active power. The BESS is connected to the DC link capacitor of the inverter to absorb and deliver power to the system when required. The strategy used to curtail PV impact is a communication network-based system which controls the steps of the SVR after receiving a signal from the PV bus as shown in Fig. 2.8. The PV controller sends signals to the smart inverter to begin controlling the active and reactive power after receiving a signal from the dead band comparator of the SVR. The investigated strategy was able to curtail voltage rise within the maximum voltage limit (±5%). However, the added cost of the communication devices makes it unattractive.

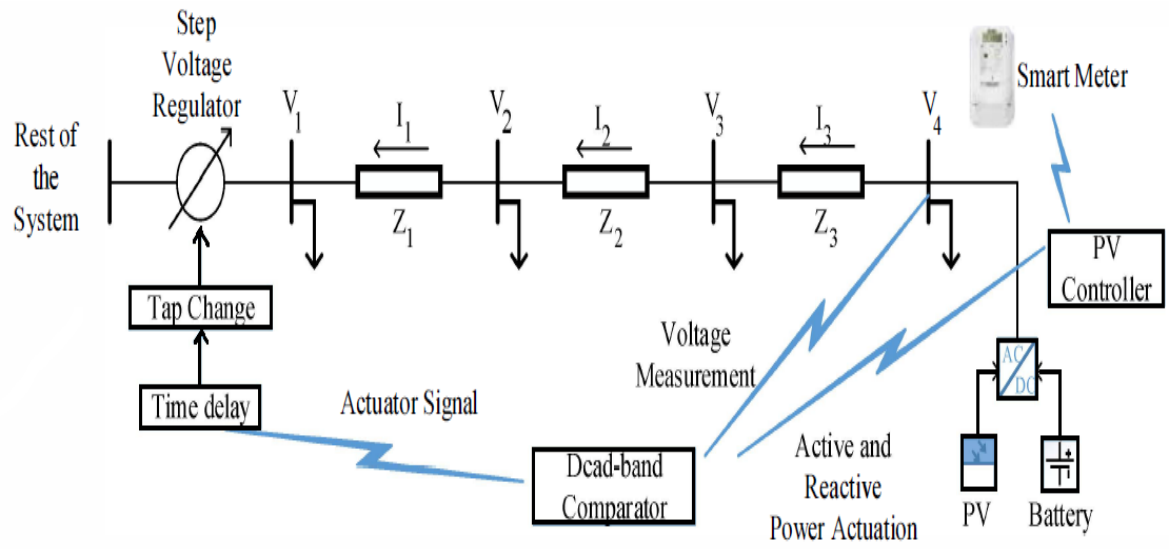

Fig. 2.8. PV Array along with SVR and Communication Layer [59]

In reference [60], the authors proposed a new ramp rate control strategy with a compensator (Battery energy system) as shown in Fig. 2.9 to control the inverter output power. The method controls the ramp rate of the PV inverter output power within the desired level at any instant of time by controlling the compensator power. The strategy introduced a dead band function that will force the ramp rate of the PV power to be zero if it is within acceptable limit using the desired ramp rate of the inverter power. The strategy also incorporates a switching function

that will decide the removal of the compensator power (ESS power). The proposed ramp rate control strategy is used to produce the appropriate amount of the compensator power so as to control the ramp rate of the PV inverter power. This is done with an inverse characteristic base desired ramp rate technique to improve mitigation performance. The proposed ramp rate control technique was deployed to control voltage dip at a household as a result of the sudden decrease in PV output by discharging the BESS to control the negative ramp rate. When sharp voltage rise occurs due to sudden increase in PV output power, the BESS is charged to control the positive ramp rate, and this action mitigates the sharp voltage rise as well.

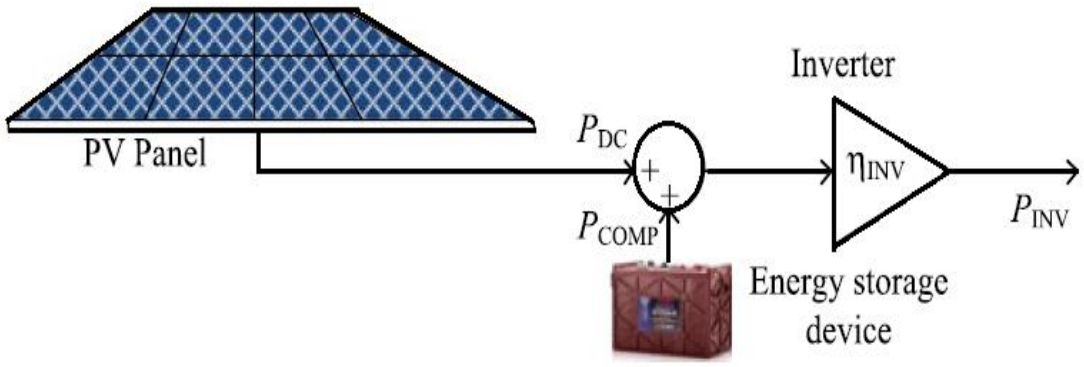

Fig. 2.9. Schematic of the Ramp Rate Control Strategy using BESS [60]

The advantage of using BESS is to slow down the rate of rise in the PV output power so as to control voltage fluctuations caused by the clouding effect or excess power on the LV distribution network. However, the problem of utilizing BESS for compensating PV output power during voltage fluctuation is the sizing of the BESS and additional economic cost due to the inclusion of BESS. The key issues of deploying BESS for active power curtailment in grid-tied PV systems, is how to control, size and estimate the appropriate amount of BESS for the fluctuation.

Various types of storage devices like lead-acid batteries, lithium-ion batteries, and electric double layer capacitors can be used to either store the excess power from the PV system or used to ramp the PV power and control the voltage at the connection point [36] [61]. Among these batteries, lead-acid batteries are the most commonly used batteries today because they are reliable, robust, and have a wide range of sizes and capacity and can deliver high current. However. they have some perceived disadvantage such as an environmental hazard, short cycle life, high maintenance requirements, low specific energy, and power. The major disadvantage of batteries for PV applications is the cost of deep cycle batteries [62]. See Table 2.4 for recent battery prices. However, the price of batteries is expected to fall due to recent breakthroughs in power electronics and manufacturing, in the near future [38].

Table 2.4: Cost of Different Deep Cycle Batteries for Residential Solar Application in South African Rand [38].

No	Item	Capacity	Price range in Rand (R)
1	Lead crystal BC-6CNFJ-40	12V, 40Ah	2236.00 incl. VAT
2	Vision sealed Deep cycle Battery	12V, 100Ah	1,992.00 incl. VAT
3	Son X RA12 100Ah 12V AGM Deep cycle battery, Valve Regulated Lead Acid	12V, 100Ah	2,462.00 incl. VAT
4	Excis smF101, C20 Taper Terminal lead calcium battery	12V, 102Ah	2,309.00 incl. VAT
5	Enervision E-Guard EFB12-100 Lead Acid battery	12V, 102Ah	1,870.00 incl. VAT
6	Deltec BD5-105N Sealed Lead Calcium Battery With Tapered Terminal	12V, 105Ah	2,522.00 incl. VAT
7	Vision Fully-sealed Deep cycle	12V, 200Ah	3,924.00 incl. VAT

2.5.4. Reactive Power Compensation/VAR Support

STATCOM, SVC and the shunt capacitor banks are used as reactive power compensators and to provide voltage regulation. Shunt capacitor banks are limited in terms of voltage regulation capabilities when compared to SVC and STATCOM because rapid voltage control capabilities are not possible. In a shunt capacitor bank, it will be very difficult to find the faulty capacitor during battery element failure. Therefore, shunt capacitor bank will not be suitable for voltage control of the LV distribution network. However, with the advancement of power electronic technology in SVC and STATCOM, rapid and flexible voltage control are possible. Reactive power compensation can also be achieved with power electronic devise such as thyristor-controlled reactor (TCR) and thyristor switch capacitor (TSC). SVC and STATCOM are extensively used to regulate the AC voltage on the power system network because the technology is well proven, and it can supply dynamic reactive power with fast response time. The development of high-power electronic devices such as transistors (Insulated-Gate Bipolar Transistor (IGBT), etc.) has increased the potential of STATCOM and SVC for dynamic reactive power control.

A device such as STATCOM has the advantage of providing a solution in fast response time with the capability of absorbing the reactive power to reduce the voltage when there is a voltage rise situation in the distribution system. The capabilities of STATCOM, D-STATCOM, and SVC to address the issue of voltage rise on the distribution network are discussed in this section. According to [41] [63], STATCOM and D-STATCOM contribute more effectively to voltage regulation and can significantly improve the transient voltage behaviour on the transmission and the distribution systems. D-STATCOM device in the reference [64] was used to evaluate the effectiveness of reactive power support to improve the steady state voltage profile of the distribution network. In [65], a dynamic reactive power support and a fast-acting energy storage system were evaluated to help alleviate some of the problems encountered

during higher PV penetration. In reference [66], the authors proposed SVC and smart inverter to control the voltage profile of a distribution network with high PV penetration. The proposed SVC strategy was able to mitigate the overvoltage issue in the LV network. In reference [67], the authors investigate the used of D-STATCOM to enhance PV penetration and control of the system voltage within the statutory limit in a Taipower distribution network. During the investigation, D-STATCOM regulates the voltage within the statutory voltage limit by absorbing some amount of reactive power in the network. The voltage at the PCC exceeds the voltage constraints limit of 2.5% with 1.475MW of PV generation without the D-STATCOM, and when the D-STATCOM was applied, the voltage was now maintained within the statutory voltage limit of 2.5% with 4 MW PV generation. In [68], the authors proposed a coordinative voltage control scheme which comprises an OLTC and D-STATCOM devices. The method uses a remote voltage value that is obtained from the PCC of each bus to activate the OLTC as shown in Fig. 2.10. The activation of the OLTC takes place only when the D-STATCOM has reached its maximum limit, and there is still the over-voltage situation. The proposed coordination was able to mitigate the voltage rise and the unbalanced voltage situation in the system.

These compensators can raise the fault ride-through capability of the PV plant within acceptable levels. However, the major drawback of these types of reactive support scheme is the high cost of these compensation devices (SVC, D-STATCOM, etc.) for LV distribution network [60] [61]. For price comparison, see prices for some of the compensation devices (SVC AND STATCOM) used in the LV distribution network in Table 2.5.

Table 2.5: Cost of Different SVC and STATCOM for Distribution Network [69] [70].

No	Item	Capacity	Price range in Rand (R)
1	Ideal SVG Dynamic Static Var Compensator	400V, 240kVar/350kVar	R95,408.057 – R152,652.89
2	Static Var Generator (SVG) SVGM-0.4-35a/T(F)L	400V, 35kvar	R38763,60/set
3	Power Distribution STATCOM SBW voltage stabilizer	380V, 200kVA	R12921,20 - R129212,00/set

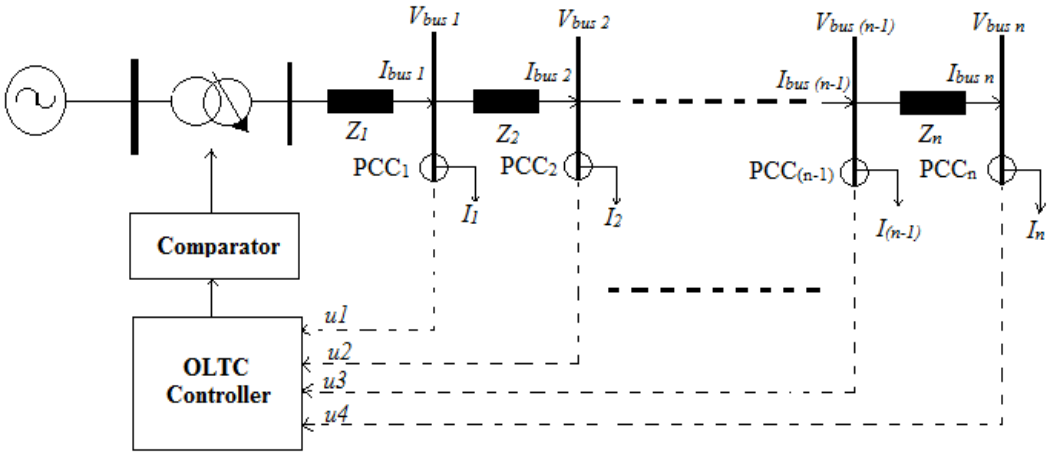

Fig. 2.10. OLTC Control Scheme

Studies into the use of inverters to regulate network voltage during high PV penetration have shown that to achieve optimal operation of the network, some form of centralized control is required [71]. Grid-tied solar inverters play a very important role in the integration of the PV system on the power system and will be discussed in chapter 3 of this thesis. One very important benefit of an inverter is that it has the ability to deliver leading or lagging reactive power or voltage-ampere (VAR) which can be used to support stability [72] [73].

One of the commonly used reactive power controls for an inverter is the local control method (known as droop based regulation method) [39] [74] [44] [75] [45]. The power factor

characteristic (Cos phi (P)) scheme and reactive power/ voltage characteristic (Q (U) scheme) for voltage control are based on the droop characteristic. The Cos phi (P) and Q (U) schemes are effectively coordinated and used to regulate the inverter output voltage. According to [40], better voltage profiles can be achieved when the reactive power is allocated to all inverters in the LV network using a central voltage control strategy, LV grid buses information from smart meters and characteristic of the LV grid as shown in Fig. 2.11. The reactive power reference of the inverters in the system is controlled using an optimal power flow (OPF) algorithm which monitors the parameters of the LV system. In this strategy, if the PV injected power is low, the reactive support is zero and when the PV power is above normal, the reactive power increases linearly to control the voltage rise.

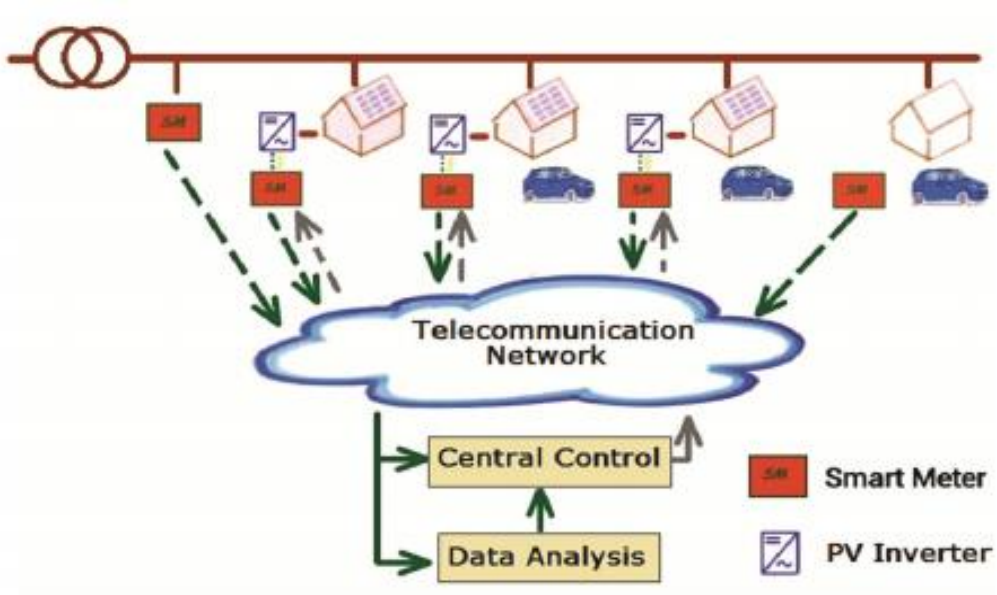

Fig. 2.11. LV Distribution Network with Smart Central Voltage Control Strategy [40]

In reference [76], the authors proposed a modified droop control technique to maintain the voltage level on the distribution network using the grid-tied inverter. The proposed method uses linear, rotational transformation matrix T from active and reactive power to create new active and reactive power components. The technique used two control modes to control the

voltage as shown in Fig. 2.12. First, the modified control mode is used to regulate the voltage when it is more than the dead band voltage while the conventional droop control mode is used to maintain the voltage within the dead band voltage. This technique can only maintain the voltage at the PCC within the dead band voltage.

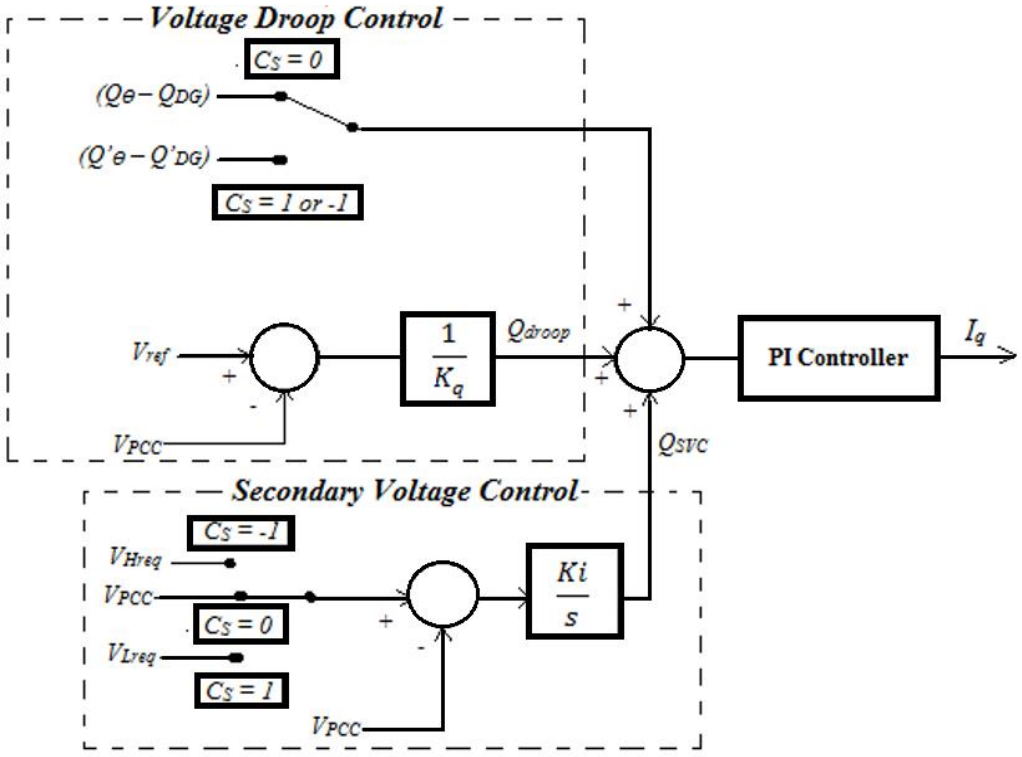

Fig. 2.12. Voltage Control Containing Control Modes [76]

In reference [77], the authors propose a reactive power/voltage characteristic regulation method. The method is optimized with a reactive power /voltage characteristic algorithm using the available capacity of all the inverters in the regulation process and avoids stressing PV at the downstream of the distribution network. The proposed algorithm maintains the voltage at the PCC within the standard limit and minimizes reactive power absorption in the overall network. In reference [78], the author developed a grid interactive PV based inverter with an additional central control system to control the reactive power injection by each inverter so as to reduce the unbalance among inverters in the network to improve the voltage at PCC.

In reference [79], the author proposed an optimal inverter VAR control to regulate voltage when there is massive PV penetration on the distribution network. The proposed technique uses the optimal power flow program to structure the inverter VAR injection. The technique is applied to a second order cone program with an additional linear term to specify the valid and optimal reactive generation and voltage magnitude, and trade off inverter losses when it is operating at non-unity power factor. In reference [80], the authors introduced the reactive power injection (RPI) technique using a droop control scheme to enhance active power curtailment (APC) for overvoltage protection. The technique reduces the active power from the PV array and increases the reactive power injection so as to control the node voltage. This means that the reduction in the active power is followed by reactive injection to maintain the voltage profile within the voltage threshold.

The use of an inverter to control voltage during voltage rise situation can be effective with low power factor, but it comes with increased losses, deteriorate power quality and congestion on the distribution line [81] [82] [42]. Sharing of the reactive power among PV inverters on the distribution network requires some communication infrastructure which can be costly. One major disadvantage in using PV inverter to absorb reactive power is the inverter power factor. The minimum power factor for most PV inverters is usually kept at 0.9. However, to effectively use an inverter to absorb reactive power, the inverter should be oversized, and this can further reduce the power factor of the inverter.

2.5.5. Active Power Curtailment (APC)

APC is also a mitigation approach that prevents overvoltage on an LV distribution network with high PV penetration. APC is an attractive strategy and requires little modification in the grid-connected inverter control [44] and it is only required when there is an overvoltage issue to minimize the PV power. APC has a direct economic effect on owners of PV plants, but

can be profitable if overvoltage is curtailed and owners feed some quantity of power, rather than disconnecting the PV inverter from the system [42]. In reference [43], residential PV operators in Germany are required to reduce the output of their PV inverter by 70% of the nominal power during an over-voltage situation so as to protect the power network. In [44] [45], the authors proposed a droop-based APC to regulate the voltage rise at the PCC. The technique is designed in a way that the power injected by the inverter must be a function of the bus voltage, the slope factor, and the droop factor. The proposed methods use the local voltage to determine how much power is needed to be curtailed by the PV inverter. Applying the APC method avoids overvoltage on the bus while keeping the installed PV power, but scarifies part of its power when it is above the standard voltage limit. The APC output power losses (OPL) method could share the curtailed power in all the PV inverter by setting different droop factor for all the PVs. In [14] the authors proposed an active power curtailment control mode and a maximum power point tracker (MPPT) control mode to regulate the voltage at the PCC. The voltage control is achieved with voltage control logic and the control algorithm is simulated in the Simulink environment in MATLAB. This proposed technique was able to adjust the active power produced by the PV according to the local voltage node using both MPPT and power curtailment mode to achieve the voltage regulation. This technique regulates the voltage rise at the PCC by regulating the active power of the renewable power source.

Reference [83], presented an active power control technique using a modified fractional open circuit voltage method to control the active power of the PV array. The technique uses the ratio of the voltage at maximum power point (V_{mpp}) and the open circuit voltage (V_{oc}) of the PV array within a reserve power margin to control the PV array output power when the system frequency changes. In this technique, the curtailed active power is determined by the ratio of V_{mpp} and V_{oc} of the PV array and can be explored for large-scale PV penetration in the LV distribution network. In reference [84], the authors proposed a control scheme that coordinates

the grid-connected PV arrays to consume reactive power and curtail the active power whenever there is overvoltage on the LV network, and to maintain maximum power transfer to the grid where there is no overvoltage situation. The control scheme operates without the communication link between the inverters. In reference [85], the authors proposed a consensus algorithm for controlling active and reactive power using a control agent which determines the reference value of active and reactive power either by absorbing reactive power or by regulating the active power when preventing overvoltage during high PV penetration through the grid-tied inverter. In reference [46], the authors proposed an active power curtailment using a predictive model, based on artificial neural network to generate the accurate power to be curtailed and determine the optimal grid-integrated inverter power to eliminate over-voltage which is a function of reverse power flow and keep the system voltage within the acceptable limits in the LV distribution network. The technique was tested, and it predicted accurate curtailed power.

The authors in [42], presented a two-wide area power curtailment strategy employing micro-inverters with a modified over-voltage prevention scheme to regulate the voltage of the LV network with higher PV penetration. The strategy uses microinverters for a string as shown in Fig. 2.13, and this converts the PV array into a segmented generator which allows for disconnection of any part of the PV array to regulate voltage on the network. This means that the disconnection will reduce the PV capacity. The method is made effective by a sequential micro-inverter tripping algorithm with time delay for each micro-inverter for the network voltage control as shown in Fig. 2.13. The strategy was used for wide area curtailment and was able to preserve about 62% - 100% of the generation when compared to typical overvoltage protection schemes. The reliability of the micro-inverters, when exposed to ambient temperature will be one major disadvantage of this method because micro-inverters are installed outdoors beneath the PV system and this can increase its failure rate which can affect

the performance of the scheme. This method is only suitable for PV systems that are connected in parallel strings as shown in Fig. 2.13.

The reduction of the active power of the PV system by the APC strategy is seen as a drawback but can be more attractive when compared with the total disconnection of the PV systems from the grid because producers can get some percentage of return on investment.

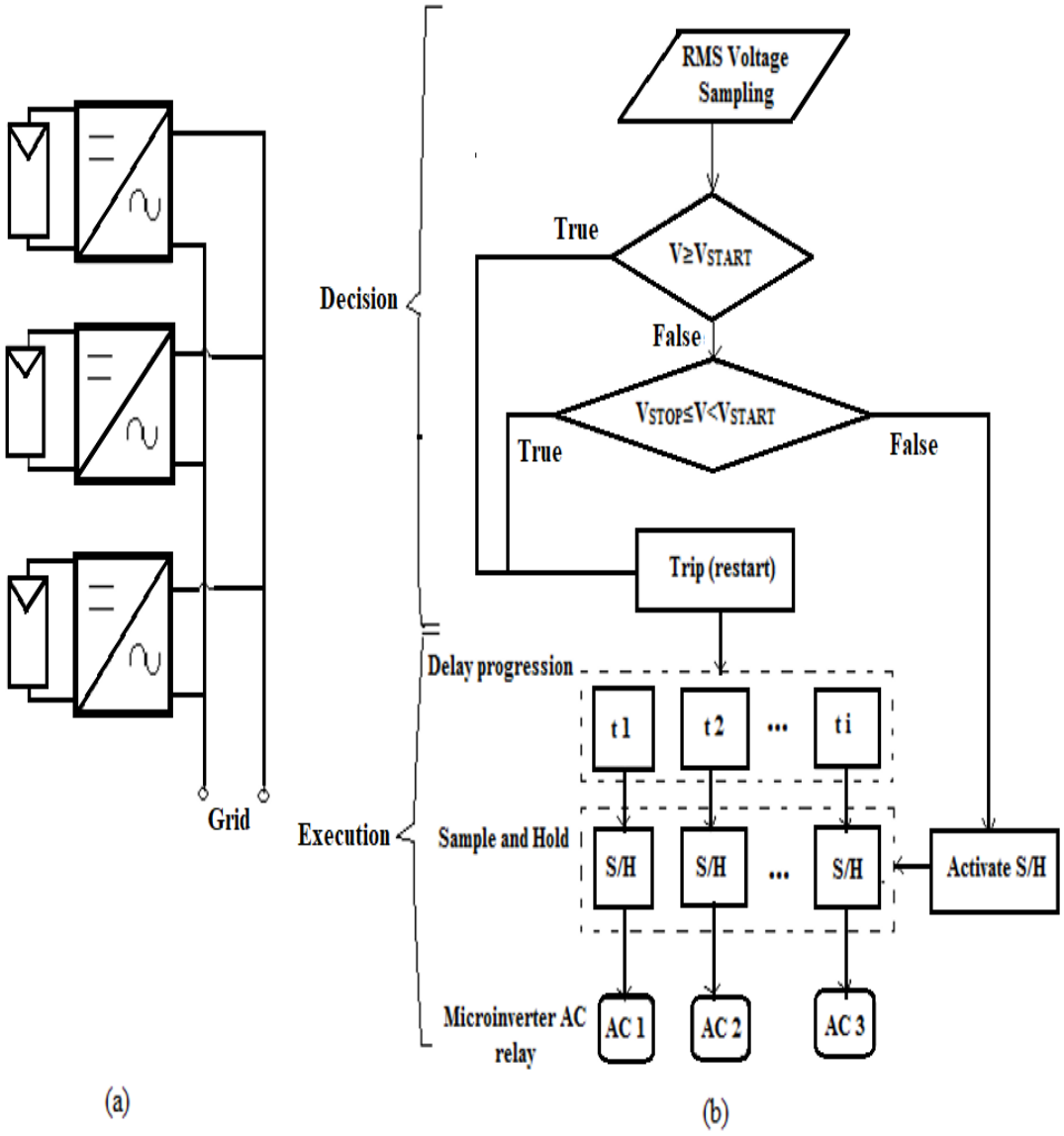

Fig. 2.13. (a) Parallel Micro-Inverter Topology (b) Algorithm of Voltage Controlled, Sequential Micro-Inverter Tripping

2.6 Future Trend of Grid Integration, Distributed Generation (DG)

These individual voltage control methods have shown the ability to control the voltage at PCC individually, but if coordinated with communication devices and control algorithm, it will improve the voltage profile and increase the penetration of renewable system technologies most especially PV systems in the near future. Due to the threats by renewable energy systems on the distribution network and the issue of frequent outages (equipment overload, circuit overload, etc.), the ultimate smart grid in this context is now seen as the next big thing in the future [86]. From a grid perspective, these new generation modes require improved control and monitoring of existing networks. Considering the aforementioned challenges, the power, and energy community is promoting the use of information and communication technology (ICT) in the electricity infrastructure [87] as shown in Fig. 2.14.

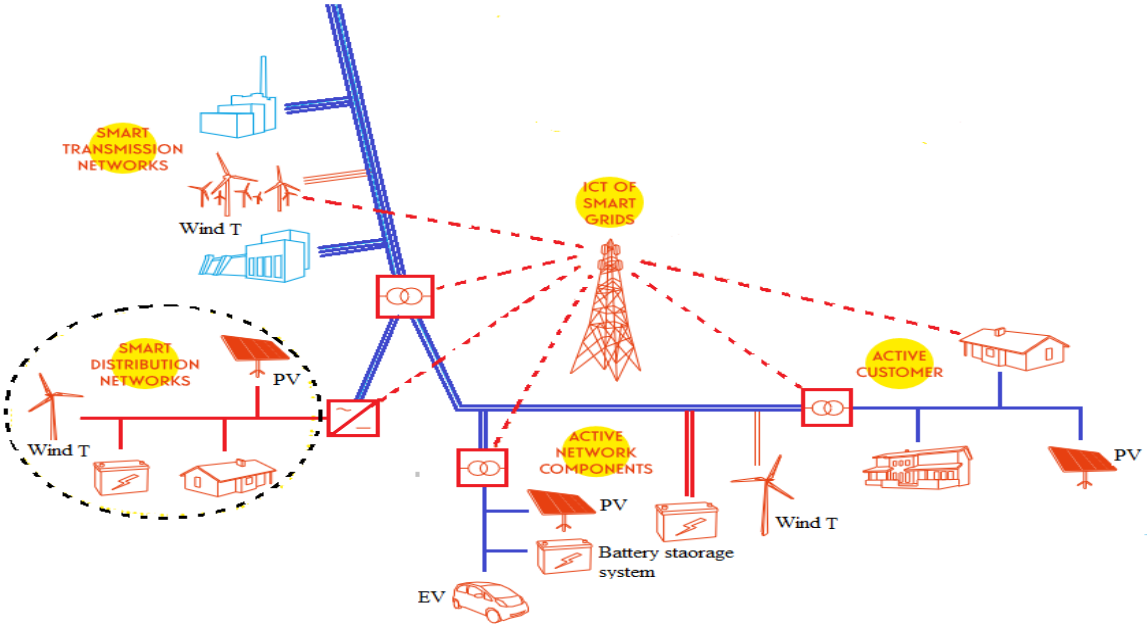

Fig. 2.14. Smart Grid Concept [88]

A smarter grid is a grid that can heal itself whenever there is an impact that can threaten the security and stability of the power network. In other words, it can be described as an active grid or self-healing grid. It will allow significant savings in energy with better interconnections and enable an active role for consumers. The drivers of the smart grid are often linked to

sustainability, renewable energy system and reducing dependence on central fossil fuel energy systems to develop more efficient and resilient systems of production and consumption. There are different perspective and understanding of a smarter grid.

According to [89]; "*The smart grid can be defined as an electric system that uses information, two-way, cyber-secure communication technologies, and computational intelligence in an integrated fashion across the entire spectrum of the energy system for the generation to end point of consumption of the electricity*".

Reference [90], also defines the smart grid as; "*The modernization of the electricity delivery system so that it monitors, protects and automatically optimizes the operation of its interconnected elements of the central and distributed generator through the high-voltage network and distribution system*".

Also, the International Electro-technical commission [91] described the smart grid as: *"Comprises everything related to the electric system in between any point of generation and any point of consumption. Through the addition of smart grid technologies, the grid becomes more flexible, interactive and is able to provide real-time feedback"*

The desire for smart grids is to re-engineer and redefine the traditional distribution network for better performance with renewable energy systems. It is seen as the next big thing in the future because of its ability to; incorporate large-scale installation and full integration of renewable energy (PV, wind, etc.) into the distribution network while maintaining reliability and better security, allow customers to play a part in optimizing the operation of the system, provide consumers with greater information and choice of supply, and reduce the environmental impact of the whole electricity supply system [91]. DG, most especially PV's are strongly connected to the idea of a smart grid and enable an active role for consumers to be actively involved in the electrical energy generation. It is well known that academia and

industry (utility) have evolved and experimented with different voltage control strategies such as OLTC, ESS, reactive power support and active power curtailment techniques over time for voltage rise mitigation with high PV penetration in the electric power system. As stated earlier, most of the developed control strategies are not self-healing when there is a sudden voltage rise situation, which is accompanied by a reverse power flow, increase losses and high transformer loading. However, few studies have incorporated smart metering, communication link and components to solve the challenges of high PV penetration in the distribution network [92] [93] [94] [95]. The incorporation of smart infrastructure in LV the distribution network can be attractive, but the cost of communication devices and infrastructure is quite expensive for LV range.

The different voltage rise mitigation strategies reviewed in this chapter will give us insight into the different control ideas and techniques to develop and improve on the voltage rise mitigation strategy that will address the instability issue caused by total disconnection of a large amount of PVs. The improve voltage rise strategy will reduce the high losses and reverse power flow caused by D-STATCOM during mitigation of voltage rise in a radial LV distribution network.

2.7 Summary

The Chapter reviews the mathematical analysis of sudden voltage rise scenario during high PV penetration on a radial LV distribution network. The analysis shows that if the voltage difference between the substation (transformer) voltage and the voltage at the PCC is greater than the upper voltage set limit, then reverse power flow will occur on the network. The chapter also identified and reviewed the different voltage rise mitigation strategies that have been employed to address the different impact issues during high PV penetration in an LV distribution network. The chapter then discusses the concept of smart grid and the need for the

combination of communication infrastructure with established control strategies such as OLTC active transformers, APC technique, and BESS. The chapter also identified some major drawbacks with the general concept of the reviewed voltage rise mitigation strategies.

Chapter 3

Grid-tied Voltage Source Inverter

In Chapter 3, the idea of DG and some standard for integration, coordination, control of DGs (PV, etc.) are discussed. The chapter also reviewed and analyzed voltage source inverter (VSI) because it is the most used interface for DG integration due to its ability to control active and reactive power independently. To develop a control strategy for voltage rise mitigation due to higher PV penetration, there is need to understand the operation, theory, and control of the VSI. The design criteria and equations of some components of grid-tied VSI such as LCL filter and phase lock loop used in the investigation of high PV penetration and methodology for voltage rise mitigation in the thesis were revised.

3.1 Distributed generation (DG)

DG which is also known as small-scale generation or embedded generation (PV system, wind turbine, etc.) is understood differently in terms of definition by researchers around the globe, for example, IEEE defines DG "*as the generation of electricity by facilities that are sufficiently smaller than central generating plants so as to allow interconnection at nearly any point in a power system"* [96] [97]. Gas Research Institute (GRI), defines DG as "*a generation between 25 W to 25MW*" [98] while reference [99], gave a more precise and direct definition of DG, as "*an electric power source connected directly to the distribution network or on the consumer side of the meter*"

The idea of DG is not new. The concept began some few decades ago, during the electrical age in the 1880's when DG technology was introduced by Thomas Edison in pearl street, Manhattan, which provided electricity to over 59 customers on the island [100]. Due to the establishment of a more unified electricity grid, which connected more load in the different section of the grid, the economic role of DG became much limited [101]. However, in the last decades, technological innovations and a changing economic and regulatory environment have resulted in renewed interest in DG [9] to increase renewable energy capacity. This has led to the establishment of different regulatory standards for integrating DGs into the power system. These regulatory standards have made it possible, for large penetration of DGs into the electrical power system. The regulatory standards are highlighted in section 3.2 of this thesis.

As a means of modernizing and strengthening electric power networks, DG sources are primarily used to increase generating adequacy of the system at micro-grids (MGs) or distribution levels [102]. As discussed earlier, the idea of DG is not new, but the approach and concept are entirely different from what they were at the beginning of the power industry. The idea is to support the existing network to improve power flow stability, backup power, improve reliability, reduce increase demand, ancillary service and reduce transmission line losses.

3.2 Standardization of Grid Integrated Systems

Today, solar PV is used as grid-connected or stand-alone systems and, to effectively coordinate the developments in the electricity sector, the IEEE, set up standard coordinating committees to develop drafts to assist with distributed generators integration into the power system [103]. The standard document is developed within the IEEE Societies and coordinating committee of the IEEE standard association (IEEE-SA) [104]. These standard IEEE documents may be superseded at any time by the issuance of new editions or may be amended from time to time. The first standard draft by the committee is IEEE 1547.1, which deals with the rules

governing the integration of distributed generation into the electrical power system. The committee also develops a standard draft IEEE 1547.3 [104], which is the guide for monitoring, information exchange, and control of distributed resources.

In 2011, IEEE adopted standard 1547.4 [105], which is the guide for design, operation, and integration of distributed resources with the electric power system. The standard provides best ways and guidelines for implementation, planning, and operation of islanded systems. To make the MG widely acceptable, IEEE 1547.7 [106] was developed to serve as a guide for DG and MG studies. To safeguard the utility grid against over-voltage and frequency issues due to distributed resources, IEEE published an amendment (IEEE standard 1547a) in 2014 which allows some flexibility in disconnection and ramping up the timing, and the use of advanced capabilities for voltage regulation support and frequency ride through. These standards deal with integration and the best ways to coordinate, control and operate DG's either as grid-connected systems or off-grid systems.

3.3 Power quality issues

Power quality is becoming an increasingly important issue to consumers, as sensitive equipment and nonlinear loads are becoming common. Power quality is also an important issue for power system utilities, as it may lead to loss of supply to customers (reducing revenue), and can also cause excessive heat in customers equipment leading to accelerated aging or component failure [107]. It is an essential impact issue for inverter-based renewable systems, most especially PV systems. For this reason, the limit for Total Harmonic Distortion (THD) of voltage and current was introduced by IEEE to improve the power quality based on the rated power of the PV.

As stated in [108], if the power rating of the inverter is not negligible with respect to the grid short-circuit power, then, the harmonic content in the injected current can have an impact on

the harmonic content of the grid voltage. According to [109], solar (PV) inverter systems typically have harmonic content of less than 1 %, because the inverters do not have protective controls such as those found in wind turbines. IEEE Standard 519 [110] recommended the limits for allowable harmonic levels for voltage at the PCC in power systems as highlighted in Table 3.1, and this standard must be followed to improve grid power quality and will be taken into consideration in the investigation of higher PV penetration on the radial LV distribution network. However, the penetration of the high PV systems in LV grid may violate the standard harmonic limit due to combine voltage harmonic generated by the grid-tied inverters, although, the individual grid-tied inverter may have complied with the grid voltage harmonic standard. Table 3.1 presents the allowable voltage distortion limit at the PCC.

Table 3.1: Voltage Distortion Limits [110]

Bus Voltage V at PCC	**Individual harmonic (%)**	**Total harmonic distortion THD (%)**
$V \leq 1.0$ kV	5.0	8.0
1 kV < $V \leq 69$ kV	3.0	5.0
69 kV < $V \leq 161$ kV	1.5	2.5
V > 161 kV	1.0	1.5[a]

"[a] *High-voltage systems can have up to 2.0% THD where the cause is an HVDC terminal whose effects will have attenuated at points in the network where future users may be connected"*

According to Table 3.1, when the voltage level is less than or equal to 1kV, the individual harmonic content shall not exceed 5% of the fundamental amplitude while the unwanted harmonic content measured by THD shall not exceed 8%. For voltage greater than 1kV and less than or equal to 69kV, the individual harmonic above the fundamental shall not be more than 3% of the fundamental amplitude, while the THD shall not exceed 5%. For voltage level greater than 69kV and less than or equal to 161kV, the individual voltage shall not exceed 1.5%, while the unwanted percentage THD shall not surpass 2.5%. These standards deal with

inverter (VSI, etc.) base DG systems such as PV, and wind turbines. In this vein, the theory of the VSI and its application as an interface are discussed in section 3.4.

3.4 Analysis of Grid-Tied VSI

According to [111], "*power electronic is said to be the study of electronic circuits intended to control the flow of electrical energy*". The birth of power electronics in the 19th century brought hope to the now enjoyed application of DG (PV system, wind turbine, etc.). It all began in 1882 when a French physicist J. Jasmine discovered a phenomenon of semi-conductance and proposed this effect to be used for rectifying. This paves the way for a series of inventions in power electronic from 1882 to 1948 before the first electronic revolution that gave birth to the invention of transistors. A notable advancement in electronic technologies today is linked to this discovery. Today, power electronic devices are rapidly expanding in the field of electrical engineering and the scope of the technology covers a wide spectrum of electronic converters [112], which is used today in grid integrated PV systems including STATCOMs and UPFCs. The development and innovations in power electronics brought so many possibilities and one of such possibility is the interface design of PV systems. Power electronic converters such as inverters are used as an interface for variable frequency power sources to the power system grid while meeting the standard requirements set by IEEE 1547 and underwriters laboratories (UL) 1741 [113].

The main function of the power electronic inverters is to deliver the maximum DG power as efficiently as possible into the external grid. Reference [37] described different power electronic topologies for PV interface with the power grid using VSI. In the different DG technologies, there have been a series of research and innovation on interface design for renewable systems. Today, almost all renewable energy sources require an inverter for grid

integration. See Fig. 3.1, which describes a complete three-phase VSI grid-connected PV system with dq PI controller.

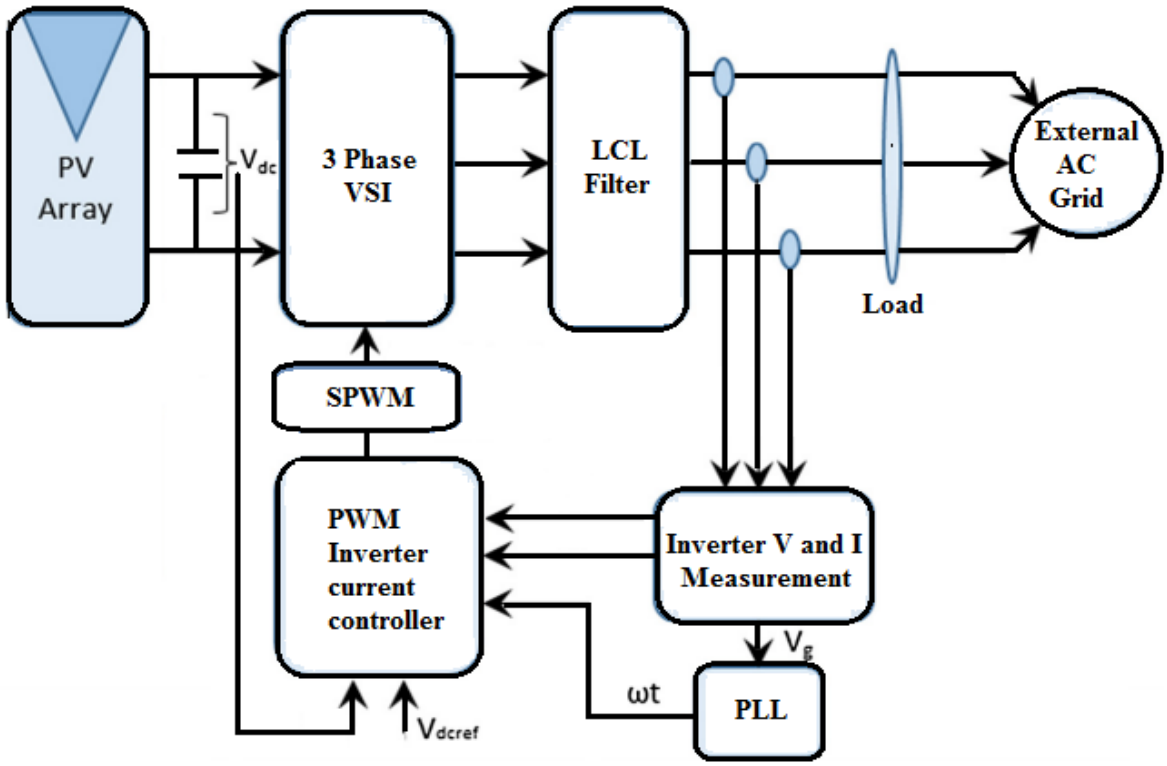

Fig. 3.1. A Complete Three-phase VSI Grid Connected PV System with dq PI Controller [114]

There are basically two main types of power electronic inverters used for grid interface with renewable power sources and, they are VSI and current source inverter (CSI). In this thesis, we will be using a three-phase VSI in our proposed topology to mitigate the voltage rise issue in a radial LV distribution network because it operates with vector control technique which allows the VSI to be flexible, and independently control its active and reactive power, making it suitable for integration into a weak AC grid. Sections 3.5 -3.9 of this thesis basically analyzed the working of a three phase-grid-connected PV system. The analysed three-phase VSI is used to investigate our proposed idea for voltage rise mitigation with high PV penetration in an LV distribution network in a MATLAB®/Simulink® environment later in this thesis. The

philosophy of the PWM current controller will be modified and used to curtail the impacts of high PV integration.

3.5 Three-Phase VSI

VSI is a power electronic device that converts fixed DC voltage into a variable frequency AC voltage by controlling the magnitude and frequency of the AC waveform. VSI's are widely used as an interface for PV systems, wind turbines, and fuel cell technology into the existing power system grid. VSI can be classified into PWM inverters, square wave inverters and single-phase inverter with voltage cancellation ability [115]. A typical three-phase, three-leg topology of VSI is shown in Fig. 3.2.

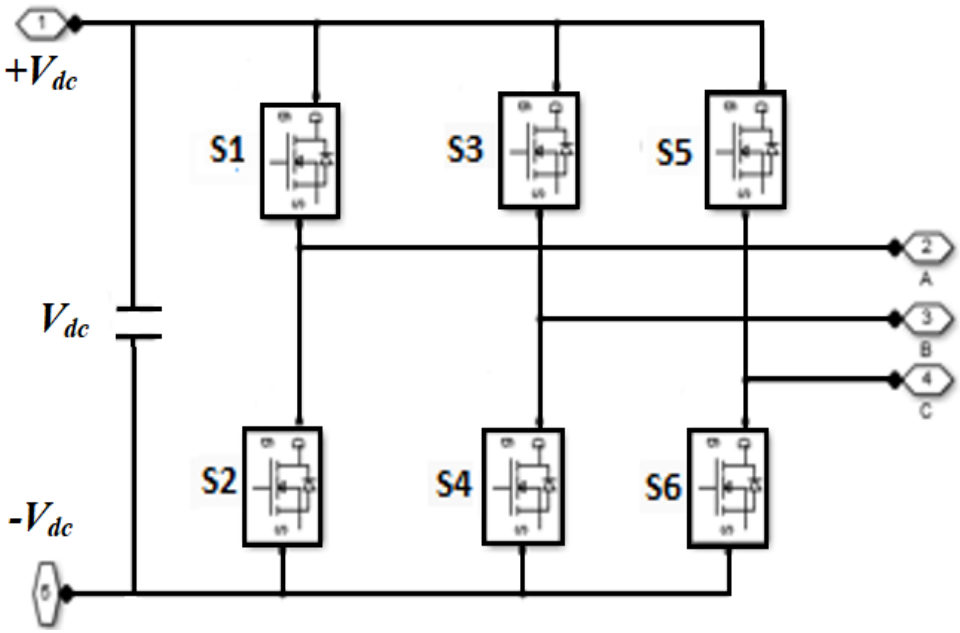

Fig. 3.2. Basic three-phase 3-leg VSI power topology

Basically, a three-phase VSI consist of six power electronic switches (IGBT's, MOSFET's, etc.) with antiparallel diodes, a DC storage capacitor across the input terminal, and an interface filter. The inverter uses the DC link capacitor voltage and the diode to rectify the line voltage, and this action is carried out using the inverter switches, and the switch type determines the

maximum switching frequency. Higher frequency of about 100 kHz can be achieved with MOSFET switches, but with the disadvantage of smaller current and voltage [116]. IGBTs are generally preferred because they have higher current carrying capacity and high switching frequency. According to [117], IGBT maximum switching frequency should be around 20 kHz with a higher power handling capacity, low power rating, and good switching speed. The VSI switching frequency for power device is described in Eqn. (3.1) [116].

$$f_{sw} = \frac{mV_m}{4hL_f}\left[1 - \frac{1}{m^2}\left(sin\theta + \frac{I_{fact}R_f}{V_m}\right)^2\right] \tag{3.1}$$

where, h is the hysteresis, L_f is interface inductance, m is modulation index, V_m is the peak AC system voltage, R_f is the filter resistance, and I_{fact} is the actual filter current and sinɵ is sin (ωt) where ω is the grid frequency.

3.5.1 Mathematical Model of a Three-phase VSI

Understanding the mathematical model of a VSI is essential because it helps us understand the control technique in the rotating (synchronous) *dq* reference frame and the nature of the VSI transfer function, which is very important in the VSI current control scheme. From Fig. 3.3, we considered the VSI connected to the power grid with the grid voltage as V_{abc}, grid current as I_{abc} and the inverter input voltage as V_{dc}, and the resistance and filter/ line inductance (L) between the VSI and the power grid. From Fig. 3.3, the voltage on the grid side is expressed in the equivalent circuit of the inverter. The analysis helps us to understand the feedback decoupling control scheme used in controlling the output of the VSI.

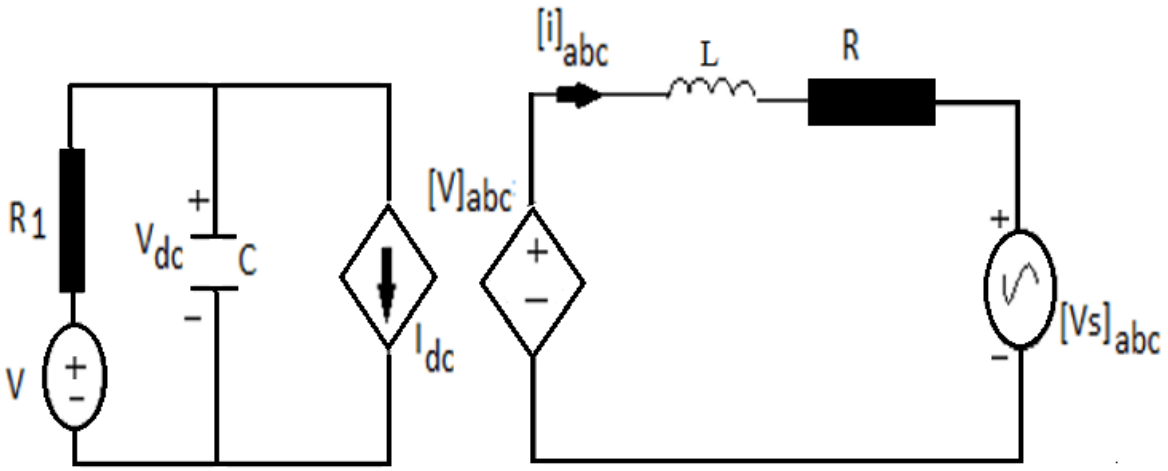

Fig. 3.3. Equivalent Circuit of VSI [118]

From the equivalent circuit, the mathematical model can be given as

$$C\,\frac{dv_{dc}}{dt} + I_{dc} = \frac{V - V_{dc}}{R_1} \tag{3.2}$$

$$L\,\frac{d[i]_{abc}}{dt} + R[i]_{abc} = \Delta[V]_{abc} \tag{3.3}$$

where,

$$\Delta\,[V]_{abc} = [V]_{abc} - [V_s]_{abc} \tag{3.4}$$

In the AC grid side of the VSI, the sum of the phase current is equal to zero as given by Eqn. (3.5):

$$i_a + i_b + i_c = 0 \tag{3.5}$$

Now, transforming the three-phase (abc) voltage and current to *d*,*q* rotating frame, we have both the current i_{abc} and voltage V_{abc} in d,q as shown in Eqn. (3.6) - Eqn. (3.9) [118].

$$i_d = \frac{2}{3}[i_a \cos \omega_1 t + i_b \cos(\omega_1 t - 120°) + i_c \cos(\omega_1 t + 120°)] \tag{3.6}$$

$$i_q = -\frac{2}{3}[i_a \sin \omega_1 t + i_b \sin(\omega_1 t - 120°) + i_c \sin(\omega_1 t + 120°)] \tag{3.7}$$

$$\Delta v_d = \frac{2}{3}[\Delta v_a \cos \omega_1 t + \Delta v_b \cos(\omega_1 t - 120°) + \Delta v_c \cos(\omega_1 t + 120°)] \quad (3.8)$$

$$\Delta v_q = \frac{2}{3}[\Delta v_a \sin \omega_1 t + \Delta v_b \sin(\omega_1 t - 120°) + \Delta v_c \sin(\omega_1 t + 120°)] \quad (3.9)$$

Differentiating Eqn. (3.6) with respect to *t*, we have [118]:

$$\frac{di_d}{dt} = \frac{2}{3}\left[\frac{di_a}{dt}\cos \omega_1 t + \frac{di_b}{dt}\cos(\omega_1 t - 120°)\right) + \frac{di_c}{dt}\cos(\omega_1 t + 120°) - \frac{2\omega_1}{3}[i_a \sin \omega_1 t + i_b \sin(\omega_1 t - 120°) + i_c \sin(\omega_1 t + 120°)] \quad (3.10)$$

Therefore, re-arranging Eqn. (3.3), we have;

$$\begin{cases} \frac{di_a}{dt} = \frac{1}{L}\Delta v_a - \frac{R}{L} i_a \\ \frac{di_b}{dt} = \frac{1}{L}\Delta v_b - \frac{R}{L} i_b \\ \frac{di_c}{dt} = \frac{1}{L}\Delta v_c - \frac{R}{L} i_c \end{cases} \quad (3.11)$$

By applying Eqn. (3.6), Eqn. (3.7), (3.8) and Eqn. (3.11), Eqn. (3.10) now become:

$$\frac{di_d}{dt} = \omega_1 i_q - \frac{R}{L} i_d - \frac{1}{L}\Delta v_d \quad (3.12)$$

If the same process is carried out with Eqns. (3.7) - (3.9) and (3.11), we have:

$$\frac{di_q}{dt} = \omega_1 i_d - \frac{R}{L} i_q - \frac{1}{L}\Delta v_q \quad (3.13)$$

Transforming Eqn. (3.12) and Eqn. (3.13) into Laplace domain (s-domain), we have;

$$(sL + R)I_d = \Delta v_d + \omega_1 L I_q \quad (3.14)$$

$$(sL + R)I_q = \Delta v_q - \omega_1 L I_d \quad (3.15)$$

Decoupling Eqn. (3.12) and Eqn. (3.13), and rearranging gives the transfer function (plant of the system) between the current I and the voltage difference of the VSI and, the grid Voltage.

Therefore, by multiplying Eqn. (3.15) with the complex number j and adding with the Eqn. (3.13) gives:

$$(sL + R)\left(I_d + jI_q\right) = \Delta V_d + j\Delta V_q + \omega_1 L(I_q - jI_d) \tag{3.16}$$

Which can be rearranged to give:

$$(sL + R + j\omega_1 L)\vec{I} = \Delta\vec{V} \tag{3.17}$$

where $\vec{I} = I_d + jI_q$, and $\Delta\vec{V} = V_d + jV_q$

$$G(s) = \frac{\vec{I}}{\Delta\vec{V}} = \frac{1}{sL+R+j\omega_1 L} \tag{3.18}$$

As shown from the mathematical model of a three-phase VSI, the plant in Eqn. (3.18) is very important because it plays a major role in the decoupling control of the d q current components as shown in Fig. 3.4 and in Eqn. (3.19) where $\Delta\vec{V}$ is the controlled voltage.

Eqn. (3.18), evaluate the coupling term ($j\omega_1 L$) used in describing the cross-coupling between d and q components. This term is compensated by the transfer function G(s) as depicted in Fig. 3.4 and used to control the active and reactive power, by independently controlling the d and q components respectively using the Proportional and Integral (PI) controllers [119]. The dq PI current control scheme which generates the SPWM signal for the switches is a function of equations of the mathematical model of the three-phase VSI.

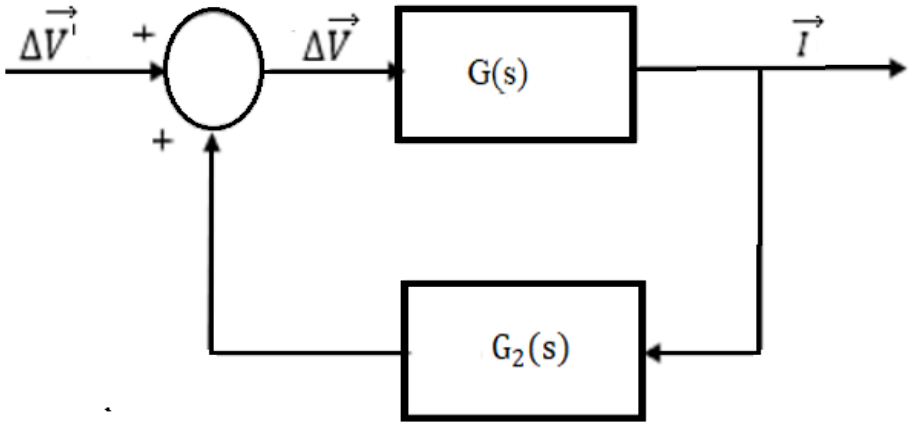

Fig 3.4. Feedback Decoupling Control Scheme

$$\Delta\vec{V} = G_2(s)\vec{I} + \overrightarrow{\Delta V'} \quad (3.19)$$

Where $\Delta V'$ is the controlled voltage from the proportional integral controller and $G_2(s)$ is the decoupling transfer function.

3.6 Sine Pulse Width Modulation (SPWM)

In this thesis, SPWM scheme is used to generate the gating signal for the three-phase VSI because it is a well-established technique and it does not require an additional component, and it generates variable voltage with a reduced number of harmonics [120]. The SPWM strategy can be used to trigger IGBT power switches of the VSI. The technique compares the sinusoidal reference (modulating signal) of the fundamental frequency to a triangular carrier signal to generate pulses at a particular switching frequency as shown in Fig 3.5. The amplitude of the sinusoidal reference wave decides the desired generated AC voltage magnitude, according to grid voltage, and the frequency of the reference wave adjusts the generated AC voltage frequency [121]. The reference signal operates at a particular switching frequency and this frequency is used to coordinate the speed at which the switches are turned on and off as shown in Fig. 3.6 and Fig. 3.7. The PWM signal is generated, when the sinusoidal reference signal is greater than the triangular carrier signal, the upper switch (S1) of the VSI is turned on

while the lower switch (S2) is turned OFF, otherwise, the upper switch (S1) is turned OFF and lower switch (S2) is turned ON as described in Table 3.2.

Table 3.2: Inverter Switch Switching Logic

Inverter Switch	**Modulating Signal Sinusoidal wave**	**Inverter Switch Logic**	
		$\mathbf{V_{Sinusoidal} > V_{Carrier}}$	$\mathbf{V_{Sinusoidal} < V_{Carrier}}$
S1	V_A	ON	OFF
S2		OFF	ON
S3	V_B	ON	OFF
S4		OFF	ON
S5	V_C	ON	OFF
S6		OFF	ON

The SPWM scheme and the duty cycle of a single switch of a VSI are presented in Fig. 3.5 and Fig. 3.6. Fig. 3.6 shows multiple numbers of pulses of different width generated from SPWM scheme of Fig. 3.5 and the width of each pulse are changing proportionally to the amplitude of the sinusoidal wave. The ratio between the amplitude of the sinusoidal reference signal and the triangular carrier signal is called the modulation index, MI. [122]. It should be noted that the modulation index is proportional (varies linearly with time) to the amplitude of the fundamental frequency of the output voltage. The gating signals depicted in Fig. 3.6 are generated by comparing the sinusoidal reference signal with the triangular carrier signals as shown in Fig. 3.5

The modulation index is given by [115].

$$MI = \frac{V_{sinusoidal\ reference}}{V_{triangular\ carrier}} \tag{3.20}$$

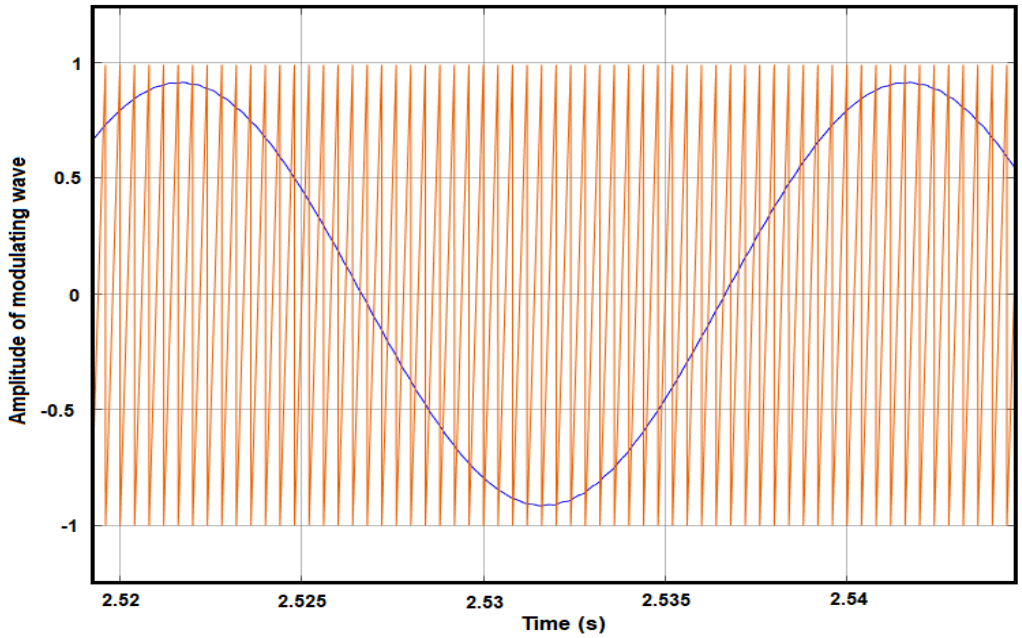

Fig. 3.5. SPWM Technique from Simulink`

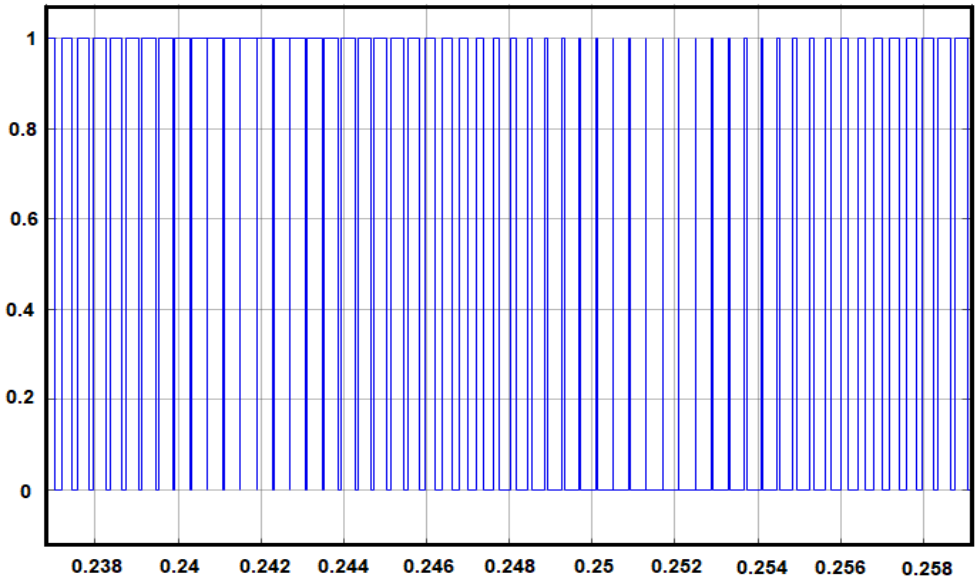

Fig. 3.6. Gating Signal from SPWM for a Switch

For a three-phase VSI, the pulses generated by SPWM for the top three switches are shown in Fig. 3.7. For the bottom switches, the phase pulses are separated by 180 degrees to avoid short circuit between the top and bottom switches of the three-phase VSI as depicted in Fig. 3.8

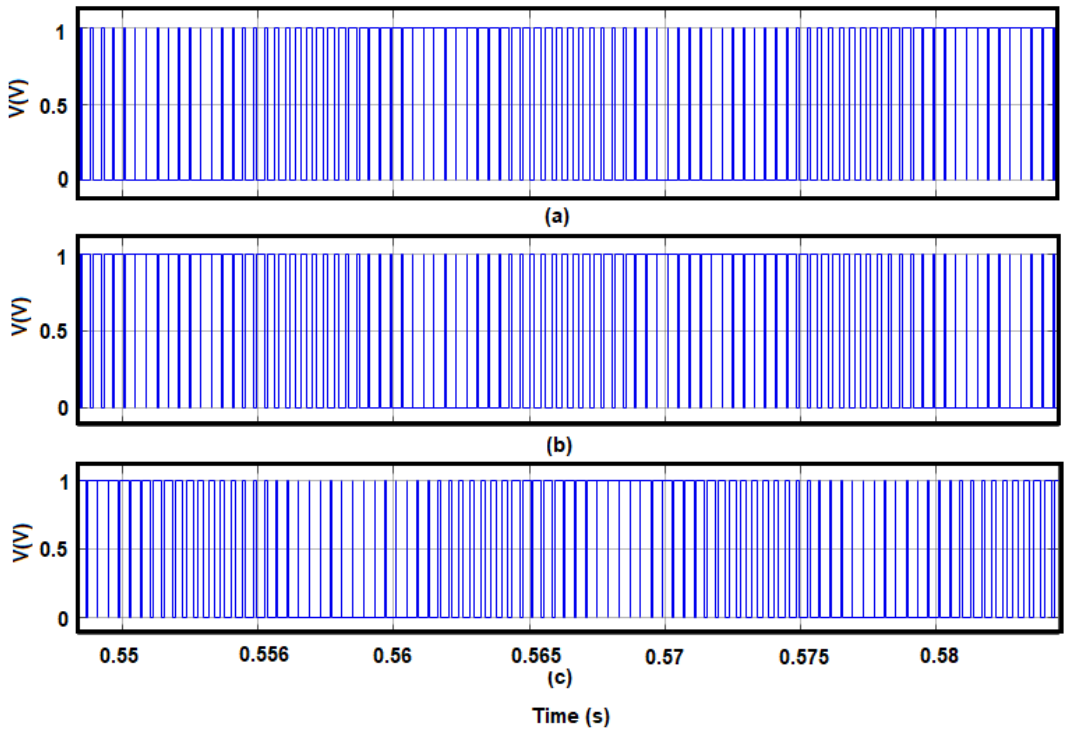

Fig. 3.7. Gating Pulses for top Three Switches of VSI Generated by SPWM in MATLAB/Simulink

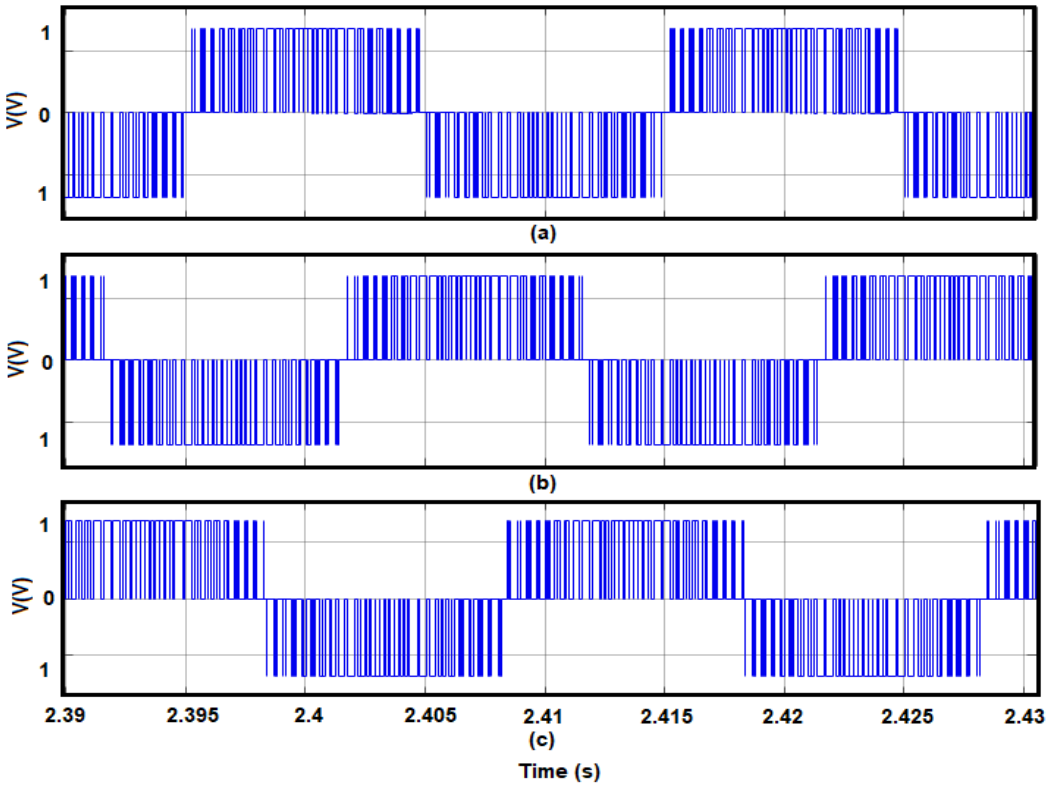

Fig. 3.8. Gating Signal from SPWM for top Three Switches of the VSI in MATLAB/Simulink (a) Phase A (b) Phase B (c) Phase C

The switches (IGBT's, MOSFET's etc.) are controlled by PWM signal to produce three-phase near sinusoidal voltage magnitude and frequency at the inverter output. The three-phase VSI operates in eight modes and the functions of each switch in the operation are depicted in Table 3.3 [123].

Table 3.3: Reference Frame dq Voltage

Mode	V_{qs}	Vds	Vos
A	0	0	$\frac{V_{dc}}{2}$
B	$\frac{V_{dc}}{3}$	$-\frac{V_{dc}}{\sqrt{3}}$	$\frac{V_{dc}}{6}$
C	$\frac{V_{dc}}{3}$	$\frac{V_{dc}}{\sqrt{3}}$	$-\frac{V_{dc}}{6}$
D	$\frac{2V_{dc}}{2}$	0	$-\frac{V_{dc}}{6}$
E	$-\frac{2V_{dc}}{2}$	0	$-\frac{V_{dc}}{6}$
F	$-\frac{V_{dc}}{3}$	$-\frac{V_{dc}}{\sqrt{3}}$	$-\frac{V_{dc}}{6}$
G	$-\frac{V_{dc}}{3}$	$\frac{V_{dc}}{\sqrt{3}}$	$-\frac{V_{dc}}{6}$
H	0	0	$-\frac{V_{dc}}{2}$

3.7. Control Scheme for VSI

The output voltage and frequency of the VSI must be synchronized with the grid frequency and voltage by a designated controller. There are basically two types of control schemes used for grid-integrated inverters. They are described as voltage and current control schemes. The current control scheme is believed to perform better because it can reach its performance indexes readily. Current control of VSI pulse width modulation (PWM) technique is the most commonly used control strategy for grid-connected PV system and over the last few years, there has been significant development of current control techniques such PI type current control technique, hysteresis current control technique, and deadbeat current control technique. To enable effective control of VSI output power, these different current control

techniques can be transformed into stationary and synchronous d-q-o rotating frame, as shown in Eqn. (3.21).

$$\begin{bmatrix} V_d \\ V_q \\ 0 \end{bmatrix} = \frac{2}{3}\begin{bmatrix} sin\,\omega t & sin\left(\omega t - \frac{2\pi}{3}\right) & sin\left(\omega t + \frac{2\pi}{3}\right) \\ cos\,\omega t & cos\left(\omega t - \frac{2\pi}{3}\right) & cos\left(\omega t + \frac{2\pi}{3}\right) \\ \frac{1}{2} & \frac{1}{2} & \frac{1}{2} \end{bmatrix}\begin{bmatrix} V_a \\ V_b \\ V_c \end{bmatrix} \tag{3.21}$$

The d-q rotating reference frame is very effective for PI current controllers due to the ability of the controllers to operate on the pseudo-stationary voltages and currents. In this thesis, the dq PI current control scheme has been selected as part of our proposed methodology for voltage rise mitigation because it is easy to implement. It can eliminate steady-state error and has a fast response when the control is decoupled. Fig. 3.9 depicts the phasor diagram for control of VSI with the dq voltage and current components, and the grid voltage and current. The dq PI controller also offers constant switching frequency, low current ripple and a well-defined harmonic content [124]. The structure of dq PI current controller is described in Fig. 3.10. The controller consists of two separate parameters known as the integral and proportional constant. The proportional constant reduces the overall errors in the control system with time while the integral constant fix small errors that cannot be reduced by the proportional constant.

Assuming that the VSI is an ideal inverter, the power transfer from the DC side to the AC side is the same, that is:

$$P_{DC} = P_{AC} \tag{3.22}$$

Active Power of Grid is then given as,

$$P_g = \frac{3}{2}\,(V_d I_d + V_q I_q) \tag{3.23}$$

The Reactive Power of Grid is given as:

$$Q_g = \frac{3}{2} (V_q I_d - V_d I_q) \quad (3.24)$$

Aligning the grid phase voltage vector with the d-axis reference frame voltage component makes the grid voltage vector to be equal to zero ($V_q = 0$), which converts the grid instantaneous active and reactive power in the LV distribution grid to Eqn. (3.25) and Eqn. (3.26) respectively [125] [126].

$$P_g = \frac{3}{2} (V_d I_d) \quad (3.25)$$

$$Q_g = -\frac{3}{2} (V_d I_q) \quad (3.26)$$

Eqn. (3.25) and Eqn. (3.26) now make it possible to independently control the active and reactive power in the AC system by regulating the d and q axis current components. In Fig. 3.10 and Eqn. (3.24), we assumed that the reactive power component is zero ($I^*_q = 0$) to make the inverter output current and grid voltage to be in phase, allowing the inverter to operate at unity power factor. Also, the active power of the inverter is maintained by controlling the active reference component (I_d^*) from the difference between the reference DC link voltage (V_{dcref}) and the measured DC link capacitor (V_{dc}). This is done by forcing the DC current component I_d of the grid to track a certain reference current I_d^* as shown in Fig. 3.10.

Fig. 3.10 shows that the outer loop provides the reference active current by constantly comparing the measured capacitor DC voltage and the reference capacitor DC voltage while the inner loop gets its reference from the outer control loop. The inner loop is made to respond faster by choosing a proper value for the PI controller which controls the modulating signal and generate the appropriate switching pulses for the VSI.

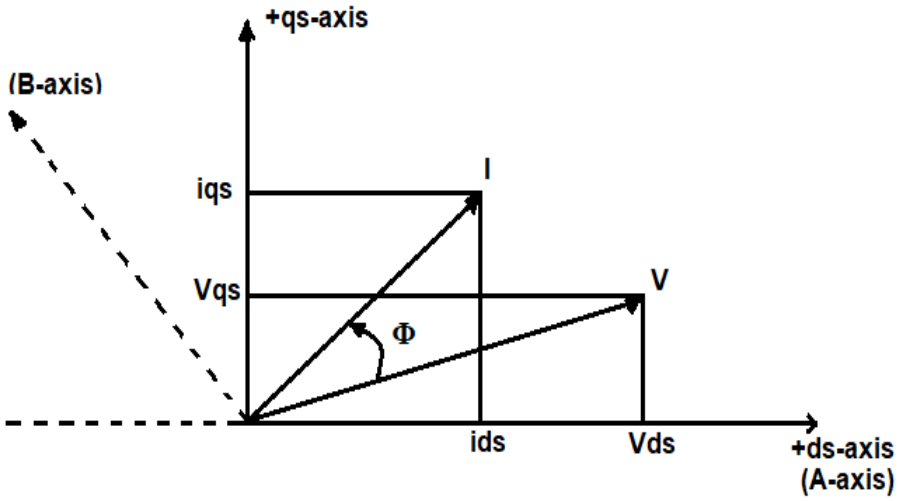

Fig. 3.9. Phase Diagram for Decouple Control System of VSI

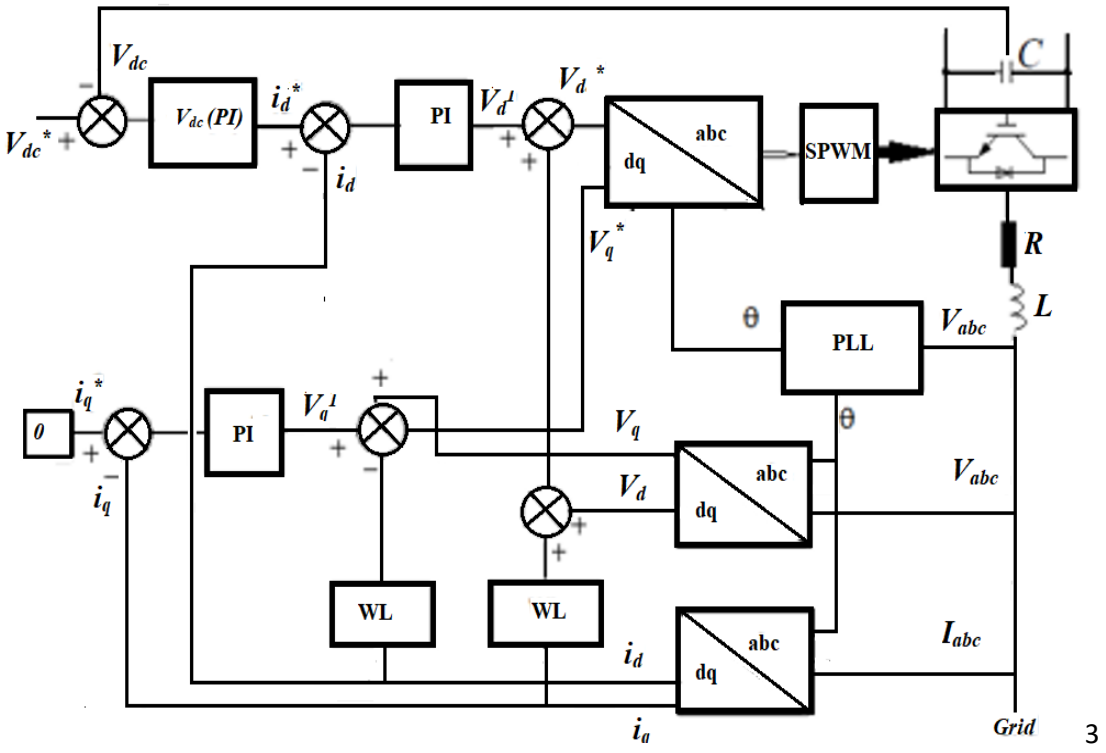

Fig. 3.10. d-q PI Current Control Method for VSI [125]

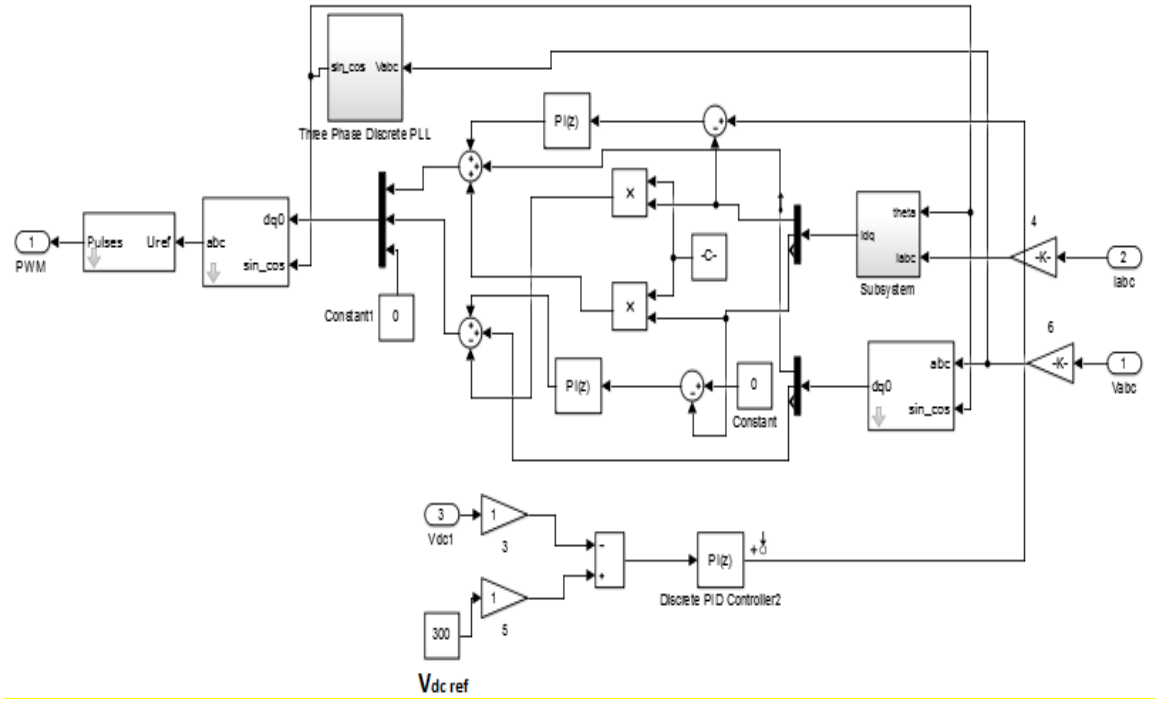

Fig. 3.11. d-q PI Current Control Method in MATLAB/Simulink

Fig 3.10 is a classical control algorithm for VSI control that is based on a nested loop dq control which usually consists of a PI controller and a DC capacitor voltage controller [127], [128]. Fig. 3.11 shows the implementation of the control scheme in the MATLAB®/Simulink® environment. The PI current controller controls both the active and reactive currents injected into the grid based on the filter and the line inductance, and resistance between the output of the inverter and the grid as shown in Fig. 3.12 and this is designed based on the system plant derived from Fig. 3.12. The plant of the system is depicted in Eqn. (3.27) while Eqn. (3.28) represent the PI controller.

The controller plant (G_C) is given as:

$$G_C = \frac{1}{R_f + sL_f} \tag{3.27}$$

where R_f is the resistance connecting the VSI line to the grid and L_f is inductance of the VSI line to the grid.

The proportional integral (PI) controller is given as:

$$PI = K_P + \frac{K_i}{s} = K_p \left(\frac{s+T_i}{s}\right) \tag{3.28}$$

where K_P is the proportional gain, *Ki* is the integral gain while $T_i = \frac{K_i}{K_p}$.

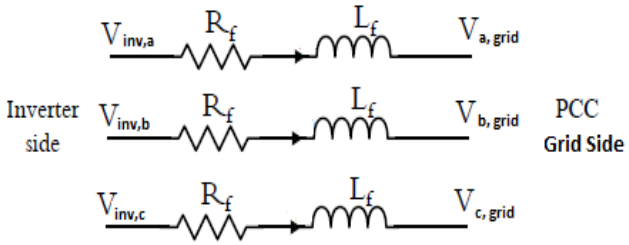

Fig 3.12. Filter Inductance and Resistance between Inverter and Grid

In many applications, the VSI is supplied by a DC voltage source and a large capacitor is used to keep the DC Link voltage within range. Usually, the VSI output voltage peak is lower than the DC link voltage value as depicted in Eqn. (3.29).

$$V_{DC} = \frac{2\sqrt{2}}{\sqrt{3}} V_{peak} \tag{3.29}$$

Eqn. (3.29), implies that in practice, the DC link voltage should meet the condition given in Eqn. (3.30):

$$V_{peak} \leq V_{DC} \leq V_{CE\ rated} \tag{3.30}$$

where $V_{CE\ rated}$ is the collector to emitter rated voltage value of the power switch.

In this research, the DC link voltage controller is designed based on Eqn. (3.31):

$$G_{DC} = \frac{V_{dc\,(s)}}{I_{gd\,(s)}} = \frac{1}{C_s} \tag{3.31}$$

where C_s is the DC link capacitance measured in microfarad (μf), V_{dc} is capacitor voltage, I_{gd} is the grid d component and G_{DC} is the transfer function of the DC Link of the plant.

3.8. Phase Lock Loop (PLL) Selection and Design of PI controller

Grid synchronization is the most important aspect of grid-connected DG systems. The output of a grid-tied VSI must provide a stable, sinusoidal AC waveform that is in phase with the grid voltage and frequency, according to utility standards. Small phase error in phase angle estimation can lead to incorrect operation of the grid-tied VSI output voltage, and current. This can cause load imbalances, instability in the grid, and damage to customer's equipment. Therefore, to prevent the issue of the phase error, a PLL is used. In general, the PLL synchronizes the output signal with a reference signal in frequency and in phase [129].

A well designed PLL can provide quick and precise synchronization information with a high degree of sensitivity to disturbance, harmonics, sags/swells, unbalances and distortion in the input signal [130]. The main types of the synchronization algorithm used for phase tracking are the stationary reference frame, synchronous rotating reference frame (SRF) based PLL and zero crossing [131]. According to [124], zero crossing synchronization algorithm is affected by higher order harmonic noise, and it also has low dynamics. The commonly implemented PLL for grid synchronization is the dq-PLL in the dq-synchronous rotating reference frame (SRF) [132], as depicted in Fig. 3.13.

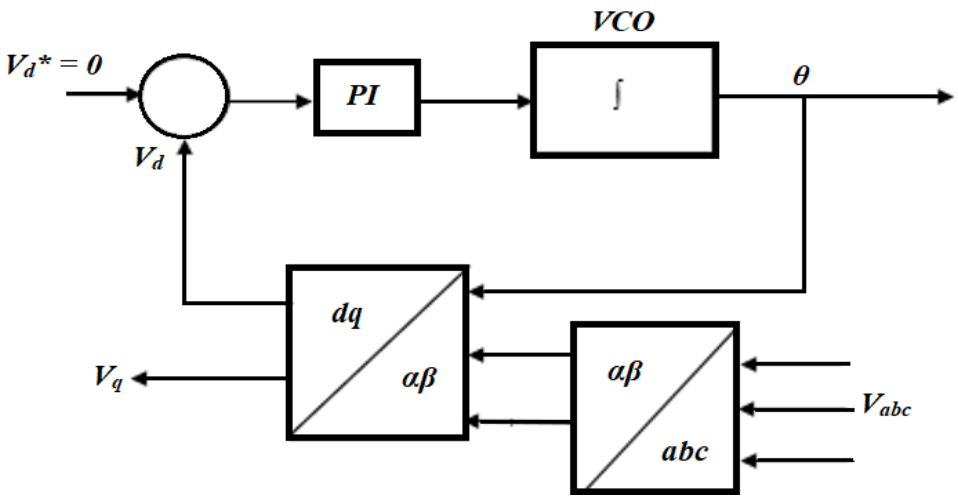

Fig. 3.13. General d-q PLL block diagram for three-phase [132]

The *dq*-PLL consists of a proportional-integral (PI) controller that determines the dynamic of the PLL and the low pass filter. The concept of the PLL is tracking of the phase angle using a feedback and a PI-regulator low pass filter to suppress high-frequency component and provide a DC control signal to the voltage-controlled oscillator (VCO), to obtain the VSI phase angle Ɵ which is then compared with the grid phase angle [133]. If the difference between the grid phase angle and the low pass filter PI output phase angle is zero, then the PLL becomes active and gives the magnitude of the grid voltage.

In this thesis, a dq-synchronous rotating reference frame (SRF) PLL was selected, designed and implemented in MATLAB®/Simulink® in chapter four and it is then used in the proposed voltage rise mitigation strategy. The SRF-PLL is designed using Eqn. (3.32) – Eqn. (3.39) to determine the parameters of the system.

Taking the time delay effect into consideration, the sample plant transfer function will be given as [134]:

$$G_{plant} = \left(\frac{1}{1+sT_S}\right)\left(\frac{1}{s}\right) \tag{3.32}$$

Therefore, the open loop transfer function of the SRF PLL G_{ol} is given as [131]

$$G_{ol} = (K_p \frac{1+s\tau}{s\tau})(\frac{1}{1+T_s})(\frac{V_m}{s}) \tag{3.33}$$

where K_p, and K_i are the PI controller gain, $\tau = \frac{K_i}{K_p}$, T_s is the sampling time and V_m is the grid RMS voltage

For the close loop (G_{cl}), the transfer function is [131]:

$$G_{cl} = \left(\frac{G_{ol}}{1+G_{ol}}\right) \tag{3.34}$$

Using the integral element in the plant, PI regulator is transferred from s-domain Eqn. (3.35) to z-domain Eqn. (3.36) [131] and is used in our discrete simulation in MATLAB®/Simulink®

$$G_{PI} = (K_p \frac{1+s\tau}{s\tau}) \tag{3.35}$$

$$G_{PI} = K_p \left(\frac{\frac{T_s}{\tau} + z-1}{z-1}\right) \tag{3.36}$$

The proportional gain, K_p, integral gain K_i and τ which is $\frac{K_i}{K_p}$, of the PI controller, are designed using the symmetrical optimum (SO) method. In the analysis, the symmetrical optimum transfer function (F_{SO}) optimizes the maximum value of its phase margin to a given crossover frequency as given in Eqn. (3.37) and this equation is compared with the open loop transfer function, given in Eqn. (3.38). The Bode plot of the transfer function will be symmetrical around the crossover frequency. The PI controller gains are derived from the comparison of Eqn. (3.37) and Eqn. (3.38). This gives the PI controller gains and other parameters as shown in Eqn. (3.39) for the system.

$$F_{SO} = \frac{{\omega_o}^2}{s^2}(\frac{ks+\omega_o}{s+k\omega_o}) \tag{3.37}$$

where *k* is a constant and will be symmetrical around the crossover frequency, $\omega = \omega_o$

$$G_{oL} = (K_p \frac{1+s\tau}{s\tau})(\frac{1}{1+T_s})(\frac{V_m}{s}) = \frac{K_p V_m}{aT_s}\frac{(as+\frac{a}{\tau})}{s^2(s+\frac{1}{T_s})} \tag{3.38}$$

The normalization factor *a*, in Eqn. (3.38), sample time T_s, proportional gain K_p, integral gain K_i, time constant $\tau = \frac{K_i}{K_p}$, grid RMS voltage (V_m), and crossover frequency (ω_c) are related as given in Eqn. (3.39) [134] and are calculated using the grid RMS voltage, crossover frequency ($\omega_c = 2\pi f_o$) and the sampling time (T_s). These equations are used to design to SRF-PLL which was employed in our investigation in Chapter 4 of this thesis.

$$\begin{cases} \omega_c = \frac{1}{aT_s} \\ \tau = a^2 T_s \\ K_p = \frac{1}{aV_m T_s} \end{cases} \quad (3.39)$$

3.9 Inductor Capacitor Inductor (LCL) Filter Specification and Design Equations

Maintaining power quality in the power system network is very important, especially on the LV network with the integration of DG like PV system. However, Voltage/current harmonic problem is one of the power quality issues associated with PV systems because of the power electronic interface such as VSI. According to [135] [136], power electronic devices generate harmonics that can damage capacitor, affect the electromagnetic environment and other grid components. Harmonic injection by renewable generators also depends on the designed specification and characteristic of these generators interfaces (converter) as revealed by the authors in [137]. Due to the impact of decentralized generator interface on grid harmonics, IEEE Std 519 was established to limit harmonic voltage and current injected into the power system. Due to the harmonic distortion problems caused by power converters on the power grid, harmonic filters such as L filter, LC filters, and LCL filters are designed to suppress these harmonics within the IEEE Std 519 standard limit. A poorly designed filter can increase distortion in the system.

In this thesis, LCL filter was selected and designed because it produces better attenuation (-60dB/decade) at frequencies more than resonance frequency and can produce low current distortion, low reactive power production and low switching frequency for giving attenuation than L and LC filter [138]. The designed procedure and equations used in our simulations are derived from [138] [139] [140] and are given in Eqn. (3.40) – Eqn. (3.47).

In designing the LCL filter, the inductance of the inductor should not be made to be too small due to high harmonic current and short circuit current but should be determined between 10%-20% of the rated current [141]. In our analysis, a 10% ripple current of the rated maximum current is selected and used for the design and it is given as:

$$\Delta I_{max} = 0.1 I_{max} \tag{3.40}$$

Where the maximum rated current is expressed as in Eqn. (3.41). In addition, the maximum output current should not exceed the maximum current rating of the inverter.

$$I_{max} = \frac{P_{n\sqrt{2}}}{3V_p} \tag{3.41}$$

where P_n is the inverter nominal power, V_p is the grid phase voltage (RMS).

The base grid Line impedance Z_b is given as:

$$Z_b = \frac{V_b^2}{P_n} \tag{3.42}$$

where V_b is the base voltage.

The filter capacitor C_f required for the LCL filter is 5% of the maximum filter capacitance, which is given as:

$$C_f = 0.05 * \frac{1}{(2*\pi*F_g)*Z_b} \tag{3.43}$$

where C_f is the filter capacitor and F_g is the grid fundamental frequency

The parameters considered in the LCL filter design are power rating of the inverter (P_n), switching frequency (F_{sw}), Line to line voltage (RMS) (V_L), grid (fundamental) frequency (F_g).

The inverter side inductance L_1 is calculated based on the percentage ripple of the rated current ΔI_{max}, VSI switching frequency (F_{sw}) and the capacitor voltage (V_{DC}) as given in Eqn. (3.44) [125] [138].

$$L_1 = \frac{V_{DC}}{8*\Delta I_{max}*F_{sw}} \tag{3.44}$$

The grid side inductance is calculated using:

$$L_g = \frac{\sqrt{\frac{1}{K_a{}^2}+1}}{C_f + W_{sw}{}^2} \tag{3.45}$$

where K_a is the desired attenuation factor, W_{sw} *(2 *π* F_{sw})* is the angular switching frequency.

The resonance frequency of the LCL filter is given by the Eqn. (3.46):

$$f_{res} = \frac{1}{2\pi}\sqrt{\frac{L_1+L_g}{L_1 L_g C_f}} \tag{3.46}$$

The resonance frequency, f_{res} of the designed filter must satisfy this condition:

$$10F_g \leq f_{res} \leq 0.5F_{sw} \tag{3.47}$$

The Eqn. (3.40) to Eqn. (3.47) were used to design an LCL filter for a 3kVA inverter in our investigations as will be seen in Chapter 4 of his thesis. The VSI, LCL filter and the PLL make up the DG integration into the power system network. These components will be designed and model to investigate the issues of voltage rise in this thesis.

3.10. Summary

The chapter starts with a brief history of DG and the concept in power system. The Chapter also highlighted in the standard guide for successful implementation, control, and integration of DG. The guideline for harmonic injection by DG inverters was also highlighted in this chapter. The theory and concept of the PI control scheme with the phasor diagram for decouple control of a VSI were also introduced in this section. PI control VSI is one of the most used interfaces for DG integration and will play a major part in our proposed voltage rise mitigation strategy. The analysis and design equations for LCL filter and SRF PLL were revised. The

scope of this chapter is limited to the analysis and design of key components of grid-tied VSI that will be useful in our proposed voltage rise mitigation strategy.

Chapter 4

Modelling and Simulation of High PV Penetration in LV Distribution Network

In Chapter 4, a comprehensive dynamic and steady-state impact assessment was carried out on a radial LV distribution network with higher PV penetration using DigSILENT power-factory® simulator software and MATLAB/Simulink software. The investigation was carried out to access the potential impact of the high PV penetration on the sudden voltage rise, transformer loading, increase line losses, and reverse power flow on a radial LV distribution network. The investigation gave us a comprehensive knowledge of how these issues affect the behaviour of the LV distribution network negatively. The dynamic investigation was done in MATLAB®/Simulink® environment with a designed three-phase VSI as an interface, and a dq synchronous reference frame PLL (SRF PLL). The Chapter also presents the designed parameters of the LCL filter used to reduce the harmonics in the LV distribution network during high PV array penetration.

4.1 Fundamental Theories of Load Flow Techniques in Distribution Network

Load flow analysis is an important numerical tool for power system planning and design. Over the years, researchers have developed different load flow algorithms such as Gauss-Seidel, Newton-Raphson, and fast decoupled load flow methods. These conventional load flow methods have been developed around transmission network and cannot meet the

robustness in the distribution network. The distribution network has multiphase and unbalance operation, many branches and node, very low impedance, voltage regulator, switches, elbows, and jumpers. In distribution network, many branches have very low impedances and these low impedances are ignored and set to zero in conventional methods. This action made the admittance approach applicable and to use this approach, the conventional methods arbitrarily assigned small non-zero impedances to the branches. This action makes the analysis ill-conditioned and difficult to converge [142]. The conventional methods are not suitable for the distribution network as more distributed energy resources (DERs) are coming online. Due to the challenges of conventional methods on the distribution network, different Load flow methods for distribution network have been developed [143] [144] [145]. In this thesis, DigSILENT power-factory software is used for the investigation of high PV penetration in a radial LV distribution network as shown in Fig 4.1. The power system tool provides a range of load flow calculation methods, including enhanced non-decoupled Newton Raphson solution and a linear DC method. The techniques exhibit excellent stability and convergence under all condition with optional relaxation and modification of constraints.

4.2. Impact Studies of High PV Penetration on Distribution Network

The negative impacts of high PV penetration on the LV distribution network have led researchers to develop analytical tools for investigating the high PV penetration so as to develop mitigation measures [146], [147], [10], [8]. The different impacts vary in severity as a function of the degree of penetration and location of PV system [7]. The voltage and system stability are also issues that are worrisome to network operators due to power fluctuation caused by intermittent radiation. The impact of voltage rise has driven research by academia, utility and the industry to focus on how these effects can be controlled to accommodate and facilitate the integration benefits and achieve the required voltage levels and stability of the distribution network [18] [148] [149]. Due to this reason and many more, the power system

network is guided by some technical regulation to maintain voltage within a certain range which is determined by each country [150]. In this thesis, we investigated the impact of the high PV penetration on a radial LV distribution network using DigSILENT Power-factory and MATLAB/Simulink environment in sections 4.3 to 4.5 to get a better understanding of the steady and dynamic nature of high PV penetration on voltage rise issues.

4.3 Simulation in DigSILENT Power-factory® Environment

Digital simulation of an electrical network (DigSILENT) power-factory is a computer-supported engineering tool for the analysis of transmission, distribution, and industrial electrical power system [151]. The engineering tool is an advanced integrated and interactive software package dedicated to the electrical power system. DigSILENT is a very powerful tool and results obtained from this simulation tool is valid and accurate and has been confirmed in many implementations by organizations involved in power system throughout the world [151]. The simulation tool provides a comprehensive suite of power system analysis function within a single executable program. The key features of the tool include

- ✓ Power system element and base case database
- ✓ Generic interface for computer-based mapping systems
- ✓ Power system network configuration with interactive or on-line SCADA access
- ✓ Integrated interactive single line graphic and data case handling
- ✓ Integrated calculation functions

The simulation tool can easily execute all power simulation functions such as short circuit analysis, load flow analysis, harmonic analysis, protection coordination, modal analysis, and stability calculation within a single program environment. The simulation tool will be used to model and simulate a radial LV distribution network in our investigation as will be seen in section 4.3.1.

4.3.1 Modelling and Simulation of High PV Penetration Level on LV Grid using *DigSILENT Power-factory*®

The power grid under investigation is a simplified 16-bus LV radial network as shown in Fig 4.1. It has a 270kW of PV systems, distributed within the network and was used to examine how high PV can perturb the assumptions on the operation of the traditional LV network. The investigated radial LV network consists of a lumped peak load of 26.4 kVA with a power factor of 0.95 situated at the end of the network. The radial LV distribution network parameters are listed in Table 4.1. Table 4.2 depicts, the distribution of PV arrays over different buses in the LV distribution network.

The length of the network is 1.4 km with a distance of 100m between terminals with 5 kW PV systems distributed across the distribution network. In the LV distribution network, different PV penetration level was carried out to ascertain the negative impact on the network. The PV inverter is assumed to operate at unity power factor. The results of the investigation are presented below from Fig. 4.2 to Fig. 4.6. Fig. 4.2 shows the voltage profile of the distribution network without PV penetration while Fig. 4.3, Fig. 4.4, Fig. 4.5 and Fig. 4.6 shows the impact of high PV penetration on the voltage profile, transformer loading, line losses and reverse power flow respectively.

Table 4.1: Parameters of the LV Network used in DigSILENT Power-factory

S/n	**LV Distribution Network Parameter**	
1	Line Voltage (V)	400
2	Line Impedance (R + jX) Ω/km	(1.652 + j1.2)
3	Line Length (km)	1.4
4	Transformer Capacity (kVA)	75 kVA
5	Lump Load (kVA)	26.4
6	Load Power Factor	0.95
7	PV Array Capacity	$5kW_p$

Table 4.2. PV Array Capacity in the LV Distribution Network

Bus Number	**PV Array Capacities (kW)**
1	0
2	0
3	10
4	20
5	20
6	20
7	20
8	20
9	20
10	20
11	20
12	20
13	20
14	20
15	20
16	20
Total	**270**

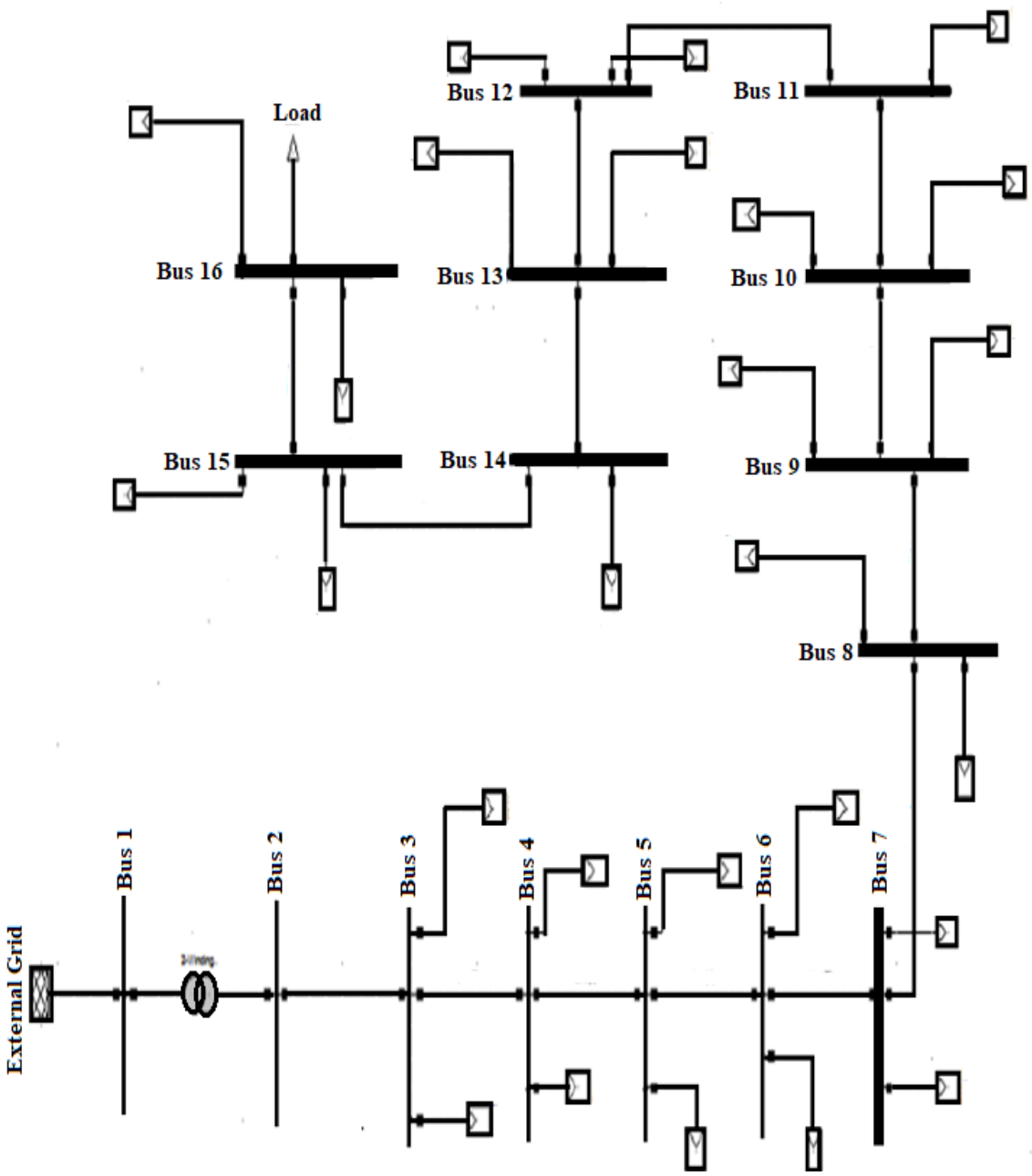

Fig. 4.1. LV Distribution Network with High PV Penetration

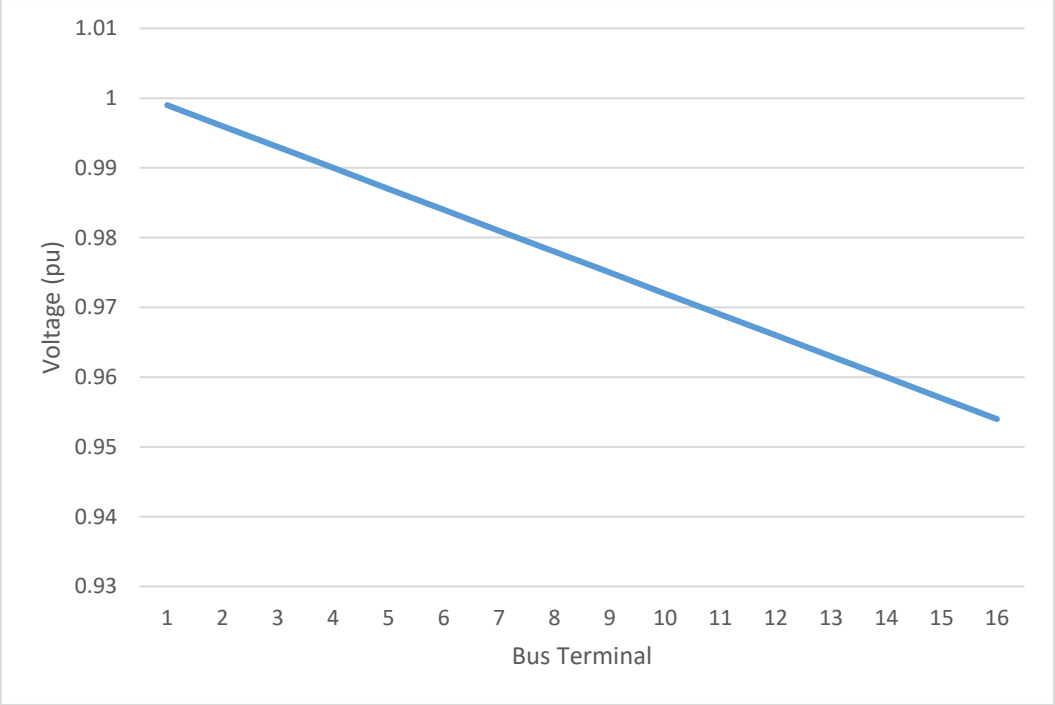

Fig 4.2. Voltage Profile without PV

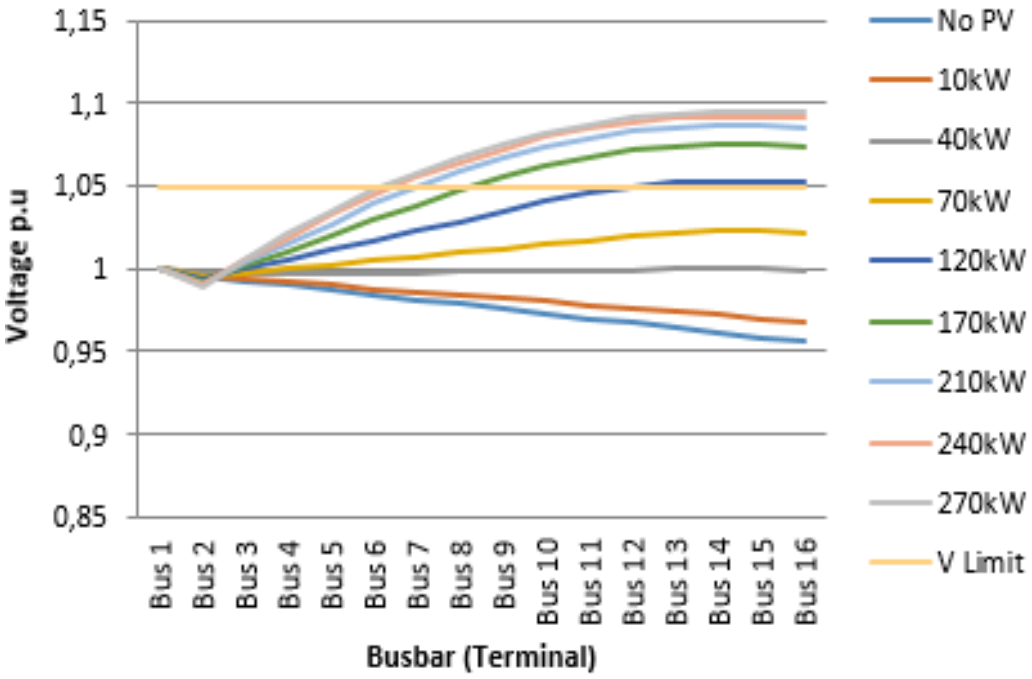

Fig. 4.3. High PV Penetration effect on Voltage Profile

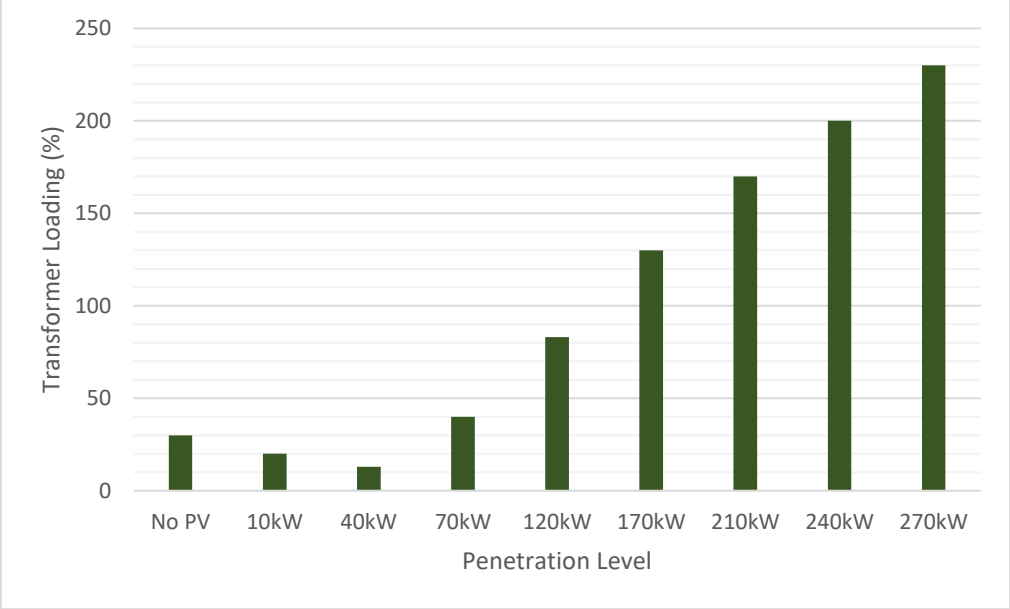

Fig. 4.4. High PV Impact on Transformer Loading

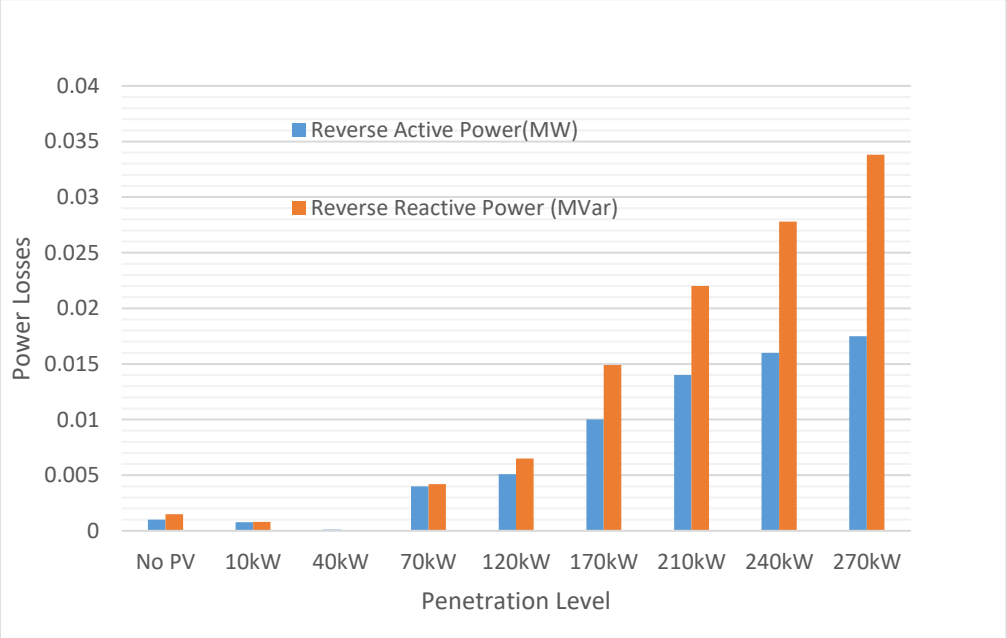

Fig. 4.5. High PV Impact on Power Losses

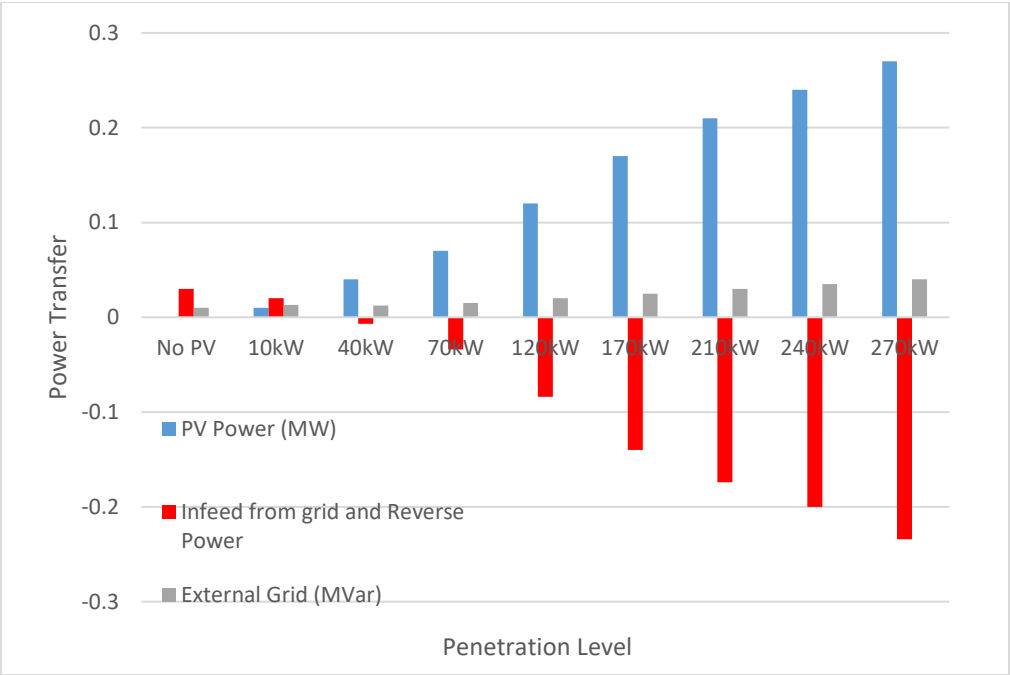

Fig. 4.6. High PV Impact on Power Flow

4.4 Discussions of Simulation Results

From Fig 4.2, it is observed that the voltage profile of the network is maintained within the acceptable voltage range (±5%) without PV penetration. Fig. 4.3 shows how high PV penetration on the LV distribution network can modify the network voltage profile and this may lead to a temporary high voltage at the end of a long LV distribution network line. This affects the acceptable voltage level and may violate utility planning limits and industrially acceptable standard. One of the main issues of high PV penetration on the LV distribution network is sudden voltage rise, which can lead to reverse power flow from the downstream of the network to the upstream (sub-Station transformer) and this condition can affect the transformer loading (rated power) and conductor ratings as shown in Fig 4.4. Fig. 4.4 shows that without PV penetration, the external grid powers the network load. In this case the transformer loading is 30% but when a 10 kW PV array was introduced the transformer loading reduced to 20% because the PV array supplies 10kW to the load. The transformer loading was further reduced to 12% due to reverse power when 40 kW of PV array was integrated.

According to [152], a PV power penetration of 150% (1.5 times) of the rated power of the transformer may either lead to overheating or unacceptable ageing of the distribution transformer. Therefore, from our investigation, the penetration of over 210 kW PV power may lead to overloading of end cable termination, overheating and unacceptable ageing of the transformer because the transformer loading is over 150%. It may also affect over-current protection coordination and line voltage regulators

It is observed in Fig 4.5 that high PV penetration can modify the current of the network which in turn increases losses along the line. Fig. 4.6 shows how the high penetration level of PV can affect the direction of power flow, that is, from the downstream of the network to the upstream (sub-Station transformer).

4.5 Modelling and Simulation in MATLAB®/Simulink® Environment

MATLAB® which means MATrix LABoratory is an advanced mathematical software which is extensively used by academia and industry because it can solve numerical computations and data visualization using highly respected algorithms with valid and trusted results. It provides a Simulink environment for application in all areas of science and engineering.

Simulink which is a tool in MATLAB® offers users the privilege to simulate, and design model based dynamic, non-linear dynamic systems, controller, plant, and embedded systems. It is integrated with MATLAB®, and it enables one to incorporate MATLAB® algorithms into models and export simulation results for further analysis [153].

Key Features of Simulink are listed as follows [153]:

- ✓ "*Graphical editor for building and managing hierarchical block diagrams*
- ✓ *Libraries of predefined blocks for modeling continuous-time and discrete-time systems*
- ✓ *Simulation engine with fixed-step and variable-step ODE solvers*

- ✓ *Scopes and data displays for viewing simulation results*
- ✓ *Project and data management tools for managing model files and data*
- ✓ *Model analysis tools for refining model architecture and increasing simulation speed*
- ✓ *MATLAB® Function block for importing MATLAB® algorithms into models*"

Simulink® is a powerful software, and it offers the opportunity to design and model, and understand the dynamic behaviour of the VSI, PI PWM current controller in the LV distribution network, under a high PV penetration.

4.5.1 Modelling and Simulation of High PV Penetration on LV Distribution Network using MATLAB®/Simulink® Environment

In this section, we have investigated the impact of high PV penetration on voltage rise, voltage harmonics, using a designed VSI, PLL, LCL filter and PI current control for PWM pattern so as to get a better understanding of the dynamic behaviour of the LV network. In this investigation, we designed and modelled a Synchronous Reference Frame- Phase Lock Loop (SRF PLL) to synchronize the output of the 3kVA VSI with the grid. Also, an LCL filter for a 3kVA VSI was designed and modelled in the MATLAB®/Simulink® Environment to reduce the injected voltage harmonic content in our system.

4.5.2. Design and Modelling of *dq* SRF PLL for 3kVA VSI Inverter

The *dq*-SRF PLL is designed using the Eqn. (3.30) – Eqn. (3.36) [131] in chapter 3. The designed parameters of the PI controller gains of the *dq*-SRF PLL were determined by the Symmetrical Optimum (SO) method. The key parameters used for determining the PI gain are listed in Table 4.3. Fig 4.7 shows the designed dq-SRF PLL with parameters in MATLAB®/Simulink®.

Table 4.3: Key Factors used in Determining PI Controller Gain

RMS Value of grid line to line Voltage	125 V
Amplitude voltage level, V_m	102.06 V
Grid Frequency, f_g	50Hz
Sampling Time	$5*10^{-4}$sec

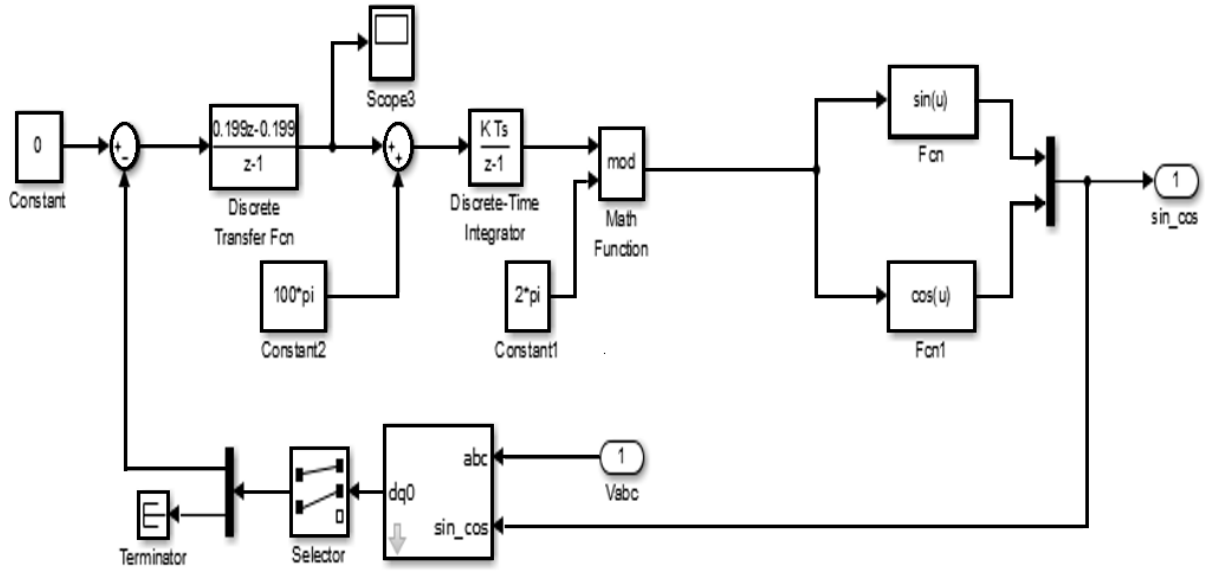

Fig 4.7. *dq*-SRF PLL Designed and Implemented in MATLAB/Simulink

Using the open loop transfer function in Eqn. (3.36) in chapter 3 gives the discrete PI controller gains, and Eqn. (3.38) gives the normalisation factor as shown in Table 4.4.

Table 4.4: Normalisation Factor and the Discrete PI Controller Gain for the SRF-PLL

Normalisation factor, a	Proportional gain, K_p	Integral gain, τ
6.365	3.0828	0.0624

Using these sets of values in Table 4.3 gave the system open loop transfer function in continuous time of the SRF PLL as:

$$G_{OL} = \frac{6.293*10^5\, s + 3.107*10^7}{s^3 + 2000\, s^2} \tag{4.1}$$

The open-loop Bode plot of the system gives a symmetrical shape, and the phase margin is about 72 degrees at the crossover frequency (314rad/s) as shown in Fig 4.8 while the Bode plot

of the closed-loop system shown in Fig 4.9 exhibit the characteristics of a low pass filter. The designed PLL will be used to handle any unbalance non-ideal conditions, harmonics and synchronize our designed VSI with the grid during high PV penetration.

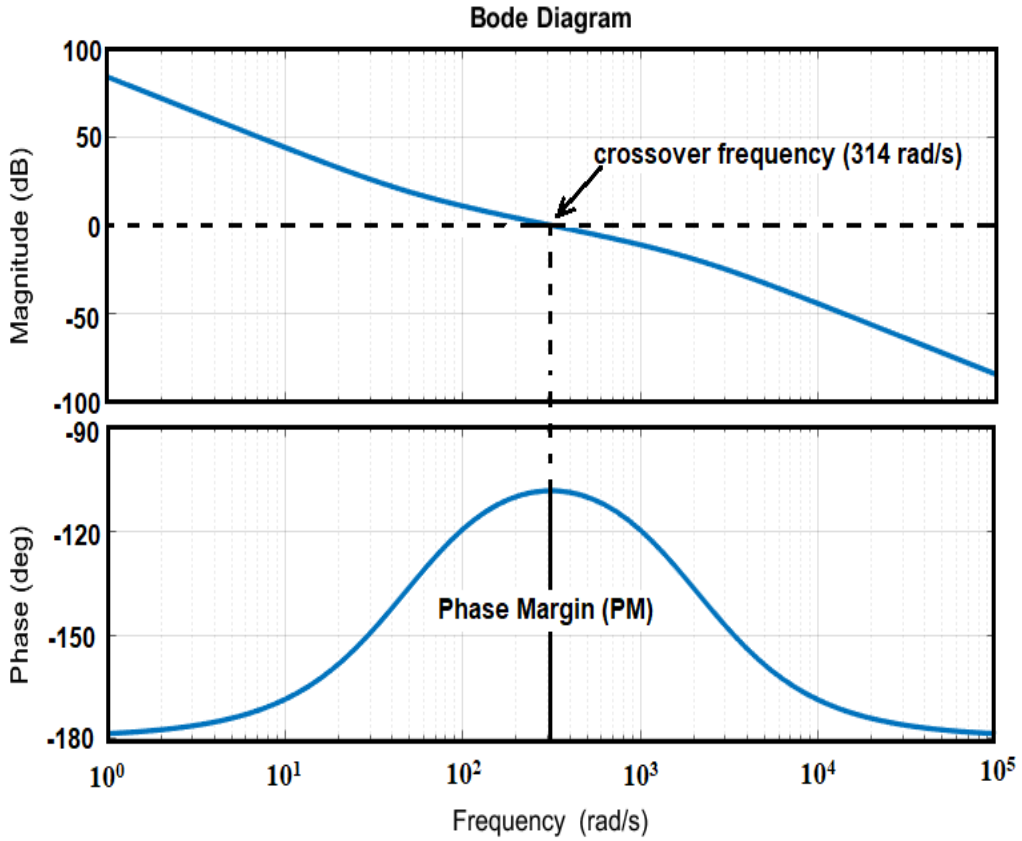

Fig 4.8. Bode Plot of the Open Loop SRF PLL System Characteristic

The closed-loop transfer function G_{CL} of the system in continuous time is calculated using Eqn. (3.32) and it is shown in Eqn. (4.2). See appendix A.1 for the derivation of the closed-loop transfer function.

$$G_{CL} = \frac{6.293*10^5 s + 3.107*10^7}{s^3 + 2000s^2 + 6.293*10^5 s + 3.107*10^7} \tag{4.2}$$

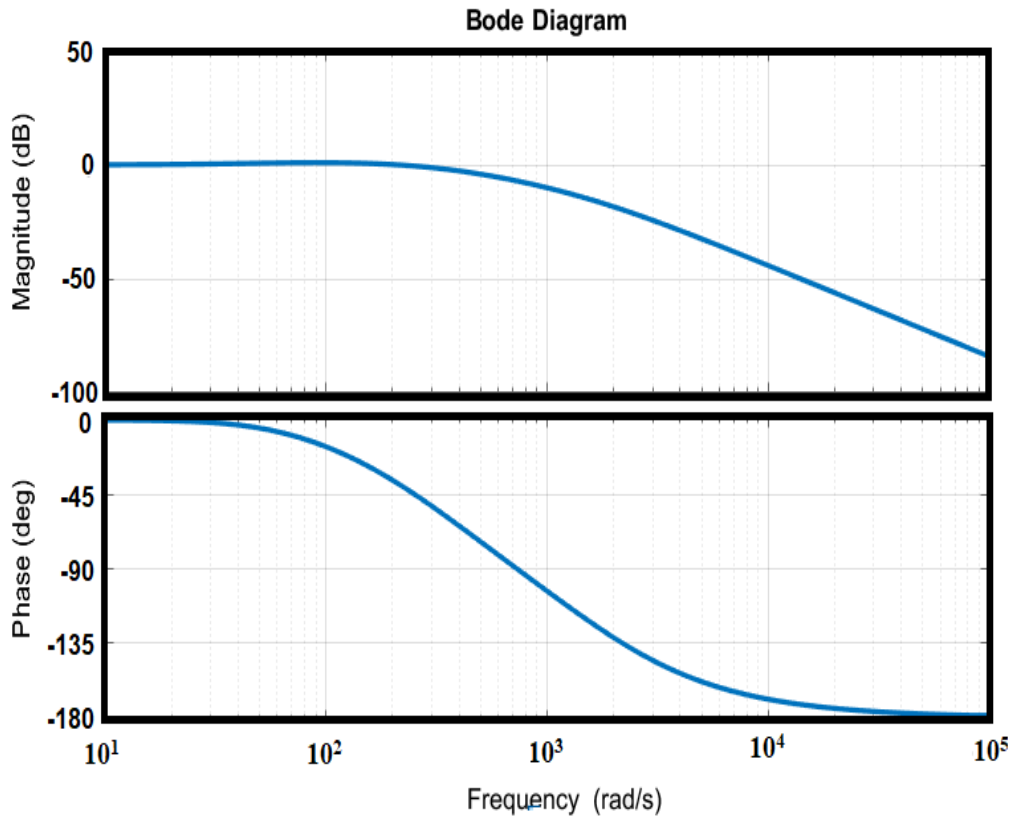

Fig 4.9. Bode Plot of the Closed Loop SRF PLL System

4.5.3 Design and Simulation of LCL Filter for 3kVA VSI in MATLAB®/Simulink®

In this section, Eqn. (3.38) – (3.45) were used to design an LCL filter which is simulated in the MATLAB®/Simulink® environment. The transfer function of the designed LCL filter, neglecting the damping resistance, gives a typical Bode plot of an LCL filter as shown in Fig. 4.10. The filter Bode plot shows that the resonant frequency is equal to the selected designed switching frequency and the attenuation rate of -60DB/decade.

$$G_{LCL} = \frac{I_g}{U_{PWM}} = \frac{1}{L_g C_f L_f s^3 + (L_g + L_f)s} \tag{4.3}$$

where I_g is the current at the PCC and U_{PWM} is the output voltage of the inverter before the LCL filter. The list of parameters used in the simulation and analysis are shown in Table 4.5.

Table 4.5: Parameters of the Inverter and the Designed Filter

Symbol	Parameters	Value
V	Grid Voltage	125 V
F_g	Grid Frequency	50 Hz
V_{DC}	DC bus Voltage	320 V
F_{SW}	PWM carrier Frequency	2500 Hz
P_n	Nominal Power	3000 W
L_f	Inverter side inductance	8 mH
L_g	Grid side inductance	0.8 mH
C_f	Filter Capacitor	30 µF
F_r	Resonance Frequency	1077 Hz

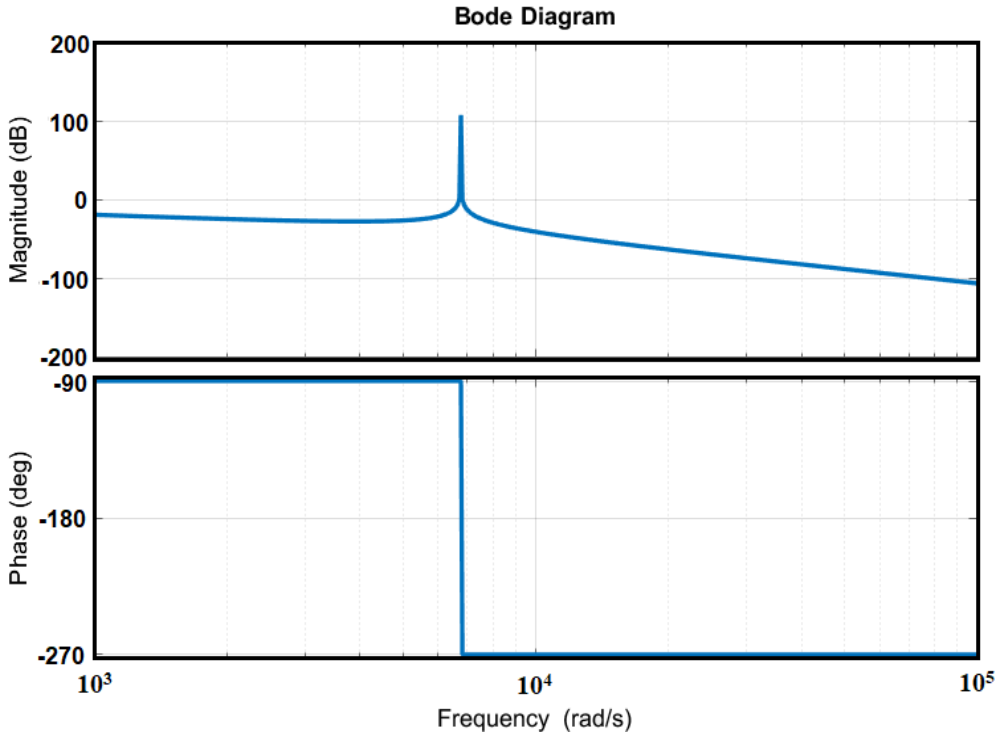

Fig. 4.10. Bode Plot of Designed LCL Filter

4.5.4 Modelling and Simulation of High PV Penetration on LV distribution network using MATLAB®/Simulink®

The three-phase VSI and LCL filter was designed for the 3kVA PV array and used for the investigation of higher PV system penetration on a scaled radial LV distribution network as shown in Fig. 4.11. Fig. 4.11 in this section was scaled down to a simple radial LV distribution

network in MATLAB®/Simulink® due to the size of the LV distribution Network, multiple VSI inverters, PWM controllers for the PV arrays and other components so as to reduce the complexity of the investigation in MATLAB®/Simulink®. The PV arrays were scaled down to 3kVA at a unity power factor, the LV network length was scaled down to 200m, and the load was scaled to 2.5KVA at 0.95 power factor while the LV transformer capacity was scaled to 10kVA, to enable the dynamic investigation of the PV systems and the controllers as shown in Fig 4.11. The 3kW PV systems were integrated 25meters from each other starting from the far end of the network as shown in Fig 4.11. The parameters used for the investigated are listed in Table 4.6.

We have investigated the behavior of the LV network with a 30% penetration level (3 kW), 60% penetration level (6 kW) and 90% penetration level (9 kW) in the scale down the LV distribution network.

Table 4.6: Parameters of the Scaled Down LV model

LV Distribution network parameter	
Line Voltage (V)	125
Line Impedance (R + jx) Ω/m	(0.001652 + j0.0007634)
Line Length (m)	200
Transformer Capacity (kVA)	10
Lump Load (kVA)	2.5
Load Power Factor	0.95
PV Array Capacity	$3kW_p$

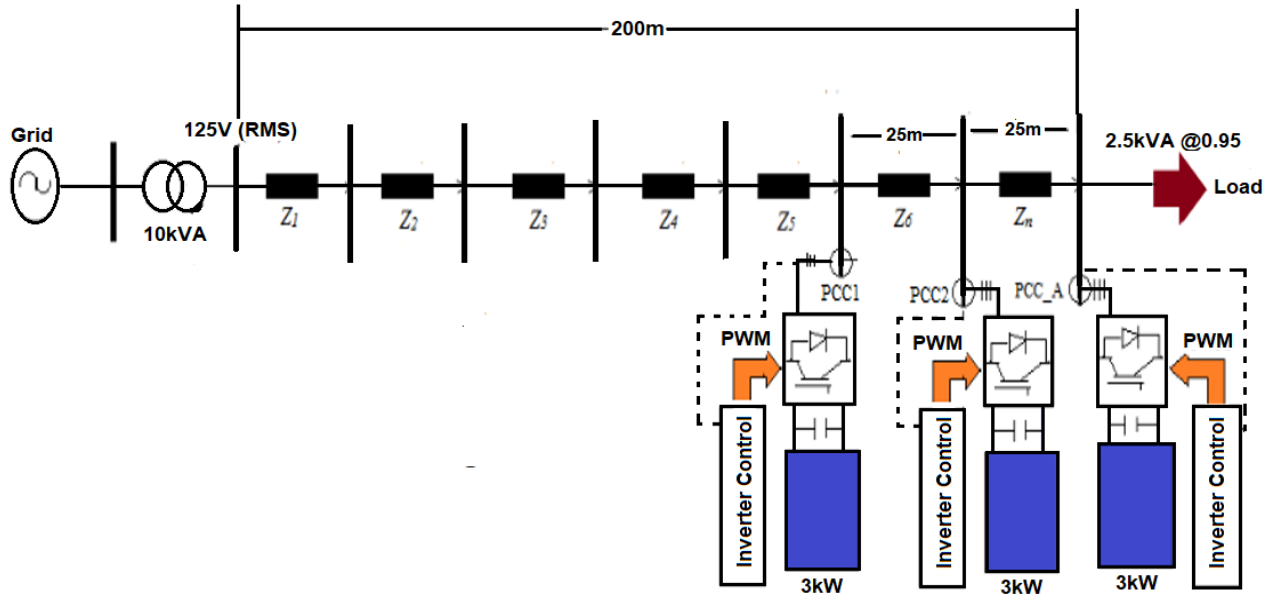

Fig 4.11. A Single Line Diagram of LV Network used with High PV Penetration in our Investigation

4.5.5 PV Array Model

The PV array used in our analysis is modelled in MatLab®/Simulink® using different experimental data. The solar PV cells were modelled using Excel and MatLab® curve fitting tool to create a three-dimensional surface which is capable of allowing direct mathematical representation of a Simulink® block which represents the PV model directly. These cells were modelled based on the environmental conditions such as irradiance (1000W/m^2) and temperature (25^{o}C). Simulink offers a different mathematical model for the various solar cell products as shown in the Appendix C. In our investigation and analysis, a Sunpower SPR-305-WHT solar cell was selected and used for the investigation of high PV penetration on the scaled LV distribution network. (see the characteristic curve of the selected PV array and the equivalent model of a photovoltaic solar cell in the Appendix C). The same PV array was used for the high PV impact assessment on the LV grid and the curtailment of voltage rise in our proposed CAPR/ramp down strategy.

4.6 Result Analysis and Discussion of Grid Voltage, current, at PCC and Power Transfer at Different PV Penetration Levels

Traditionally, with no solar PV integration, voltage along the LV distribution network is typically reduced from the transformer bus along the network, due to the voltage drop across the network. Figs. 4.12 and 4.13, show the instantaneous bus voltage and line current respectively at the end of the LV grid when there is no PV penetration. It can be seen that the voltage at the PCC_A is about 0.945 pu, as shown in Fig. 4.12 and falls within the grid voltage standard voltage limit (±5%) in this study. The current along the distribution network is about 0.225 pu, as shown in Fig. 4.13. Fig. 4.14, shows a voltage rise from 0.95 pu to 1.035 pu when a 3kW solar PV (30% penetration level) is integrated into the LV network. However, the voltage level still falls within the ±5% voltage range. The voltage profile at the PCC further increases from 1.035 pu to 1.067 pu when the penetration level increases to 6kW (60% penetration). In this case, the standard voltage limit of ±5% is violated as shown in Fig. 4.15. The voltage at the PCC was further increased from 1.067 pu to about 1.1 p.u when the penetration level increase to 9kW (90% penetration) as shown Fig. 4.16 and this voltage level violates the prescribed voltage standard limit of ±5%. Under the grid code, this violation may be detrimental to customers because some of the customers loads and equipment are sensitive to voltage perturbation. The increase in penetration also affected the LV distribution network current which is accompanied by reverse active and reactive power flow. Fig. 4.13 shows the current in the LV distribution network when there is no PV system in the network. To account for the fact that the 3kW solar PV (30% penetration level) is now integrated on the load side, the current from the external grid reduced from 0.225 p.u to about 0.085A p.u in our simulation as shown in Fig. 4.17 because the PV is now supplying the load. The increase in solar PV penetration from 30% to 60%, increases the line current from 0.085 p.u to about 0.3 p.u as shown in Fig. 4.17 due to increasing PV power. The same trend was also observed when the

PV penetration increased from 60% to 90% (9kW), in this case, the line current increased from 0.3 p.u to about 0.52 p.u as shown in Fig. 4.17 and this can affect overcurrent protection device and increase losses across the network. The increase in current is accompanied by a reverse power flow from the load end to the external grid.

From our analysis, the external grid provides an active power of 0.2755 p.u and a reactive power of 0.192 pu to the load when there is no PV in the LV distribution network as shown in Fig. 4.18 and Fig. 4.19. However, when 3kW (30% PV penetration) was integrated, a reverse active and reactive power flow of 0.03 pu and a reactive power flow of 0.125 p.u were observed as shown in Figs. 4.20 and 4.21 respectively. When the PV integration increases from 30% to 60%, both the reverse active and reactive power flows were increased from 0.03 pu and 0.125 p.u as shown in Figs. 4.20 and 4.21 to 0.37 p.u and 0.27 p.u, respectively as shown in Fig 4.20 and Fig 4.21. This represents a percentage increase of 34.3% of active power and 40.63% for reactive power. The reverse power flow further increases when the solar PV penetration increased to 90%, under this condition, both the reverse active and reactive power increased to 0.72 p.u and 0.32 pu respectively as shown in Fig. 4.20 and Fig. 4.21. This represents an increase of 161.3% of active power and 66.67% for reactive power when compared to the LV distribution network with no PV system, and this may have a detrimental effect on the transformer loading.

In chapter 5**,** we will describe the new technique used to address the sudden voltage rise and other related issues.

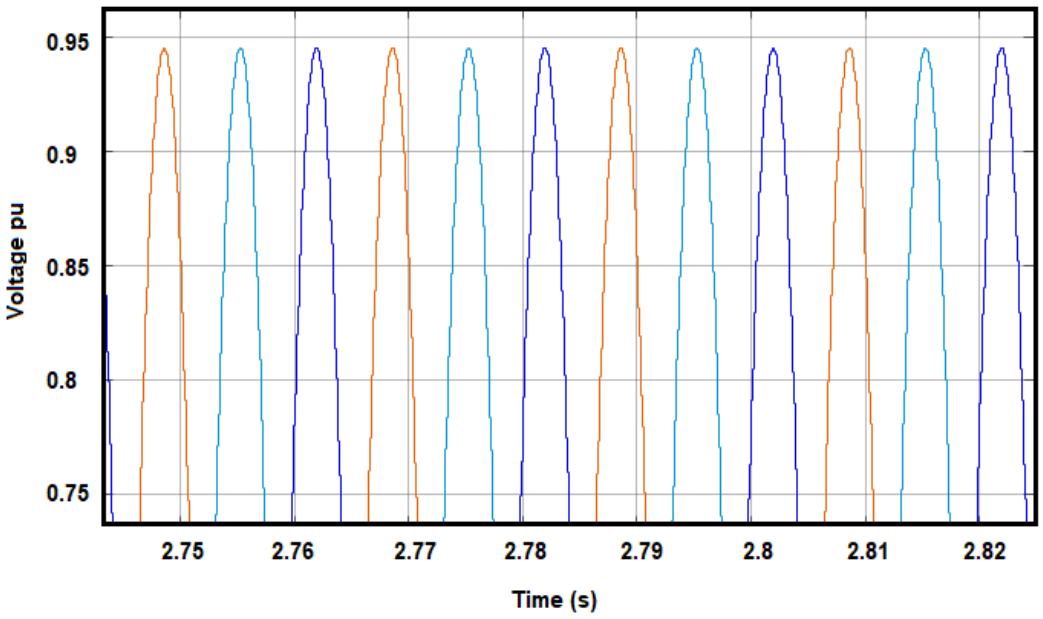

Fig. 4.12. Voltage (0.945pu) at the End of the LV Grid without PV

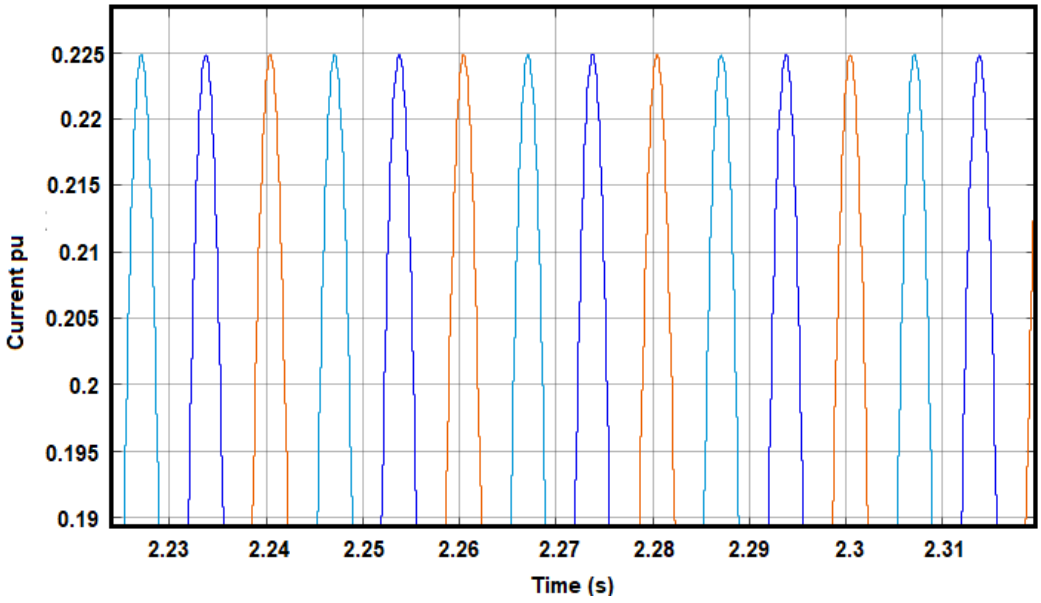

Fig. 4.13. Current (0.225pu) at the LV Network without PV

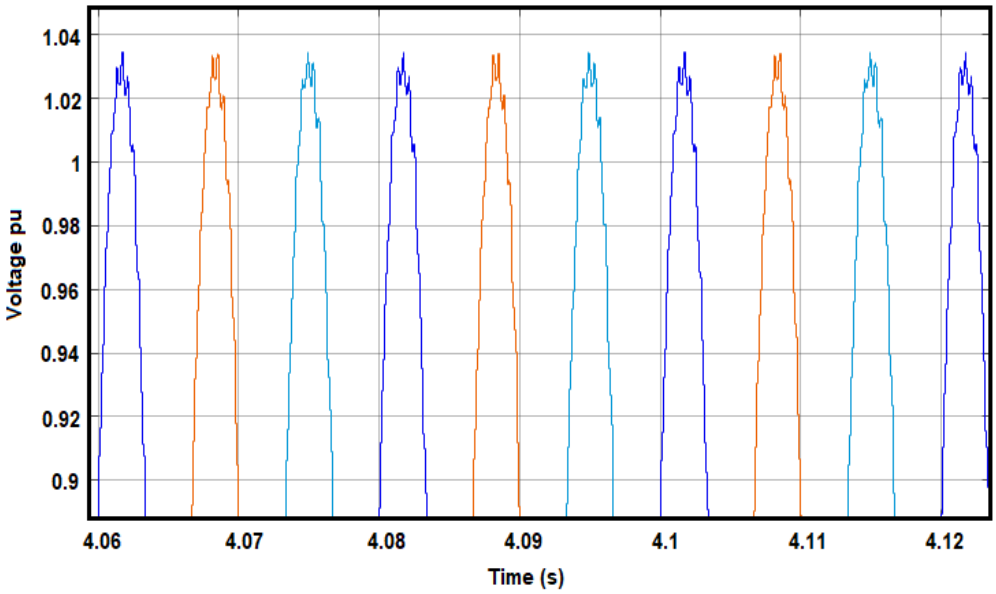

Fig. 4.14. Voltage Profile (1.035 pu) at 30% Penetration Level

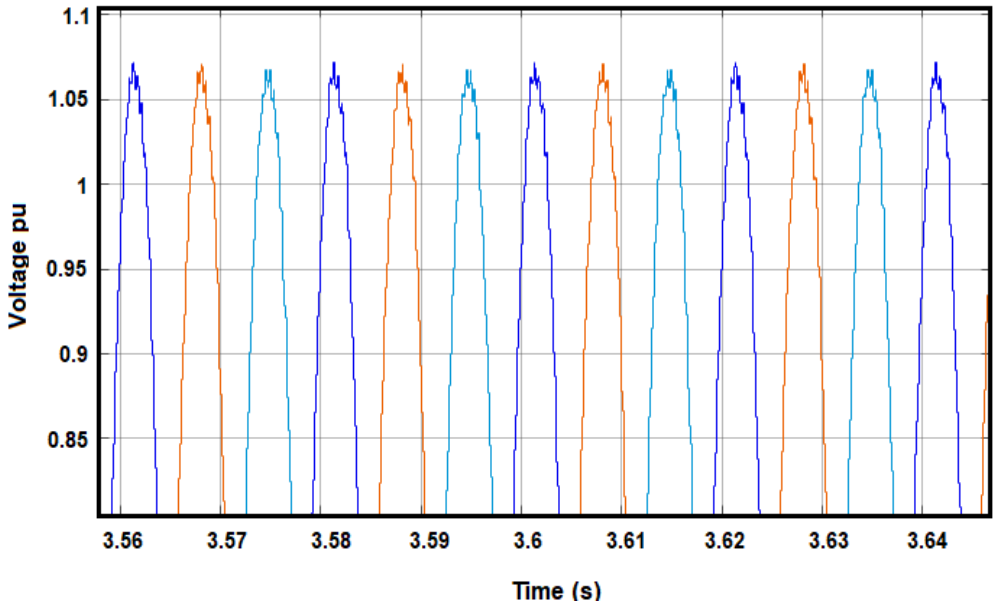

Fig. 4.15. Voltage Profile (1.067 pu) at 60% Penetration Level

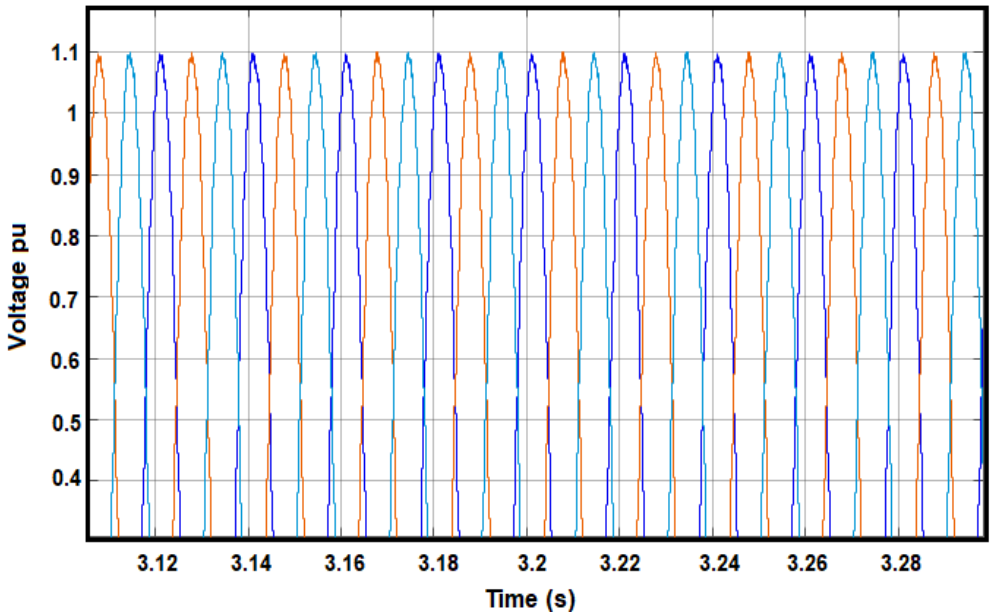

Fig. 4.16. Voltage Profile (1.1 pu) at 90% Penetration Level

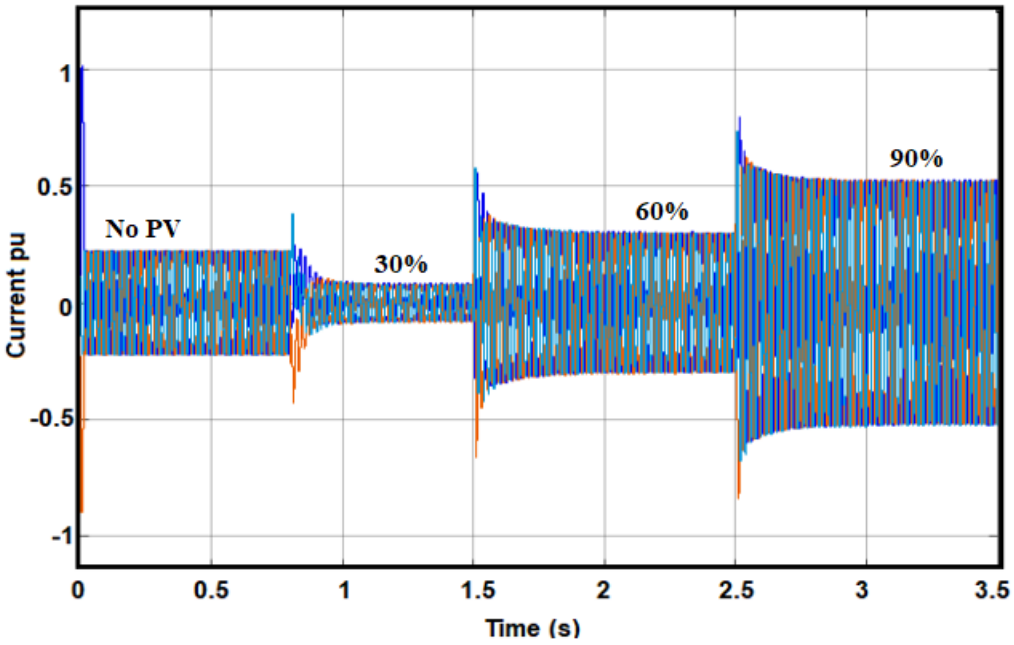

Fig. 4.17. Current Modification on Transformer Bus at Different Penetration Level

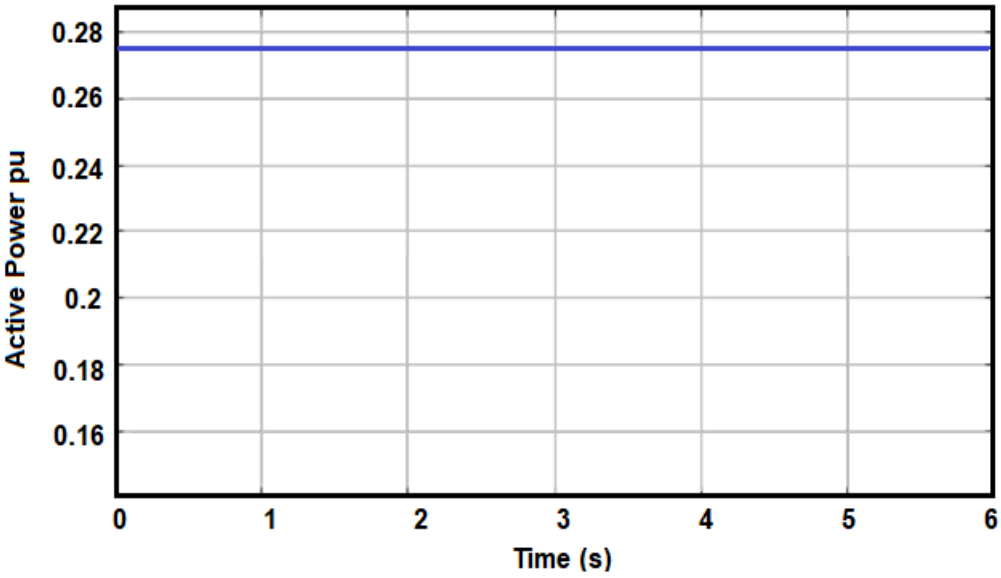

Fig. 4.18. Active Power Transfer without PV Penetration

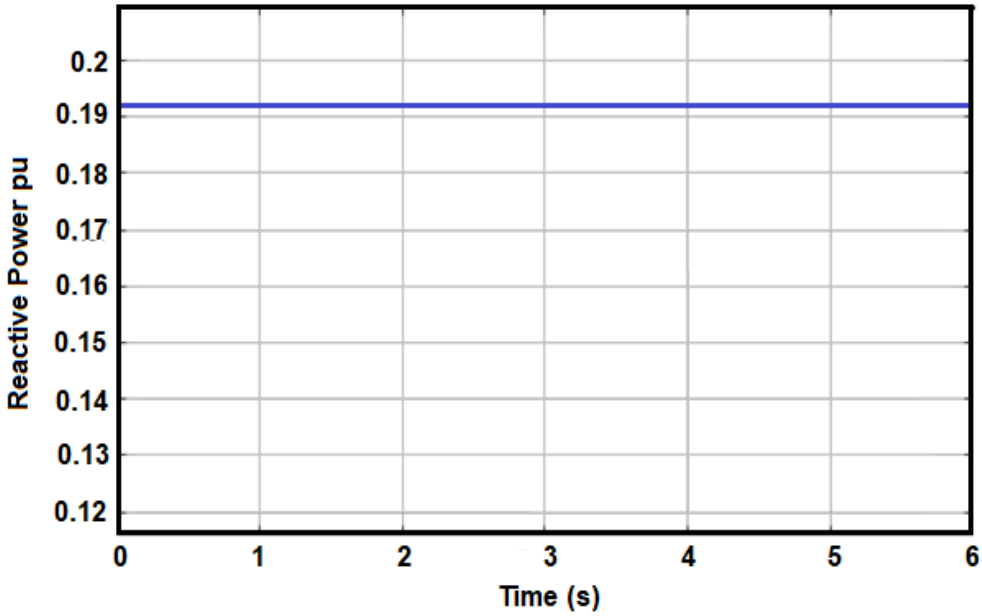

Fig. 4.19. Reactive Power Transfer without PV Penetration

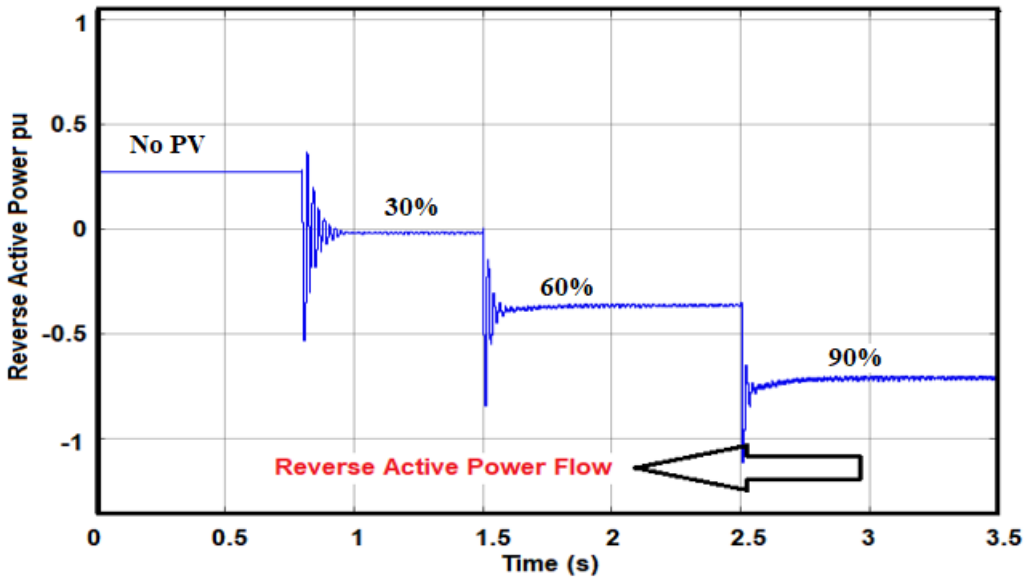

Fig. 4.20. Active Power Transfer on the LV Network at Different Penetration Level

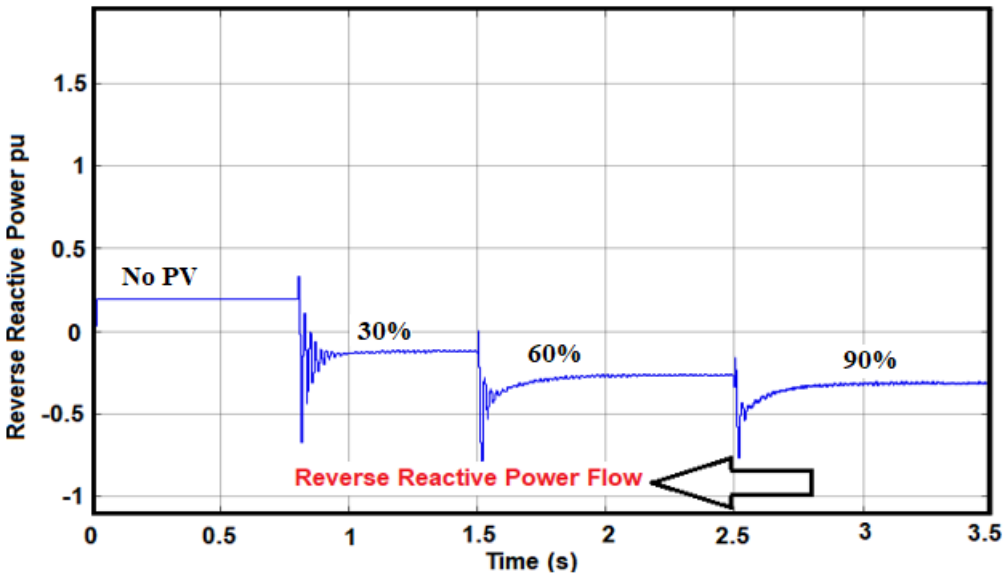

Fig. 4.21: Reactive Power Transfer at Different Penetration Level

4.7 Results Analysis and Discussion of Voltage Harmonics Level at PCC with Different PV Penetration Levels

Fig. 4.22, shows the approximate THD levels at the PCC when the PV penetration into the LV distribution network was at 30%, 60%, and 90%. The analysis shows a voltage THD value at PCC of about 1.86%, which complies with the IEEE standard 5194 as described in Table 3.1

above. According to IEEE Standard 5194 requirements, the THD level for voltage less than 1kV should be less than 5%. As shown in Fig. 4.22, the voltage THD values almost doubled due to the increase in PV penetration, but it is still within the IEEE Standard 5194 requirements. In the investigated case, the individual and combined PV inverters did not violate the voltage harmonic limit. However, a high distributed PV penetration may violate the harmonic limit due to the overall combined voltage harmonic generated by the PV inverters.

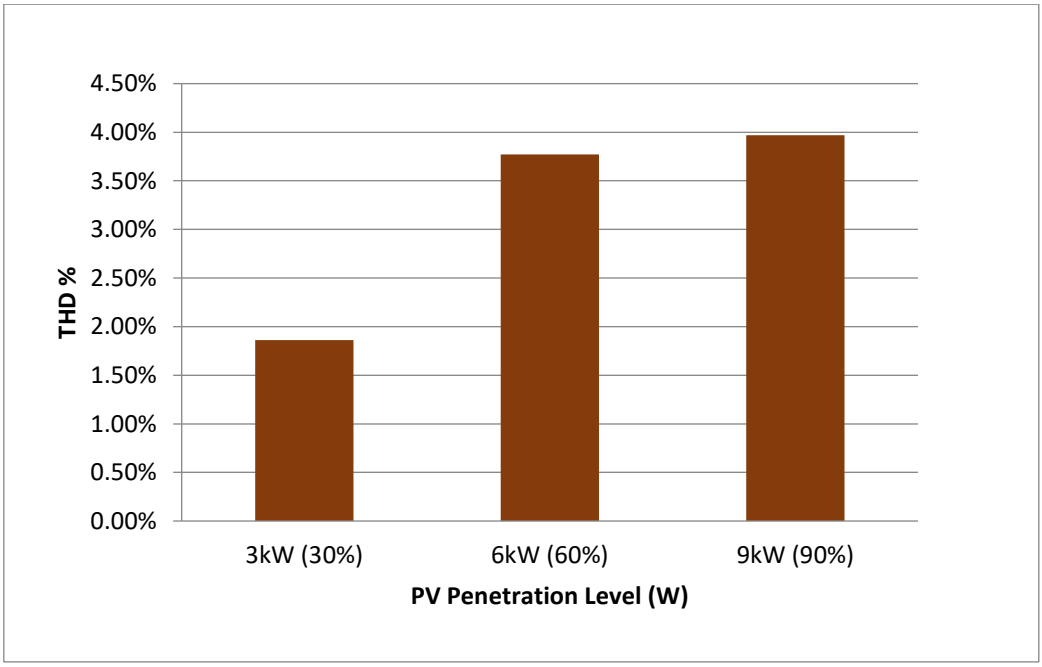

Fig 4.22. Voltage Total Harmonic Distortion (THD %) at the PCC

4.8 Summary

In this Chapter, two different investigations were carried out using DigSILENT power-factory and MATLAB®/Simulink® software's to understand the potential impact of increasing PV penetration in the LV distribution networks and develop a mitigation strategy. In the steady state analysis, DigSILENT power-factory software was used to model the potential impacts or danger of increasing penetration of PV on a radial LV grid. The potential impacts are listed as transformer loading (rating), network line losses, voltage rise, reverse power Flow

MATLAB®/Simulink® software environment was also used to investigate the dynamic analysis of higher PV penetration on a scaled radial LV distribution network. The investigation clearly identifies the dynamic of a sudden voltage rise issue with high PV penetration.

Chapter 5

Proposed Voltage Rise Mitigation Method and Simulation

Chapter 5 describes the proposed CAPR strategy for sudden voltage rise mitigation in the LV distribution grid based on the reactive power absorbed by a three-phase VSI, which provide instantaneous setpoint changes with a ramp down PV inverter output power. This action is activated in response to an input command received from a control DC capacitor current as a result of voltage perturbation at the PCC. The proposed CAPR strategy was simulated in MATLAB/Simulink® environments using a scaled down radial LV distribution network with two 3kW PV arrays to evaluate the performance of the control technique.

5.1 Methodology

In this section, we will describe the strategy (methodology) used in harnessing the inverter capability so as to reduce or regulate the PV output power during a high PV penetration in an LV distribution grid. In the proposed power reduction strategy, the amplitude of the modulating signal or sinusoidal signal is regulated downward to change the duty cycle of the switching frequency for the transistors as shown in Fig. 5.1 and Fig. 5.2. The downward regulation of the modulating signal increases the inverter gate pulse Off-time and reduce the on-time, which shut down the PV array momentarily in an extremely short time. This action allows the inverter switch to absorb reactive power through the freewheeling diode as depicted in Fig. 5.3 and Fig. 5.4. The increase of the off time of the switch will enable the freewheeling

diode to conduct and become forward bias. In this case, some current from the grid decays to zero in the switches while the remaining current charges the DC link capacitor as shown in Fig. 5.3. This action will ramp down the maximum power generated by the PV array.

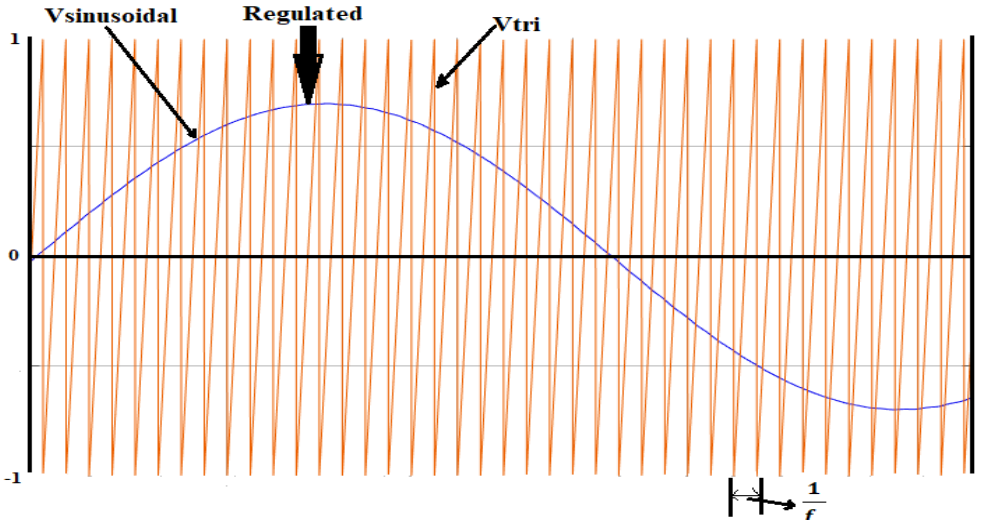

Fig. 5.1: Regulated amplitude of modulated signal

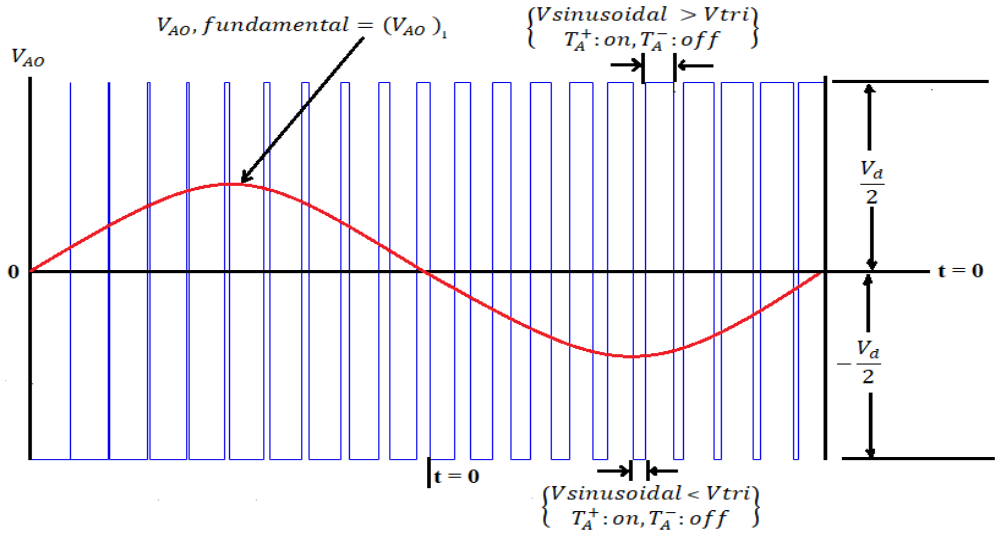

Fig. 5.2: Impact of Regulated Modulated Signal to IGBT Switch OFF Time

In this way, the output current of the inverter is stopped for a few microseconds delaying transients between the output filter and the grid while reducing the inverter input current and forcing the PV output voltage to move toward open circuit while shifting the PV power away

from the maximum power point. This action is carried out by the inverter after receiving a command indicating that the measured voltage at the PCC is higher than the predetermined set voltage value as shown in the threshold algorithm in Fig. 5.5.

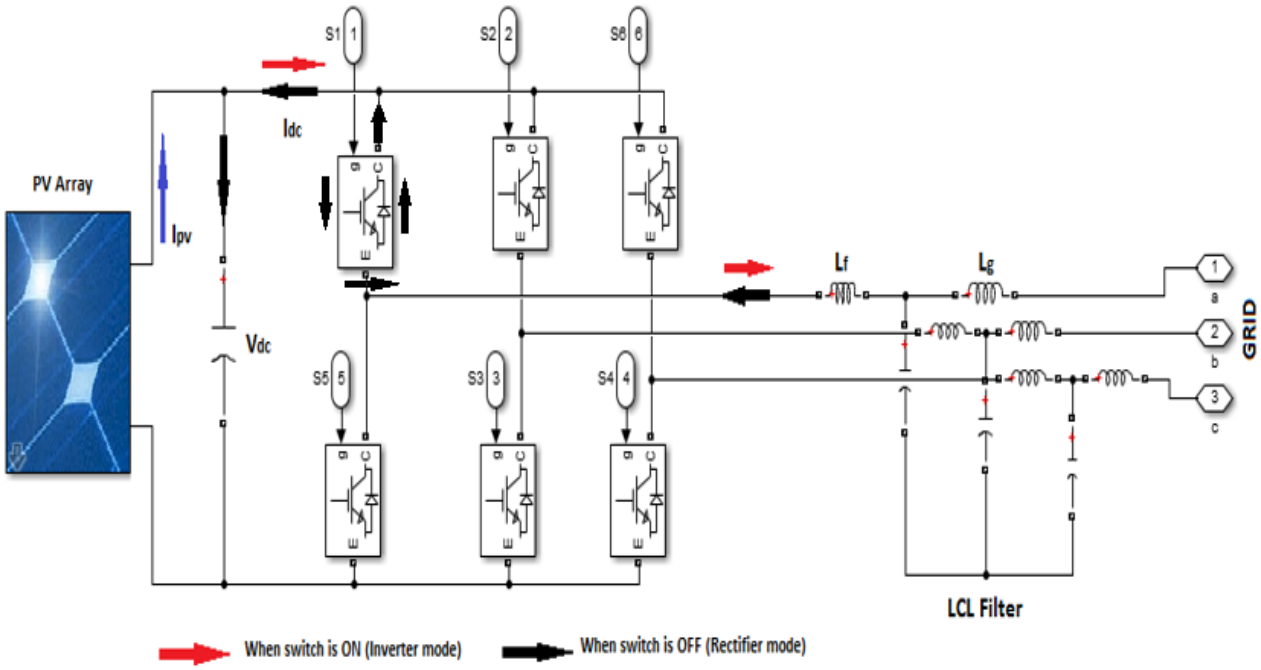

Fig. 5.3: Operation of VSI when IGBT Switch OFF Time is Increased

This technique will reduce the active power with associated ramp rate and set a new maximum power point for the PV array which leads to a reduction in the inverter output voltage. The ramping of the inverter output power results in a reactive power transfer and create an amplitude difference between the inverter output voltage and the external grid voltage. According to [154], if the inverter output voltage is less than the grid voltage, but still remain in phase with the grid voltage, the inverter will absorb reactive power as shown in Fig. 5.4.

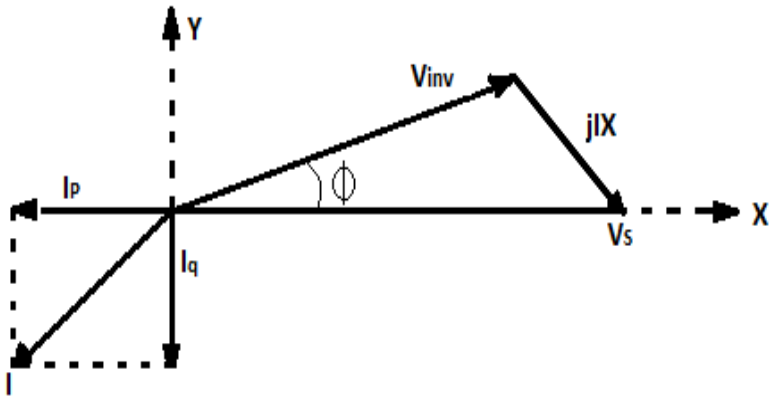

Fig. 5.4: Phasor Diagram of Inverter Supplying both Active and Reactive Power [154]

In Fig. 5.4, V_{inv} is the inverter output voltage, V_s is the grid voltage, ϕ is the phase angle while I, is the inverter output current, I_P, and I_q are the active and reactive current vector respectively. The ability of the inverter to absorb and inject active power is dependent on the changes of the active and reactive current vector.

Regulating the amplitude of the modulating signal and ramping down of the PV array power was carried out through a modified PI controller using Fig. 5.5. The regulation of the amplitude of the modulating signal of the inverter was carried out by generating different reactive power reference using a regulated DC link capacitor current value known as I_c. The threshold algorithm is used to regulate the DC capacitor current (I_c) so as to generate a new current called I_c^* and this current determine the reactive reference based on the voltage at the PCC as shown in Fig. 5.5.

The threshold algorithm is used to control the inverter reactive reference component by creating new values for I_c^*, which changes based on the standard upper voltage set limit (which is usually ±5% or ±10% as the case may be). In this thesis, a voltage limit of ±5% was used in our investigation and analysis. The threshold algorithm measures the voltage at the VPCC and compares it with an upper voltage set point limit (V_{set_Upper}) and if the difference between the

voltage is zero (that is V_{set_Upper} = VPCC), the power reduction is initiated. If the V_{set_Upper} is less than VPCC, the algorithm disconnects from the zero-reactive component (Q_{ref}=0) and connect the switch to the reactive reference component Q_{ref}^{*} as shown in Fig. 5.5. The reactive reference component is a function of the regulated DC link capacitor current, I_c^* as shown in Eqn. (5.8), therefore, if I_c^*, is regulated, the reactive reference component is then varied to keep the VPCC below the set upper voltage limit (V_{set_Upper}). The voltage at the PCC is regulated by varying the I_c^* value by a factor of 0.1 until the voltage at the PCC is below the set upper voltage limit (V_{set_Upper}) as shown in Fig. 5.5. This action ramps down the PV power and the output voltage of the VSI leading to absorption of some reactive power as described in Figs. 5.3 and 5.4. Also, if the measured voltage (VPCC) is less than the lower voltage limit of the LV distribution grid, the threshold algorithm disconnects the connector from the reactive reference component Q_{ref}^{*} and connect the connector back to zero reactive reference (Q_{ref}=0) that is when Q_{ref}^{*} is zero. This action now makes the inverter to transfer maximum power to the LV distribution network.

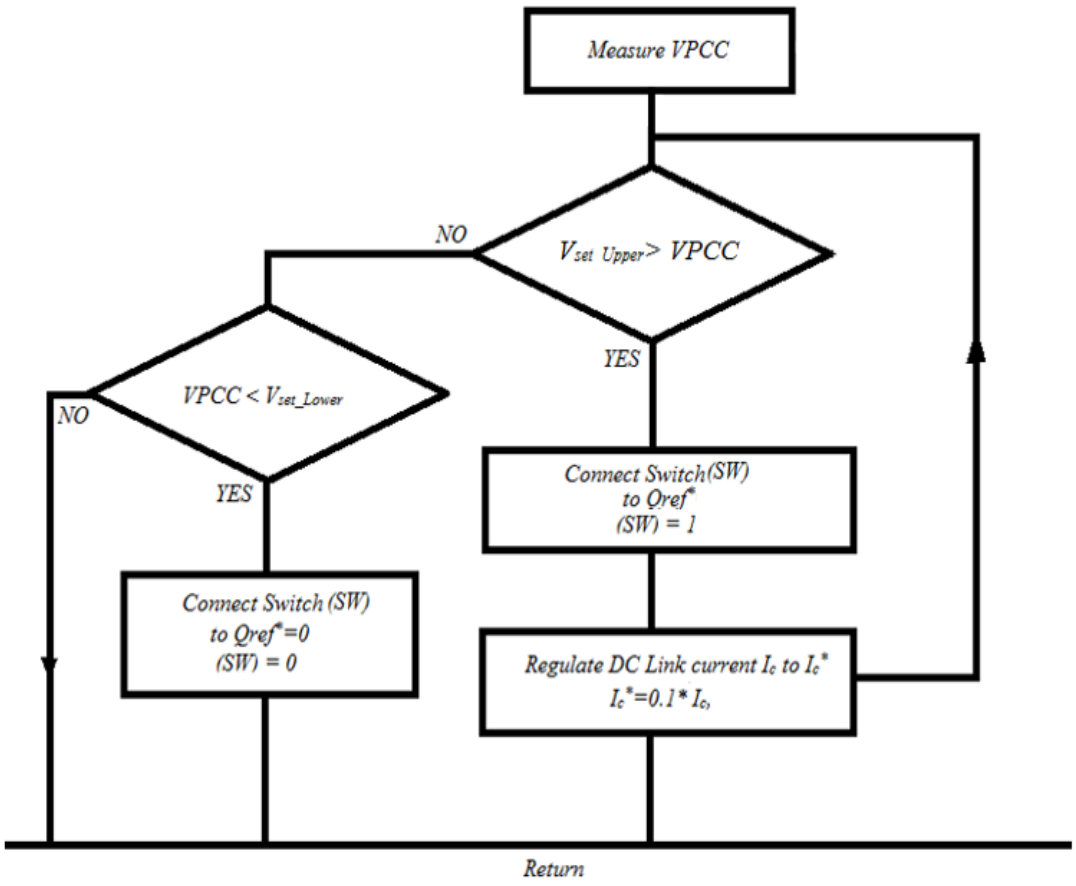

Fig. 5.5: Threshold Algorithm used for the Control of *Ic** Value during Voltage Rise

It is known that the active power injected into the LV distribution grid by the PV system via the VSI is given as

$$P_{PV} = V_{dc} I_{dc} \tag{5.1}$$

Therefore, from Eqn. (5.1), it is shown that the V_{dc} voltage on the DC side of the inverter plays a key role in the transfer of active power into the grid. The inverter acts as an interface between the PV system and the grid, and the output voltage in the time domain is given as:

$$\begin{pmatrix} U_a \\ U_b \\ u_c \end{pmatrix} - \begin{pmatrix} U_{ag} \\ U_{bg} \\ u_{cg} \end{pmatrix} = L_f \frac{d}{dt} \begin{pmatrix} I_a \\ I_b \\ I_c \end{pmatrix} + R_g \begin{pmatrix} I_a \\ I_b \\ I_c \end{pmatrix} \tag{5.2}$$

where U_{ag}, U_{bg}, and U_{cg} are the grid voltage, I_a I_b and I_c are the inverter output current and L_f is the filter inductor. In Eqn. 5.2, we also have U_a, U_b, and U_c as the inverter output voltages

For effective control of the injected current and power, the three-phase voltage and current at the PCC and the inverter in Eqn. (5.2) are transformed into the *d-q* component using the park transformation as shown in Eqn. (5.3).

$$\frac{d}{dt}\begin{pmatrix} I_d \\ I_q \end{pmatrix} = \begin{pmatrix} R_g & -\omega L \\ \omega L & R_g \end{pmatrix}\begin{pmatrix} I_d \\ I_q \end{pmatrix} + \frac{1}{L_f}\begin{pmatrix} U_d & -U_{dg} \\ U_q & -U_{qg} \end{pmatrix} \tag{5.3}$$

where U_{dg} and U_{qg} are the grid *d-q* voltage components. U_d, U_q, I_q, and I_d are the inverter voltage and currents *d-q* axis while R_g and L are the resistance and inductor of the distribution line respectively.

Now, from Eqn. (5.3), the active and reactive power of the system can now be controlled independently by controlling the current reference components (I_d^* and I_q^*). Eqn. (5.3) will play a key role in our proposed control strategy with slight modification on the reactive component to control voltage at PCC.

We understand that the PV system injects only active current and power into the grid. However, to control the active current and PV power, the PV output voltage will be shifted towards open circuit to reduce the maximum power point (MPP) of the PV system. In this way, the PV output power will be ramped down by forcing the inverter current to lag or lead.

In the analysis, the inverter input current is assumed to be inversely proportional to the DC link voltage. Therefore, to ramp down the inverter input current, the V_{dc} must be increased. To increase the DC link voltage, the transistor off time will be increased by reducing the modulating signal as highlighted above and to do this we assumed that the PV system inverter generates a reactive current as shown in Eqn. (5.4). The assumed reactive reference current component ($I_{q\_ref}^*$) is termed as the subtraction of the regulated DC capacitor current (I_c^*) from the DC source current which is assumed to be proportional to the reciprocal of the DC link voltage (V_{dc}) (that is, the PV output voltage) as shown in Eqn. (5.4). The voltage at the PCC

will be sensed and compared with the set voltage value and then the error is used to determine the I_c^* value which generates the reactive reference component ($Q_{ref}{}^*$) The generated reactive reference component ($Q_{ref}{}^*$) is used to regulate the VSI switching pattern, which is then used to control the reactive power that is absorbed by the inverter.

$$I_{q\_ref}^* = \frac{1}{V_{dc}} - I_c^* \tag{5.4}$$

where $I_c^*$is the controlled DC capacitor current.

The active and reactive power of DG systems can be expressed as [155]:

$$P_{DG} \backsimeq I_d V_s \tag{5.5}$$

$$Q_{DG} \backsimeq I_q V_s \tag{5.6}$$

where V_s, I_d, I_q, are the system voltage, active and reactive current components respectively

Therefore, to apply Eqn. (5.6) to the PV system, we assumed that the reactive power reference component generated by the PV through the inverter can be given as;

$$Q_{ref}{}^* = I_{q\_ref}^* V_s \tag{5.7}$$

Hence, substituting Eqn. 5.4 into Eqn. 5.7 gives the reactive power compensation as;

$$Q_{ref}{}^* = \left(\frac{1}{V_{dc}} - I_c^*\right)\sqrt{V^2{}_d + V^2{}_q} \tag{5.8}$$

The inverter active power curtailment is a function of the reactive power control. Therefore, the reactive power reference component ($Q_{ref}{}^*$), is activated according to the measured voltage at the PCC, as given by Eqn. (5.9):

$$Q_{ref}^* = \begin{cases} \left(\frac{1}{V_{dc}} - I_c^*\right)\sqrt{V^2{}_d + V^2{}_q}, & V_{meas} > V_{set_{upper\ limit}}\ [Q_{ref}^* \neq 0] \\ 0, & V_{meas} < V_{set\ lower\ limit}\ [Q_{ref}^* = 0] \end{cases} \tag{5.9}$$

where V_{meas} is the voltage measured at the PCC.

To curtail the active power injected from the PV while reducing the PV current and increasing the PV output voltage towards open circuit, Eqn. (5.8) needs to be compared with the grid reactive power as given in Eqn. (5.10):

$$Q_g = (V_d I_q - V_q I_d) \tag{5.10}$$

where, V_d, V_q, I_d, and I_q are the *d-q* components of the voltage at the PCC in the synchronous rotating reference frame.

The reactive power error generated from Eqn. (5.11) is then used to curtailment or ramp down PV power of the PV, and this is also based on the regulation of I_c^* value. This action shifts the power of the PV away from the maximum power point, creating a reduced maximum power point for the PV system array.

$$Q_{error} = Q_{ref}^* - Q_g \tag{5.11}$$

The smaller the error, the greater the amount of reactive power absorbed by the inverter. That is, the Q_{ref}^* determine the current deviation for the IGBT switch to absorb more reactive power so as to reduce the inverter output power and the voltage at the PCC during high PV penetration in the distribution network. The active and reactive power transfer of the inverter is limited by the power rating of the inverter. Therefore, in this strategy, the interface filter inductance and the inverter can be oversize by 30% to allow more reactive power absorption.

The proposed CAPR strategy is simulated in MATLAB®/Simulink® Sim power system environment, on a 200m long radial LV distribution network so as to curtail over-voltage due to high PV penetration as described in Chapter 4. The simulation results of the CAPR strategy are presented in section 5.2.

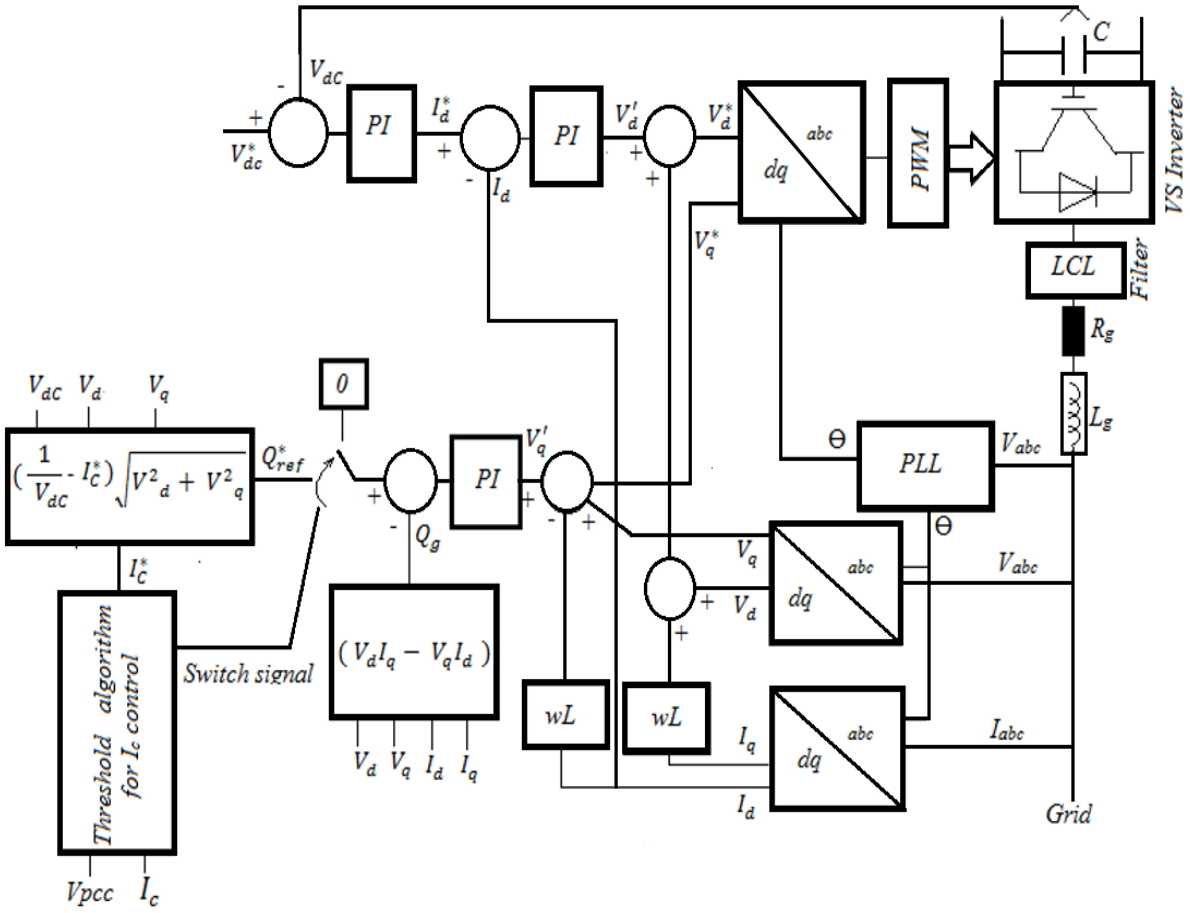

Fig. 5.6: Proposed Active Power Reduction Strategy Schematic for Voltage Rise Mitigation

5.2. Simulation Results and Analysis of CAPR Strategy with 60% PV penetration on the Scaled-Down Radial LV Distribution Network

The LV distribution network used in Fig. 4.1 was scaled down due to the complexity of the simulation and the inability of the software to simulate the system with a lot of PI current controller, and PV system arrays. See Appendix D for the CAPR control and the overall system in the MATLAB/Simulink® environment.

The results described in this section were investigated with the scaled down LV network shown in Fig 4.11 using the proposed CAPR technique. In the analysis, the DC capacitor current *(I_c)* was regulated to $I_c^* = 5.8\,\mathrm{A}$ and the VSI's absorbed reactive power of about 1.83kVar to reduce the inverter output active power from 3kW to about 2.37kW. See Table 5.1

for the impact of regulated I_c^* on the active power, reactive power, PV output power, PV output current and VPCC in a 3kVA inverter.

Table 5.1: Impact of the Controlled I_c^* on the Input and Output of the VSI

	DC side of Inverter			**Inverter**		**LV grid Parameters**			
I^*_c *(A)*	I_{dc} *(A)*	V_{dc} (V)	P_{dc} (W)	Pf	Q pu	Vpcc pu	Igrid pu	$P_{Reverse}$ pu	$Q_{Reverse}$ pu
0	11.02	272.00	2994.0	0.998	0.0189	1.0670	0.3000	0.3730	0.2800
4	9.33	294.29	2744.7	0.914	0.1211	1.0670	0.2680	0.3200	0.2400
5	8.60	298.88	2642.2	0.880	0.1426	1.0520	0.2440	0.3100	0.1900
5.2	8.36	299.79	2602.8	0.867	0.1495	1.0480	0.2380	0.3000	0.1800
5.4	8.17	300.63	2466.8	0.822	0.1709	1.0460	0.2350	0.2900	0.1800
5.6	8.02	301.17	2418.9	0.806	0.1776	1.0450	0.2330	0.2800	0.1600
5.8	7.87	300.83	2376.7	0.792	0.1832	1.0400	0.2300	0.2750	0.1400

5.2.1 Impact of CAPR Strategy on Voltage Rise and Network Current with 60% PV penetration.

From the investigation in section 4.5, we discovered that the PCC voltage increased to 1.067 with 60% PV penetration level and we observed that the voltage is above the standard voltage limit of ±5%. However, when the proposed CAPR strategy was used in the investigation, the voltage at the PCC was ramped down to 1.04pu with an I^*c current of 5.8A which is based on the threshold algorithm. The measured PCC voltage is now below the standard voltage upper limit set point of +5% as shown in Fig. 5.7 and Fig. 5.8. The proposed CAPR strategy gradually reduces the voltage at the PCC, and it took about 6s to reduce the voltage below the upper voltage set limit. The current was also reduced from 0.3 pu to about 0.23 pu with a reduction of 0.07 pu as shown in Fig. 5.9 and Fig. 5.10.

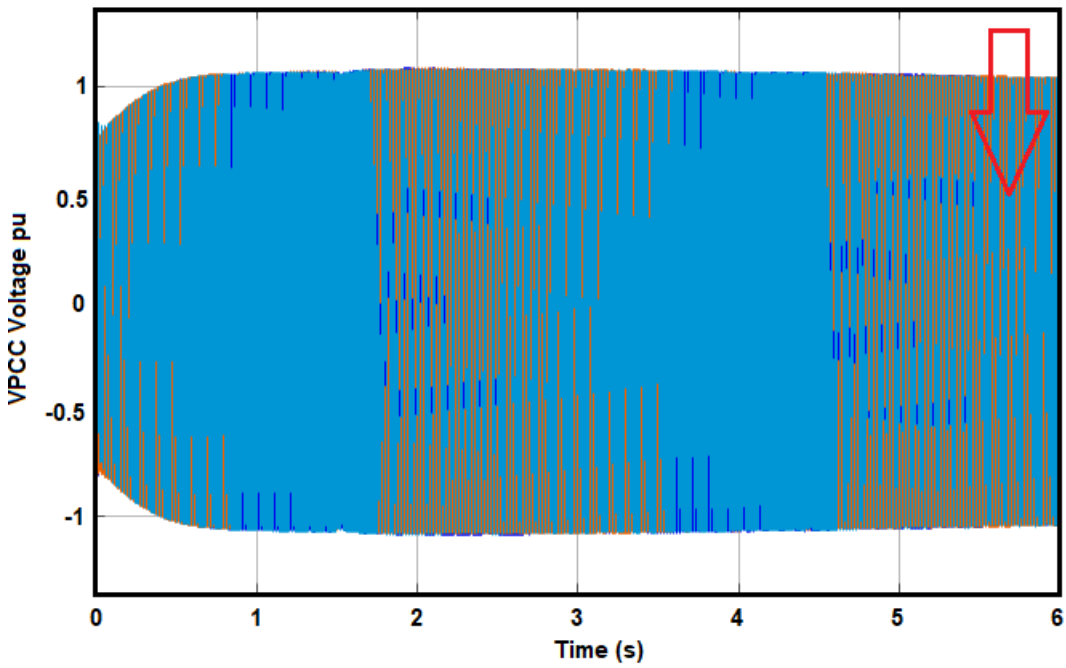

Fig. 5.7: Waveform of the PCC Voltage at 60% PV Penetration with CAPR Strategy

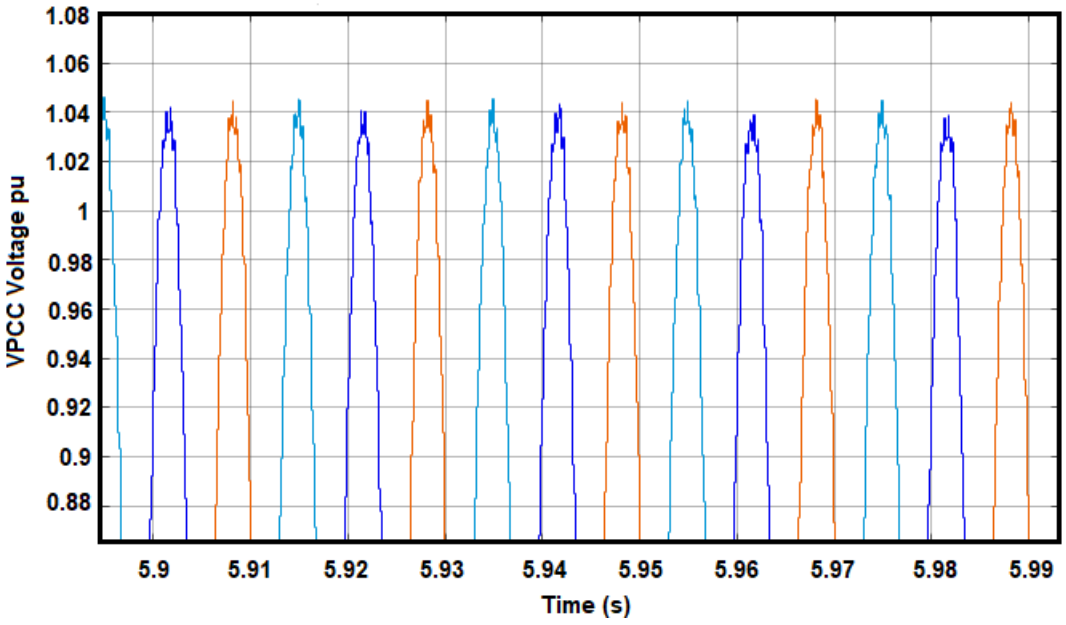

Fig. 5.8: Zoomed PCC Voltage Profile with 60% PV Penetration with Proposed CAPR Strategy

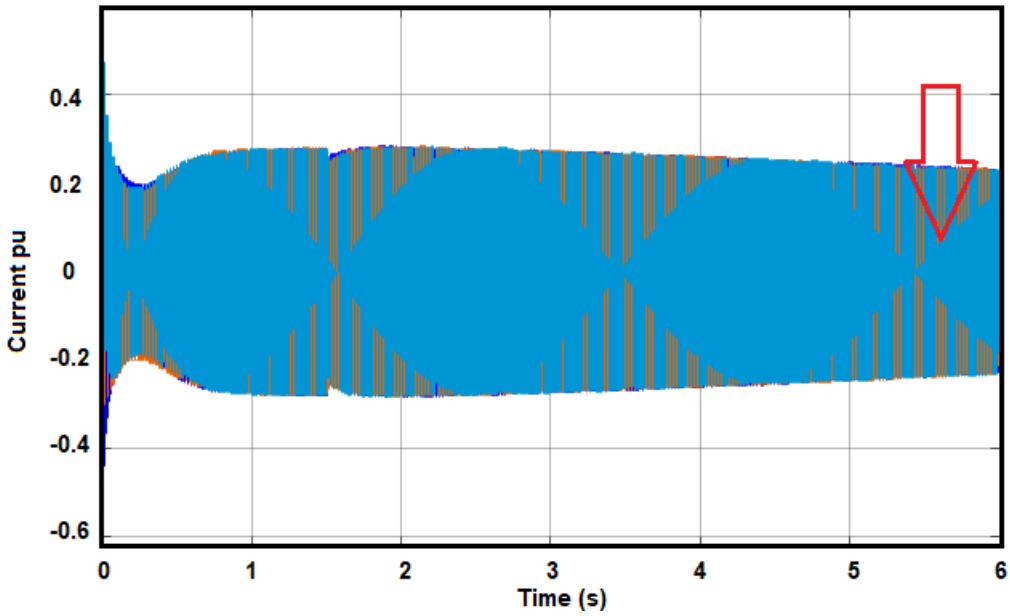

Fig. 5.9: Current Waveform at 60% PV Penetration with CAPR Strategy

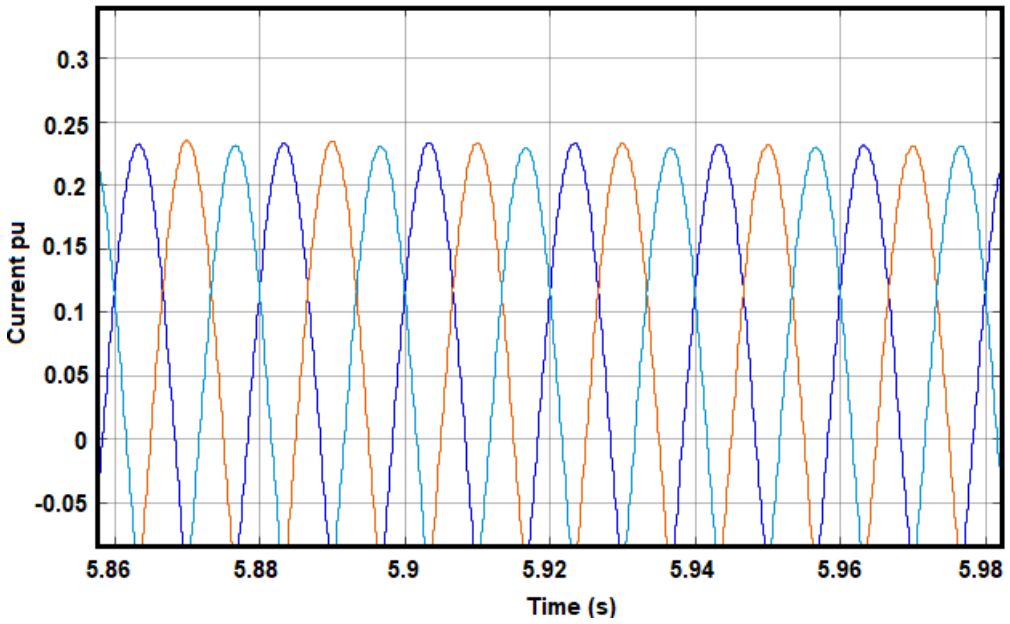

Fig 5.10: Zoomed LV Network Current at 60% PV Penetration with Proposed CAPR strategy

5.2.2 Impact of CAPR Strategy on the Reverse Power flow with 60% PV penetration.

The proposed CAPR technique also reduces the amount of reverse active and reactive power in the radial LV distribution network. The reverse active power was reduced from 0.37 pu to 0.3 pu, as shown Fig. 5.11 and Fig. 5.12. This corresponds to a reverse active power reduction

of 0.07 pu. Also, the reverse reactive power was also reduced from 0.28 pu to 0.14 as shown in Fig. 5.13 and Fig. 5.14.

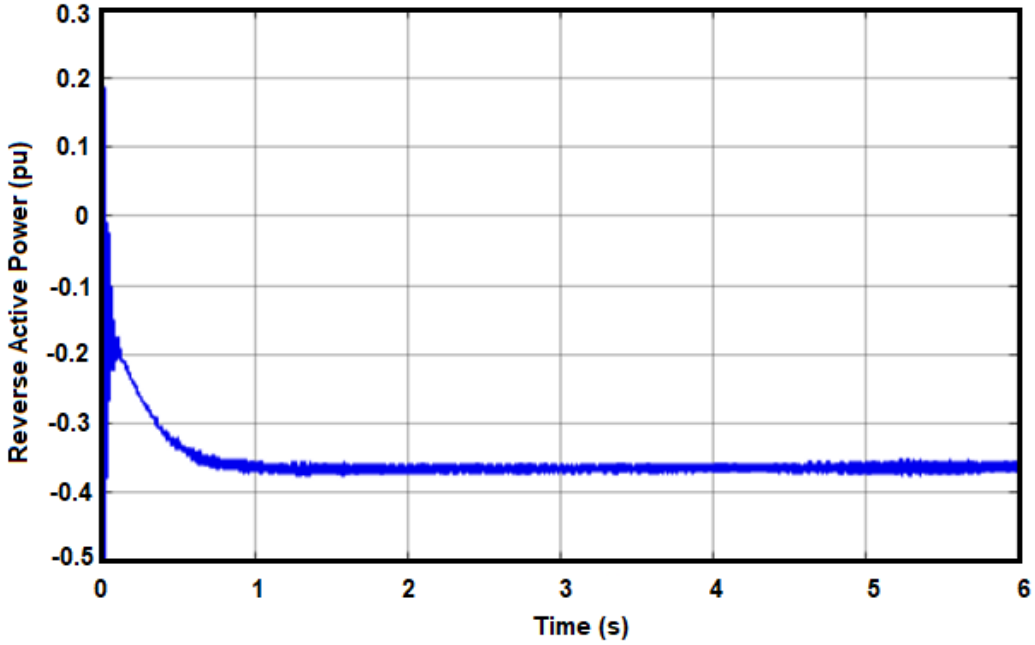

Fig 5.11: Reverse Active Power Flow with 60% PV Penetration without CAPR

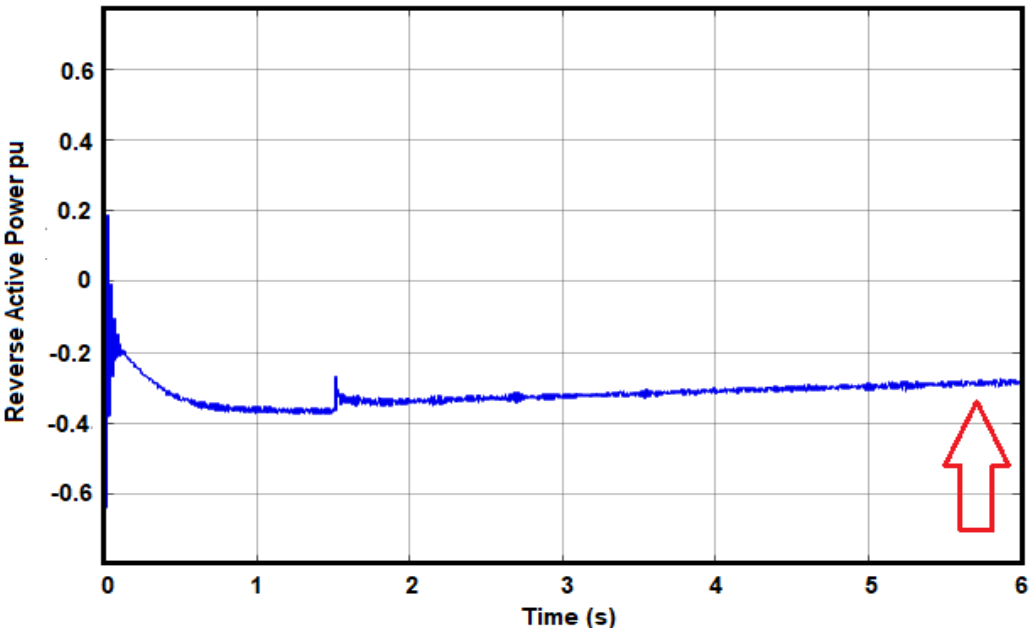

Fig. 5.12: Reverse Active Power at 60% Penetration with Proposed CAPR strategy

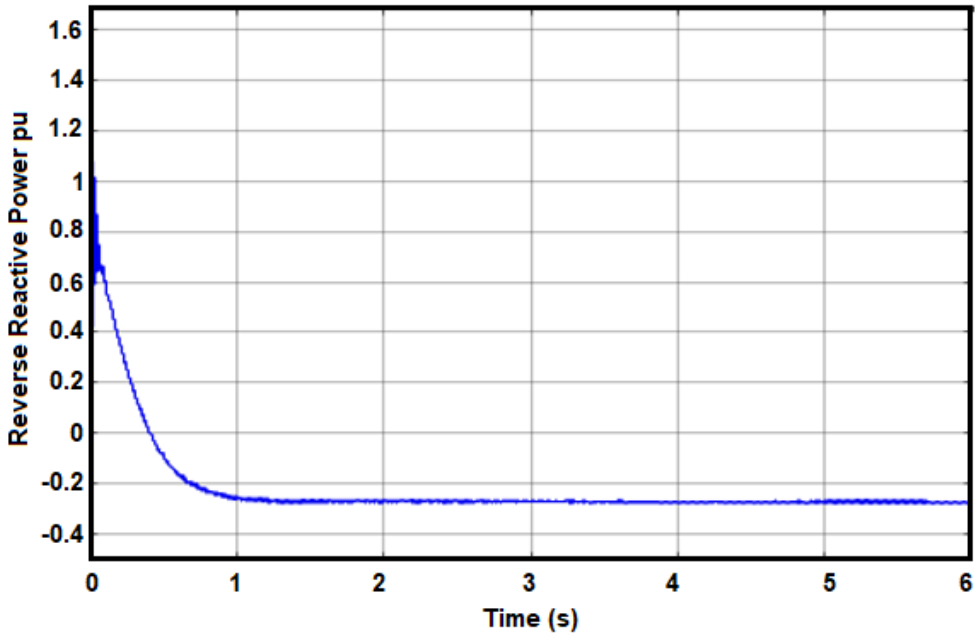

Fig. 5.13: Reverse Reactive Power Flow with 60% PV Penetration without CAPR

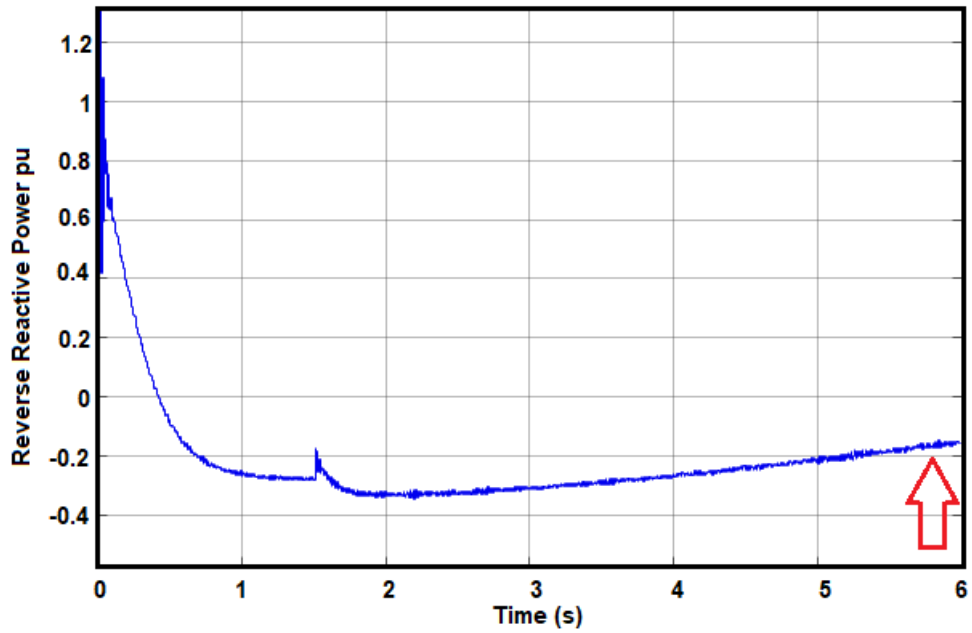

Fig. 5.14: Reverse Reactive Power at 60% PV Penetration with Proposed CAPR strategy

5.2.3 Impact of Proposed CAPR Strategy on the PV Array Output Parameters such as the PV output Power, Voltage and Current.

The proposed CAPR ramps down the PV output power from 3kW to 2.37 kW as shown in Fig. 5.15 which is due to the increases the off time of the PWM signal, thereby absorbing reactive

power and reducing the PWM signal on time, and this results in the DC link capacitor being charged. This action forces the PV output voltage to move towards its open circuit voltage (301.8 V) as shown in Fig 5.16 and reducing the PV output current from 12 A to 7.87A as shown in Fig 5.17. The degree of ramping down of these parameters depends on the reactive reference Q^*_{ref} which is based on the regulation of the controlled I^*_c current.

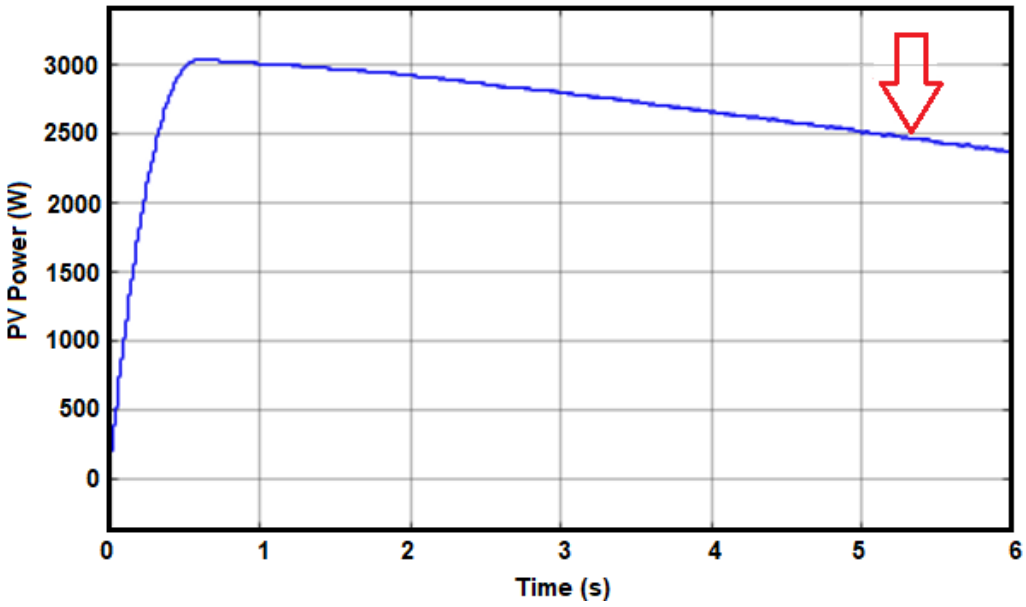

Fig. 5.15: PV output power (2376 W) with proposed CAPR strategy

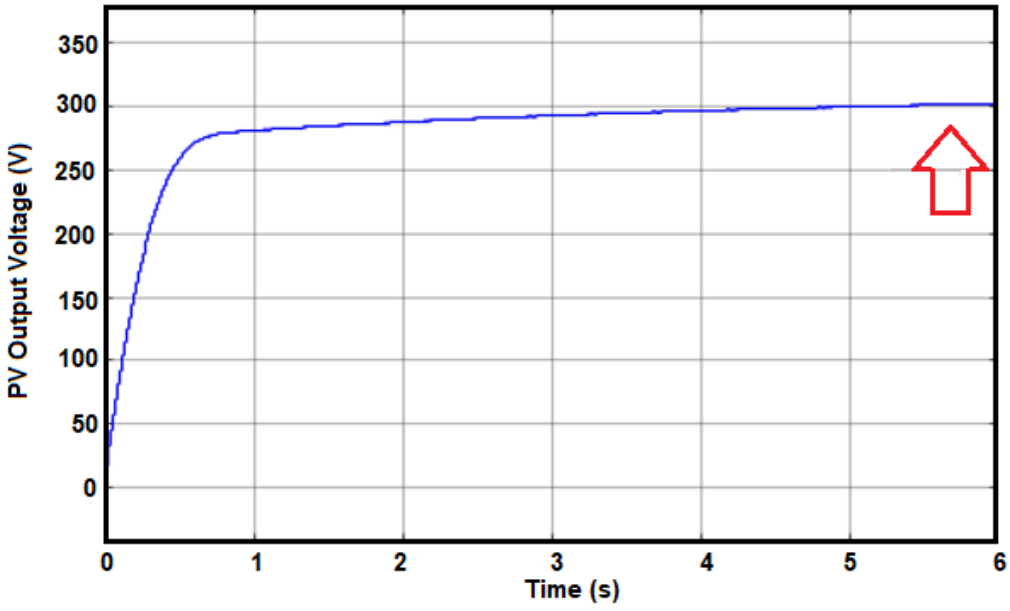

Fig. 5.16: PV Output Voltage Push Towards open circuit voltage (301.8 V)

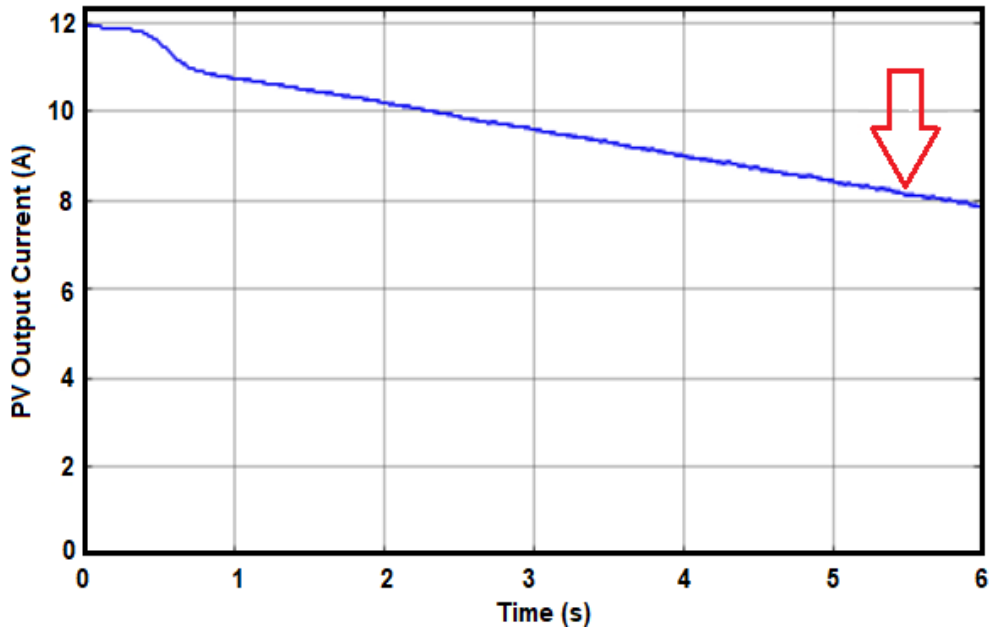

Fig. 5.17: PV Output Current Push Down (7.87 A)

5.3 Summary

The methodology of the proposed CAPR technique was analysed and used to investigate the impact of 60% penetration of PV arrays on a 200m long LV distribution network. The technique used is based on Proportional integral PWM current controller with a reactive component reference which is based on the regulation of the DC link capacitor current. From the results in section 5.2, it can be seen that the control technique was able to control the voltage rise below the +5% of the standard voltage limit and it also shows a slight reduction of the reverse power flow (both active and reactive).

Chapter 6

Comparison of the Proposed Active Power Reduction Strategy with BESS and D-STATCOM

In this Chapter, BESS and D-STATCOM were introduced into the system to address the impact of the high PV penetration on the scaled LV distribution network. D-STATCOM was selected because it is the most effective, flexible alternating current transmission system (FACTS) device available for distribution networks. It has a fast response time when compared to other FACTS devices like a static Var compensator (SVC), and it can be dynamically controlled to regulate voltage by either absorbing or injecting reactive power into the distribution network. The dynamic flexibilities and capabilities of the D-STATCOM for voltage rise mitigation are analysed. BESS was also selected because it is an established technique for voltage rise mitigation. It also possesses sub-second response capability that can be utilized to offset the sudden changes in PV output. The results obtained from the proposed CAPR strategy are compared with those obtained using BESS and D-STATCOM. The analysis was based on the effect of the strategies on voltage rise issues, reverse power flow, network losses and system response time.

6.1. Distributed Static Compensator (D-STATCOM)

FACTS devices such as Static VAr Compensators, fixed or passive capacitor banks and dynamic voltage restorers (DVR) are matured technologies in power systems and can be used

in transmission and distribution networks to regulate voltage during a voltage disturbance. However, these devices have some drawbacks such as poor dynamic performance, fail under LV conditions, etc. [156]. but with the introduction of D-STATCOM, these drawbacks can be addressed in the distribution network.

D-STATCOM is a promising and mature device with fast dynamic response that can provide voltage stabilization, voltage regulation, harmonic control, power factor correction, voltage flicker suppression, and sustain reactive current at LV level, and can be used for voltage and frequency support by changing the capacitors with an energy storage system (ESS) [157] [158] [159]. D-STATCOM technology is a three-phase shunt bi-directional power electronic device (converter) and is mostly connected close to the load and can be used to supply and absorb reactive power. The D-STATCOM components consist of a DC storage capacitor, a three-phase inverter with either Thyristors or IGBTs as switches, PWM gate pulse, AC filter inductor, and a control system which maintain the voltage across the inverter DC storage capacitor as shown in Fig 6.1. Basically, the output voltage of the D-STATCOM must be in phase with the LV distribution network voltage so that there will be no exchange of active power between the D-STATCOM and the grid but allows only reactive power exchange either by absorption or injection which is due to the change in the amplitude of the D-STATCOM output voltage. That is, D-STATCOM will operate in capacitive compensation mode if the D-STATCOM output voltage is greater than the voltage at the PCC (terminal voltage) or in an inductive compensation mode if the voltage at the PCC is greater than the D-STATCOM output voltage [159].

D-STATCOM is an established technology used in the industry to control voltage sag at the bus level caused by arc furnaces in the steel manufacturing industries [160] [161]. Some researchers [162] [163] have also investigated the flexibilities and capabilities of the D-STATCOM to improve power quality and regulate the system voltage in LV distribution

networks. Therefore, in this thesis, D-STATCOM will be designed and used to control the voltage within the standard voltage limit of -5% ≤ V ≥+5% at the PCC of the scaled LV distribution network with high PV penetration.

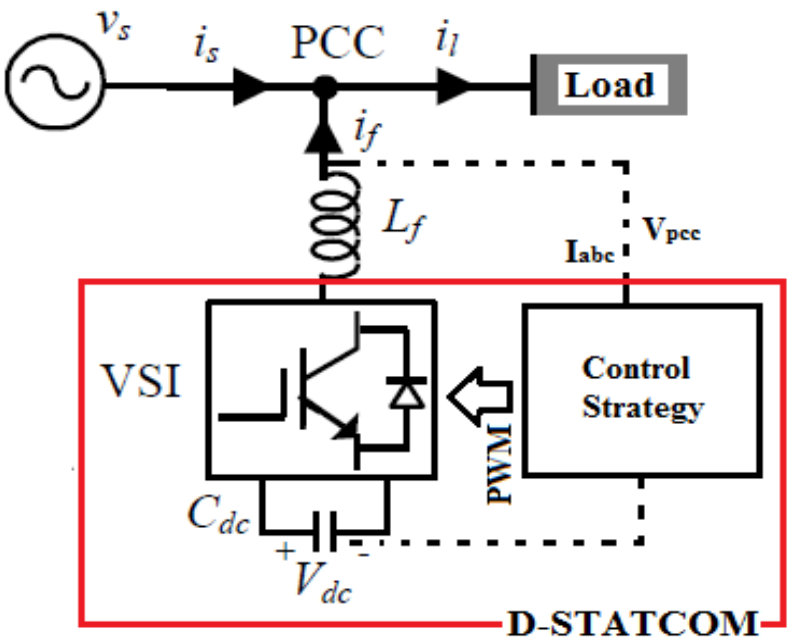

Fig. 6.1: Structure of a Three Phase Three Wire D-STATCOM

6.2 Switching Strategies for D-STATCOM

The technological advancement in power electronic devices has led to the development of low switching loss IGBT's which has resulted in a paradigm shift from the fundamental frequency switching to pulse width modulation (PWM) strategy for D-STATCOM application [156]. The generated PWM signals (pulses) are used for triggering the VSI switches as shown in Fig 6.1. It is reported that the generation of the PWM pulses applies to the different control scheme for D-STATCOM. The different control schemes used in the D-STATCOM are phase shift control, carrier-based PWM control, and carrier less hysteresis control. In this thesis, the carrier-based PWM control algorithm is used because it incorporates a self-supporting DC bus, it is easy to implement, inherently linear, and robust. The PWM control algorithm was modelled and simulated to regulate the voltage at the PCC as shown in Fig 6.2 The PWM

carrier-based algorithm is based on instantaneous power theory, where the voltage and current are transformed into a synchronous rotating reference frame using park's transformation. This allows for independent control of I_d and I_q components of the PWM carrier-based algorithm so as to facilitate the exchange of reactive power using a DC bus voltage controller and the terminal or PCC voltage controller.

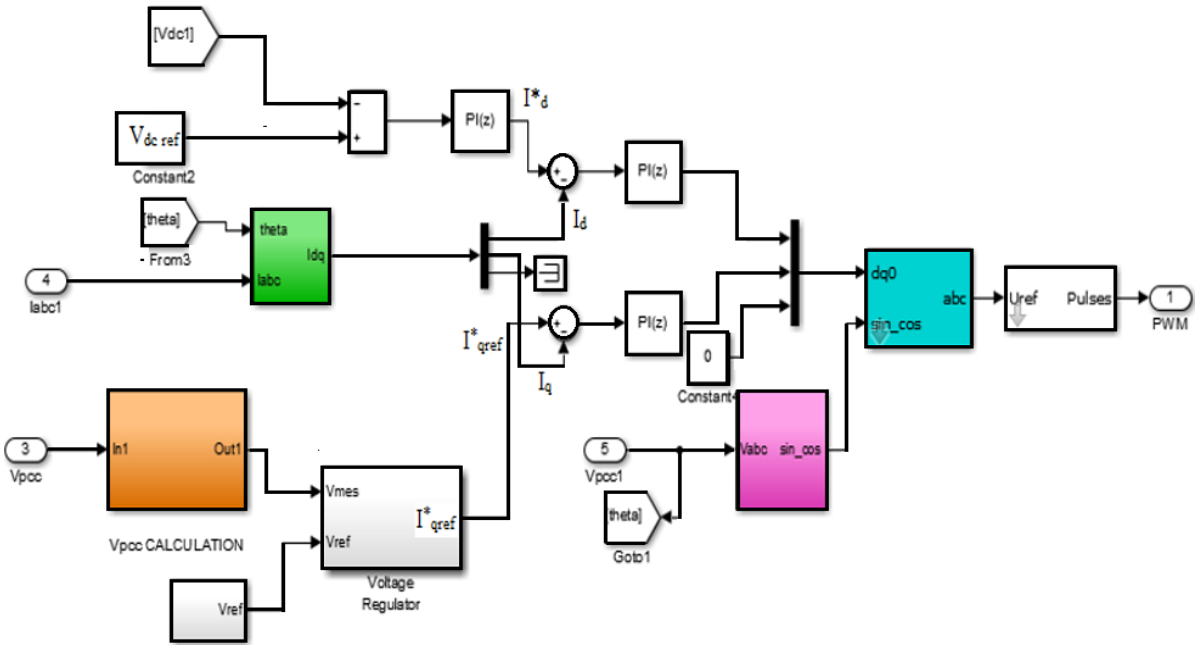

Fig 6.2: Algorithm of Carrier-Based PWM Control of D-STATCOM Implemented in MATLAB/Simulink

6.2.1 Analysis of the D-STATCOM Control using Carrier Based Algorithm

The PWM pulse signal of the carrier-based algorithm is generated from the measurement and control of the terminal voltage at the PCC, and the D-STATCOM DC side voltage. These measurements and proportional – integral (PI) controllers are used to generate the active and reactive components that are used to compare the d-q component of the grid current, and the error is used to generate the V_d and V_q components of the modulating signal (the carrier signal) of the SPWM. The control equations of the terminal (V_{pcc}) and DC side voltage of the D-STATCOM are discussed below. The transfer function used for designing PI regulator gain for the VPCC measurement in the D-STATCOM is given as:

$$G_D = \frac{1}{R+sL} \tag{6.1}$$

where G_D is the plant of the system, R is the line resistance, and L is the line inductor

A. *D-STATCOM VPCC Voltage Control*

The amplitude of the voltage at the PCC (V_{pcc}) is measured as shown in Eqn. (6.2) and compared with the desired PCC voltage ($Vpcc\_{ref}$), and the error at the nth sample instant is given in Eqn. (6.3) [156]:

$$V_{pcc} = \sqrt{(\frac{2}{3}){V_{sa}}^2 + {V_{sb}}^2} + {V_{sc}}^2 \tag{6.2}$$

$$V_{error(n)} = V_{pcc\_ref} - V_{pcc(n)} \tag{6.3}$$

where V_{sa}, V_{sb}, and V_{sc} are the system terminal (PCC) phase voltages and $V_{error(n)}$ is the difference between the reference voltage and the measured voltage

The error established in that sample instant is fed into an outer regulator (proportional integral controller (PI)) to generate the reference reactive current component (I^*_{qref}) as shown in Eqn (6.4).

$$I^*_{qref(n)} = I^*_{qref(n-1)} + K_{OP}\left(V_{error(n)} - V_{error(n-1)}\right) + K_{OI}V_{error(n)} \tag{6.4}$$

where K_{OP} and K_{OI} are the proportional and integral gain of the outer PI regulator of the terminal voltage that is the voltage at the PCC.

The V_q is generated from the inner controller after comparing the I^*_{qref} component at the nth sample instant, to the network current I_q which is generated from the Park's transformation (abc to dq components).

The value of I_q is generated using the park's transformation (abc to dq) over the load current. The $I^*_{qref(n)}$ and I_q components are compared and the error is fed to the inner PI regulator to generate V_q.

$$I^*_{qref(n)} = I^*_{qref(n)} - I_{q(n)} \tag{6.5}$$

$$V_{q(n)} = V_{q(n-1)} + K_{inP}\left(I^*_{qref(n)} - I^*_{qref(n-1)}\right) + K_{inI} I^*_{qref(n)} \tag{6.6}$$

where K_{inP} and K_{inI} are the proportional and integral gain of the inner PI regulator of the voltage measured at the PCC.

B. *D-STATCOM DC Capacitor Voltage Control*

The DC terminal voltage of the D-STATCOM is controlled by comparing the capacitor voltage at the DC side (V_{dc}) of the D-STATCOM with the reference or desired voltage (V_{dc_ref}) at the nth sampling time as shown in Eqn. (6.7)

$$V_{dc\_error(n)} = V_{dc\_ref} - V_{dc(n)} \tag{6.7}$$

where $V_{dc\_error\ (n)}$ and $V_{dc\ (n)}$ are the DC voltage error and the sensed DC voltage of the D-STATCOM at the nth instant.

The DC voltage error in Eqn. (6.7) is fed into a PI regulator to generate the reference d-component as given in Eqn. (6.8)

$$I^*_{dref(n)} = I^*_{dref(n-1)} + K_{dcP}(V_{dc\_error(n)} - V_{dc\_error(n-1)}) + K_{dcI} V_{dc\_error(n)} \tag{6.8}$$

where K_{dcP} and K_{dcI} are the proportional and integral gain of the D-SATCOM DC voltage regulator.

For the DC side outer regulator, the I_d generated from the measured Iabc grid current is compared to the reference component of Eqn. (6.8) as shown in Eqn. (6.9). Now, Eqn. (6.9) is then used to determine the V_d component of the carrier signal as shown in Eqn. (6.10).

$$I_{d\_error\,(n)} = I_{dref} - I_{d(n)} \tag{6.9}$$

$$V_{d(n)} = V_{d(n-1)} + K_{Pin}\left(I_{d\_error(n)} - I_{d\_error(n-1)}\right) + K_{Iin}I_{d\_error(n)} \tag{6.10}$$

where K_{Pin} and K_{Iin} are the proportional-integral gain of the inner d-component regulator of the D-STATCOM DC voltage.

From the analysis, Eqn. (6.5) and Eqn. (6.10) are converted to the sinusoidal carrier signal that is used to generate the PWM pulses which control the absorbed or injected reactive power.

6.3 Design, Modelling and Simulation of D-STATCOM with High PV Penetration on an LV Distribution Network

To demonstrate the impact of D-STATCOM in term of voltage rise issues in the scaled LV distribution network with high PV penetration, several key parameters of the D-STATCOM such as DC link voltage, DC capacitor value and interface AC inductor (filter) need to be determined (see Fig 6.3). These key parameters are the deciding factors for determining the reactive power to be injected or absorbed by the D-STATCOM to regulate the voltage at the PCC when the voltage rise situation occurs. As shown in Fig 6.3, the D-STATCOM was placed 50m away from the load so as to operate within a wider range. In this thesis, the key parameters of D-STATCOM such DC link voltage (V_{dc}), DC capacitor (C_{dc}) and interface filter (L_f) are determined and calculated using Eqn. (6.11) to Eqn. (6.14) [164] [165] [166].

The DC link voltage (V_{dc}) is determined based on the available instantaneous energy at the D-STATCOM and it can be calculated using Eqn. (6.11).

$$V_{dc} = \frac{2\sqrt{2}V_{L-L}}{m\sqrt{3}} \tag{6.11}$$

where *m* is the modulation index, $V_{L\text{-}L}$ is the line to line AC output voltage of D-STATCOM.

To determine the D-STATCOM DC capacitor, the principle of energy conversation is applied and used to estimate the capacitor value as given in Eqn. (6.12).

$$\frac{1}{2}C_{dc}[V_{dc}^2 - V_{dc1}^2] = 3V_{Ph}(\alpha I)t \tag{6.12}$$

where V_{ph} is the phase voltage, I is the phase current, V_{dc} is the DC voltage, V_{dc1} is the minimum DC voltage, α is the overloading factor while t is the recovery time of the DC voltage.

According to [122], the response time *(t)* of the STATCOM is typically between 200μs to 350μs while the overloading factor may likely vary from 1.2 to about 1.8 because, during transients, the current rating of the D-STATCOM varies from 120% to 180% of the steady-state value [167]. The value of the inverter side inductor can be calculated to filter high-frequency components on the AC side. The inductor value depends on the current ripple, DC link voltage, and switching frequency. The current ripple can be selected from 10% to 20% of the inductor rated current. The inductor can be calculated using Eqn. (6.13).

$$L_f = \frac{mV_{dc}\sqrt{3}}{12\alpha f_s I_{Cr(p-p)}} \tag{6.13}$$

where f_s is the switching frequency, $I_{cr\ (p\text{-}p)}$ is the current ripple.

The D-STATCOM VAR rating can be calculated using the following equation;

$$VAR = \omega * C_{dc} * V_{L-L}^2 \tag{6.14}$$

where ω is the angular frequency (314.2 rad/sec), $V_{L\text{-}L}$ is line to line voltage

The calculated parameters are listed in Table 6.1. See complete system in MATLAB®/Simulink® in Appendix. D

Table 6.1: Parameters of Modelled D-STATCOM and System

D-STATCOM and system Parameters	
DC capacitor	304µf
DC link Voltage	300V
Interface inductance	22mH
Switching frequency	20kHz
D-STATCOM Var rating	3kVar
System line voltage (RMS)	125 V
Fundamental frequency	50Hz
Terminal Voltage (PCC) controller gain, K_{OP}, K_{OI}	K_{OP} = 0.8, K_{OI}=500
PI regulators K_{Pin}, K_{Iin}	K_{pn},= 0.0088 K_{in}= 0.0054

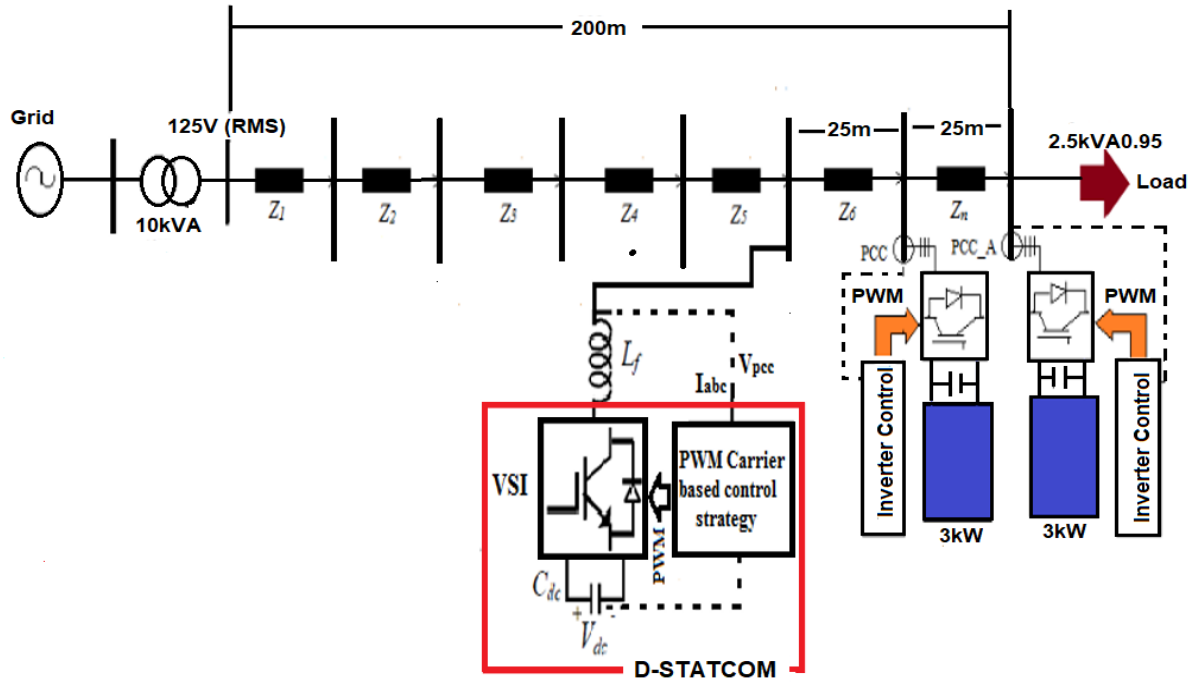

Fig. 6.3: A Simple Scaled Down Radial LV Network with D-STATCOM and High PV Penetration

6.4. Discussion of Simulation Results

The simulation is performed on the scaled down radial LV distribution network with high PV system penetration (60% penetration level) and the D-STATCOM as shown in Fig 6.1 using MATLAB/Simulink® environment. The results show the effect of D-STATCOM with 60% PV

penetration on the parameters of the LV distribution network. See Appendix E for configuration and control of D-STATCOM in MATLAB®/Simulink®.

6.4.1. Impact of D-STATCOM on Voltage Profile of the Scaled-Down Radial LV Distribution Network with 60% PV Penetration

The D-STATCOM regulates voltage by either supplying reactive power to improve voltage or absorbing reactive power to reduce the system voltage. In our investigation, the D-STATCOM was introduced into the LV distribution network in 1.5s when the voltage profile is above the voltage upper set limit of +5 %. From Fig. 6.4 and Fig. 6.5, the voltage profile at the load PCC was reduced from 1.067 p.u to 1 p.u when the D-STATCOM was injected. The LV distribution network current was simultaneously increased from 0.3 pu to 0.382 p.u as shown in Fig. 6.6 and Fig. 6.7.

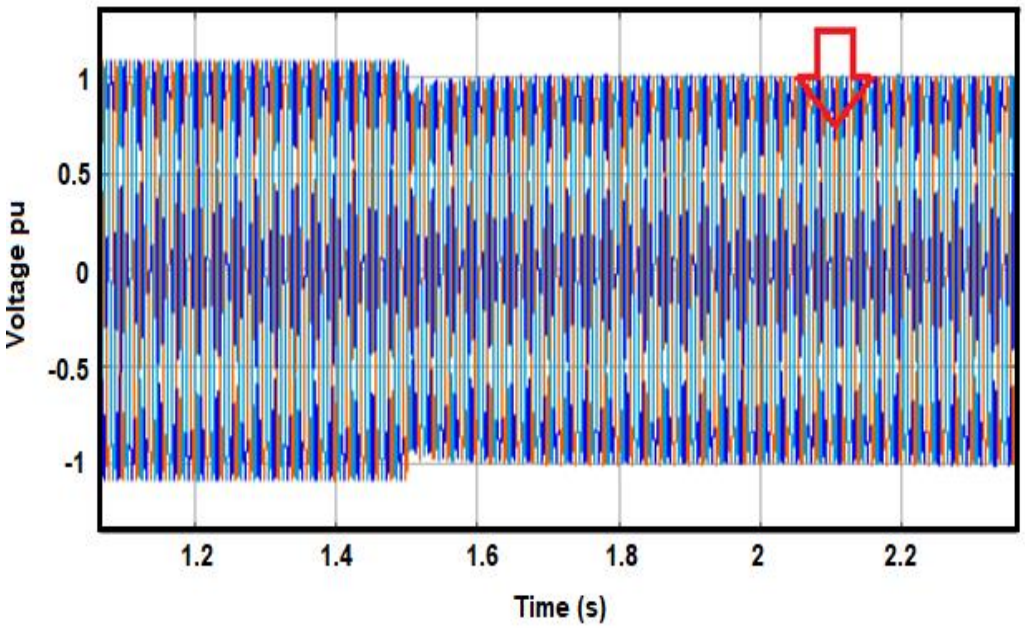

Fig. 6.4: Voltage Waveform at PCC after Introduction of D-STATCOM at 1.5s

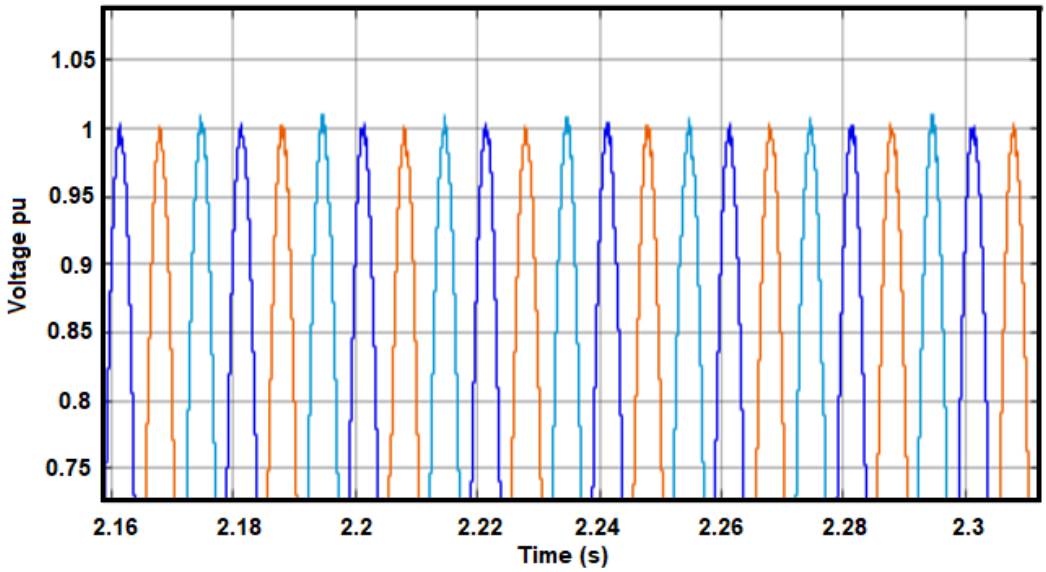

Fig. 6.5: Voltage at PCC Reduce to 1pu with D-STATCOM Application at 1.5s

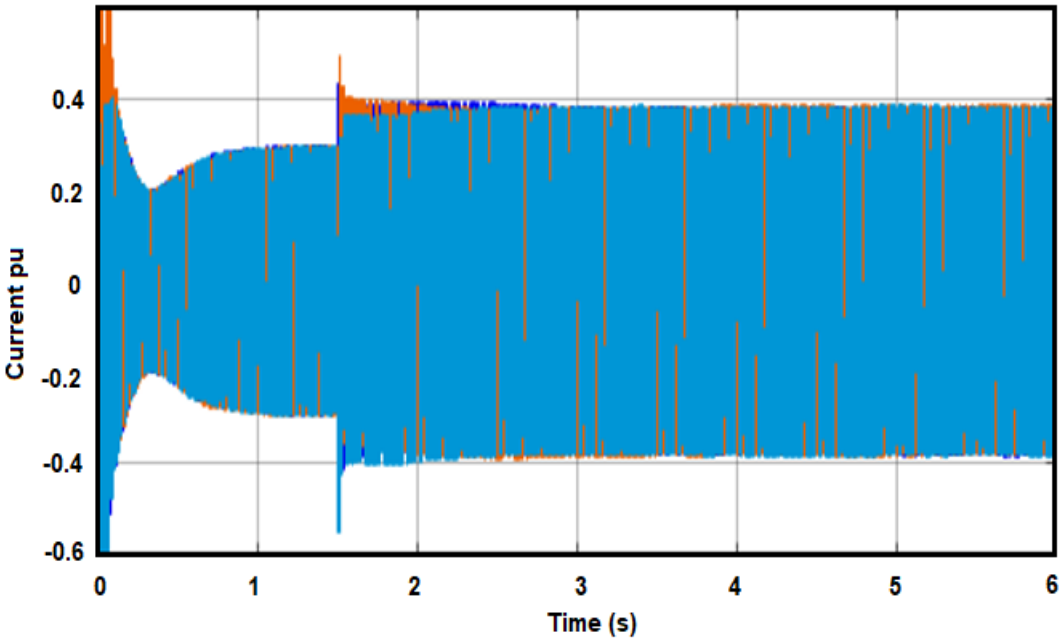

Fig. 6.6: Current Waveform in Distribution Network with D-STATCOM

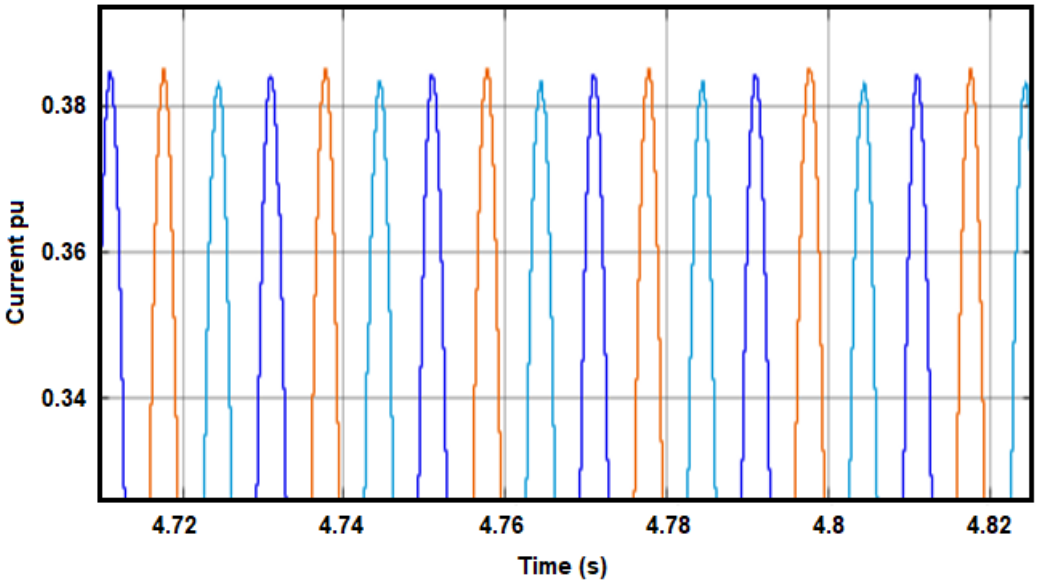

Fig. 6.7: Network Current Increased to 0.382 (pu) with D-STATCOM Application at 1.5s

6.4.2. Impact of D-STATCOM on the Power flow of the Scaled-Down LV Distribution Network

The injection of D-STATCOM in 1.5s into the LV distribution network was to regulate the system voltage and maintain stability in the system. By introducing the D-STATCOM at 1.5s in the LV distribution network system, we were able to maintain the maximum level of PV penetration while reducing the voltage, the reverse active and reactive power. As observed in Fig. 6.8, the reverse active power was slightly reduced from 0.37 pu to 0.35 p.u. The reactive power was reduced from 0.27 at 60% PV penetration to 0.1 p.u when the D-STATCOM was applied as shown in Fig. 6.9.

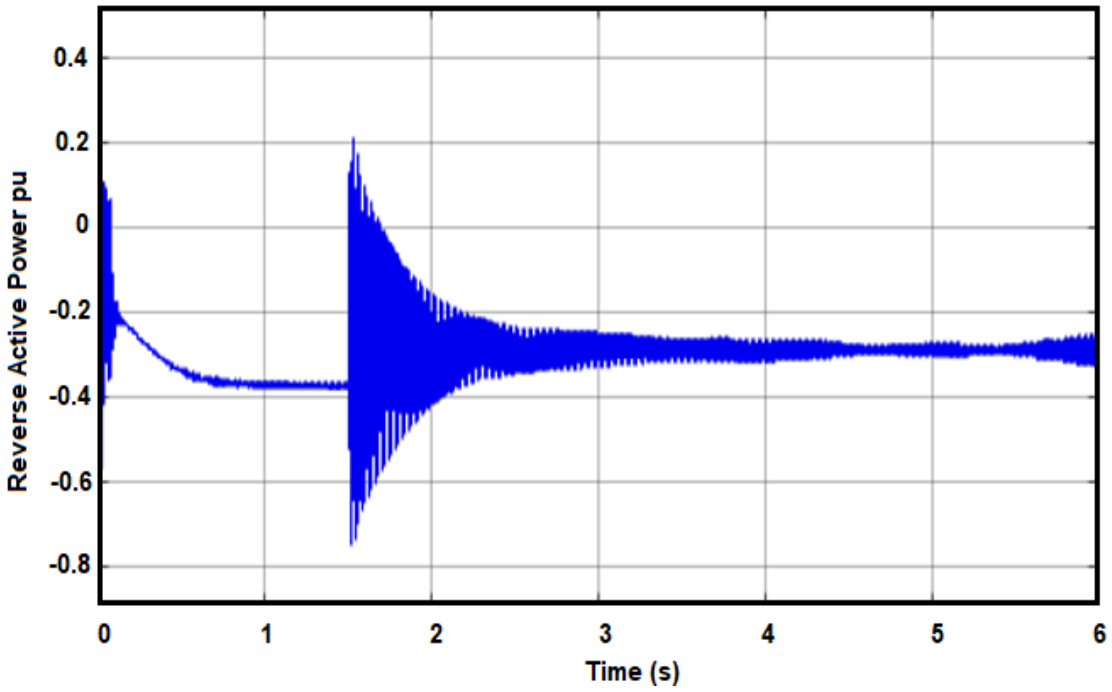

Fig. 6.8: Reverse Active Power when D-STATCOM and High PV are Applied on the LV network

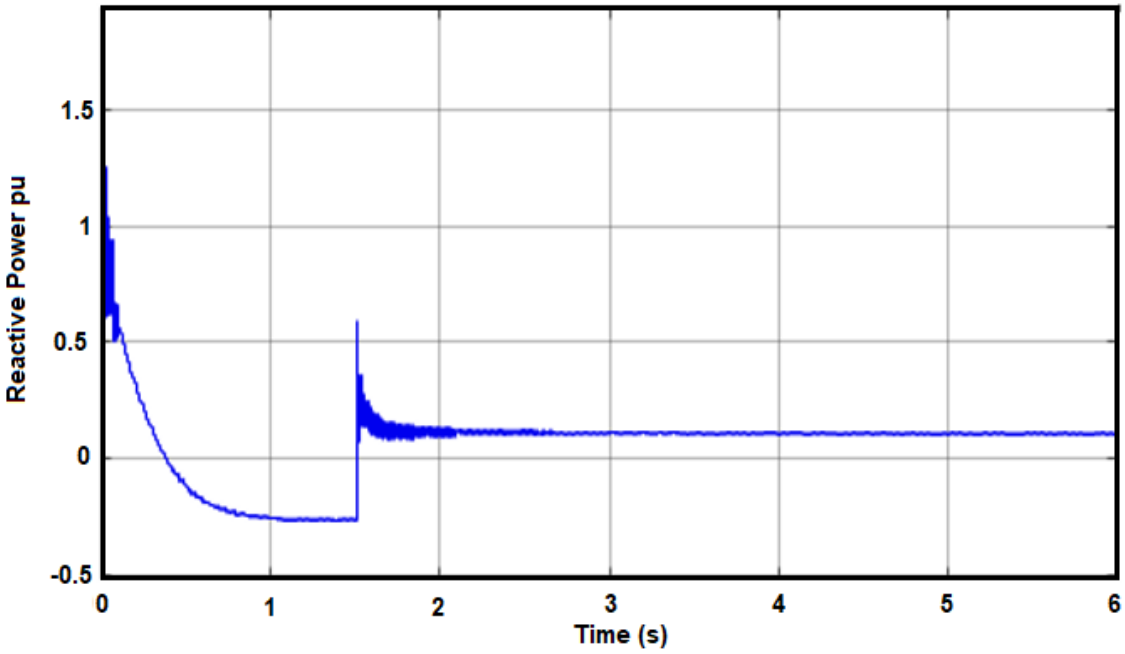

Fig. 6.9: Grid Supply Reactive power to Network with D-STATCOM

6.5. BESS for Voltage Rise Mitigation

Voltage control is usually the responsibility of the utilities during disturbance (e.g. Voltage rise or voltage dip) on the MV and LV distribution network. However, BESS can be used to curtail voltage disturbance in the distribution network by limiting the active power (controlling active power ramping) of the PV system. This function of the BESS helps to keep the system voltage within specific limits during high PV penetration or cloudy conditions. In most cases, The BESS is used to ramp the inverter output power during voltage fluctuations in the distribution system. The BESS is used because it possesses sub-second response capability that can be utilized to offset the sudden changes in PV output which affects the power quality [59]. The BESS's are used to slow down (ramp down) the PV output during voltage disturbance. A Coordinated BESS tied to the PV array can act as a damper to reduce or ramp down the grid-tied PV inverter output power. In addition to PV power curtailment, BESS can also be used to regulate the grid frequency, emergency power, peak power shaving and grid healing. The objective of this section is to analyze the operation of the BESS to reduce or ramp down the inverter output power in order to curtail voltage rise situations.

6.6. BESS Operation

A MATLAB/Simulink® modelled BESS without temperature effect is used theoretically in this section to reduce the PV inverter output power to curtail the voltage rise situation during high PV penetration in a scaled down LV distribution network. When the voltage at the PCC is greater than the standard voltage limit (±5%), the BESS is activated to store some of the PV power so that the power received by the grid via the inverter reduces. When the voltage at the PCC does not exceed the standard voltage limit (±5%), the BESS does not interfere with the output power of the PV array. At that point, it is considered as normal operation and the output power of the PV array via the PV inverter goes directly to the grid.

The BESS control system checks the voltage at the PCC in every second and when the voltage at the PCC exceeds the standard voltage limit (±5%), the BESS is activated as shown in Fig. 6.10.

6.7. Simulation of BESS with High PV Penetration on an LV Distribution Network

This section demonstrates the impact of BESS to reduce the inverter output power and to curtail the voltage rise situation on a scale down LV distribution network. In our investigation, a lead acid battery type modelled by MATLAB/Simulink was selected and used in our investigation. See Appendix F for different battery type. A 200Ah Battery at 48V with about 40% SOC was used in the simulation as shown in shown in Appendix F. The energy absorb by the BESS is determined by the voltage at the PCC over a given time interval (i.e the voltage level above ±5%). It is only required to temporarily absorb some amount of the PV power so as to reduce the voltage at the PCC during high PV penetration. The BESS is connected in parallel with the individual PV array as shown in Fig. 6.10. In the analysis, the ramp rate control of the BESS was not investigated.

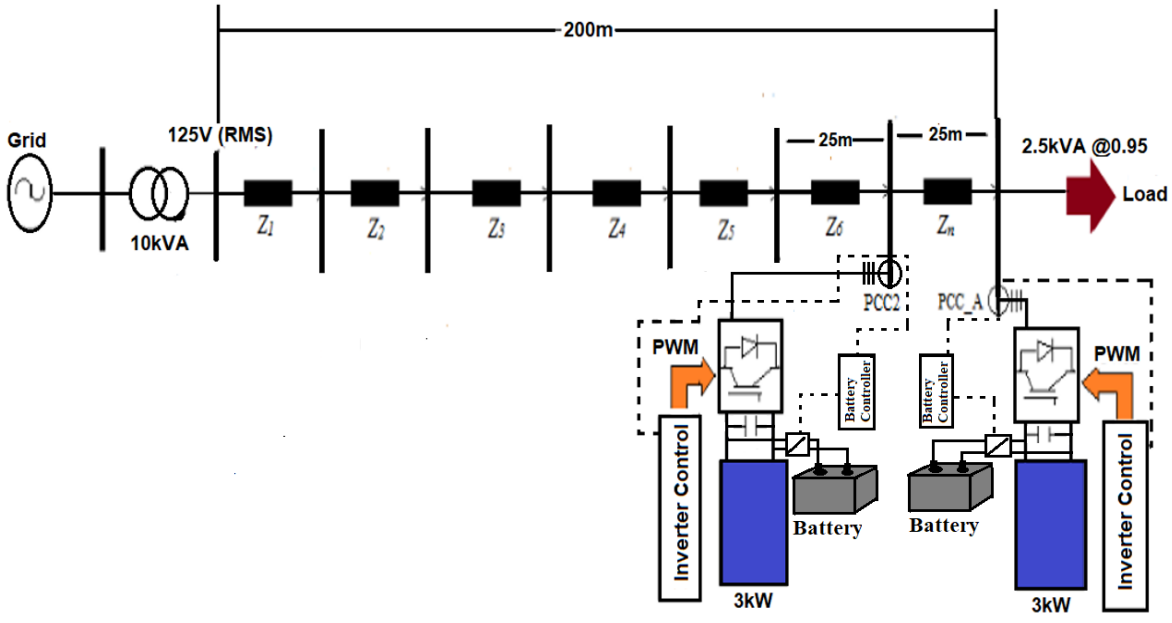

Fig. 6.10. A Simple Scaled Down Radial LV Network with BESS and High PV Penetration

6.8. Discussion of BESS Simulation Results

The MATLAB/Simulink® environment was used to simulate the inverter controllers, BESS and PV penetration level (60%) as shown in Fig. 6.10. See Appendix F for BESS and 60% PV penetration.

6.8.1. Impact of BESS on Voltage Profile and Network Current of the Scaled-Down Radial LV Distribution Network with 60% PV Penetration

BESS strategy is implemented using MATLAB/Simulink® environment to mitigate voltage rise issues with high PV penetration on a scaled down LV distribution network. The result shows that the voltage profile at the PCC is reduced from 1.067 pu to 1.038 pu when the BESS was activated as shown in Fig. 6.11 and Fig. 6.12. The change in the voltage profile is as a result of the reduction of the inverter power due to the absorption of some of the PV array power by the BESS. The LV distribution network current was reduced from 0.3 pu to 0.241 pu as shown in Fig. 6.13 and Fig. 6.14.

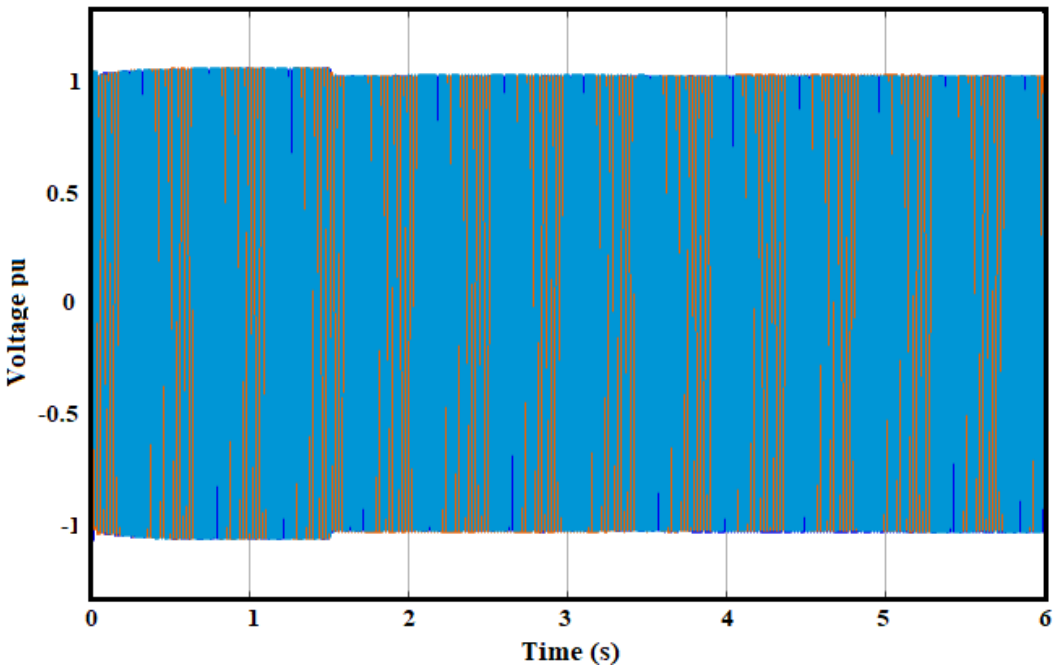

Fig. 6.11. Voltage Wave at PCC after Introduction of BESS

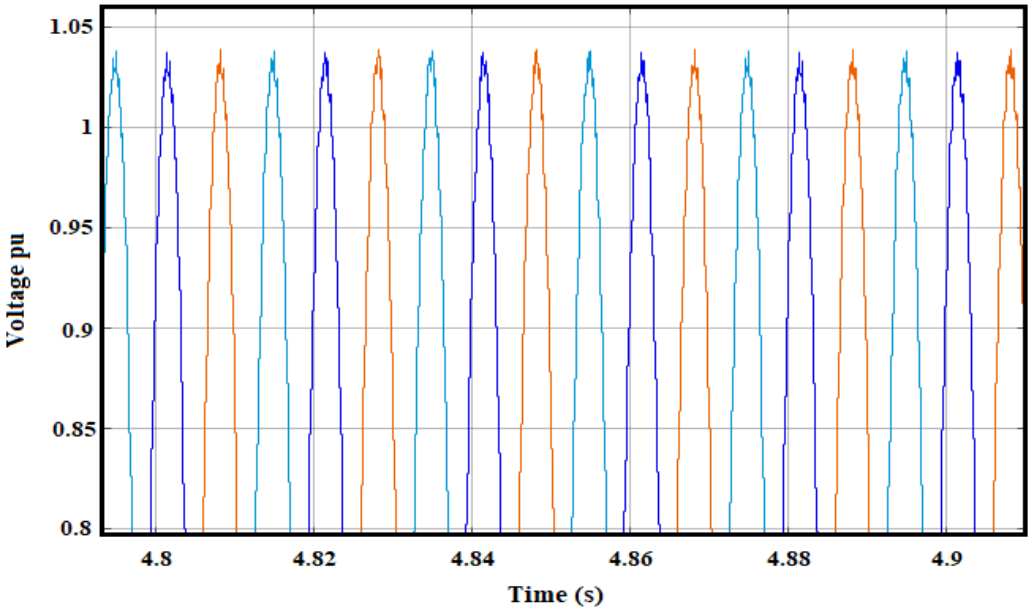

Fig. 6.12. Zoomed Voltage Profile at PCC Reduced to 1.038 pu with BESS

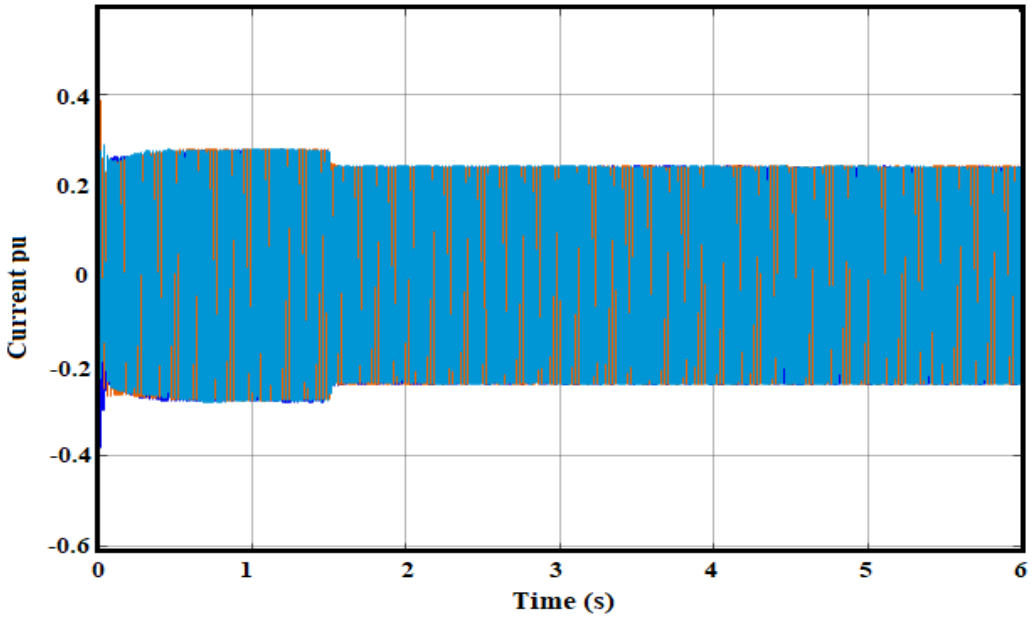

Fig. 6.13. Current Waveform in the Distribution Network with BESS

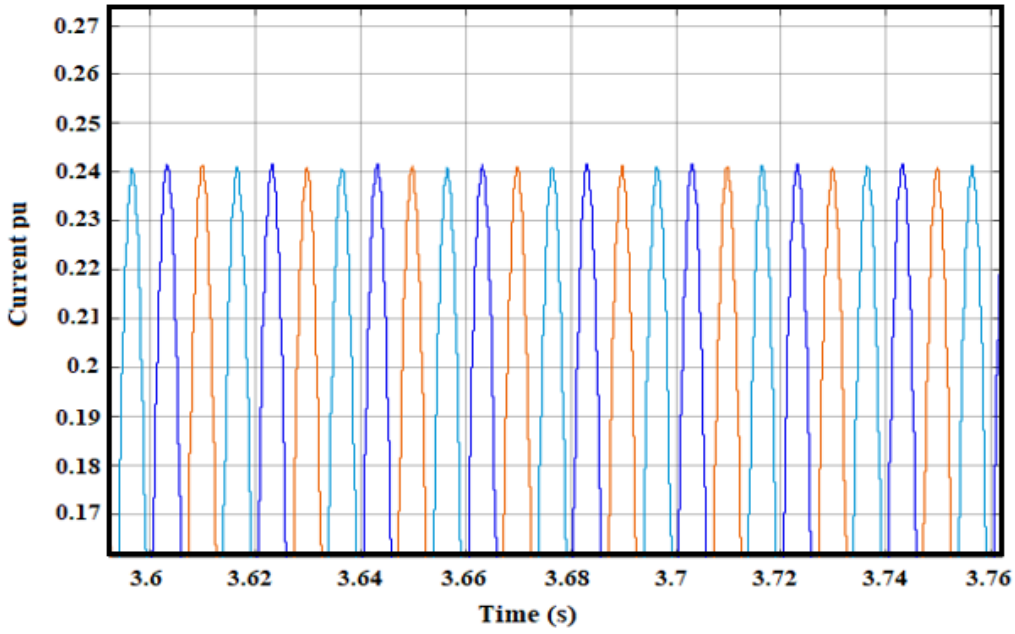

Fig. 6.14. Zoomed Distribution Network Current Reduced to 0.241 pu with BESS

6.8.2. Impact of BESS on the Power flow of the Scaled Down LV Distribution Network

It is observed from Fig. 6.15 and Fig. 6.16 that the introduction of BESS reduces the active and reactive power flow in the LV radial distribution network to maintain the voltage at the PCC within the standard voltage limit of ±5%. The reverse active power was reduced from 0.37 pu at 60% PV penetration to 0.33 pu when the BESS was connected in parallel with the PV array as shown in Fig. 6.15. This is because the individual PV array powers were reduced from 3 kW to 2.7 kW by the BESS. The system reactive power was also reduced from 0.27 pu at 60% penetration to 0.13 pu when BESS was introduced as shown in Fig. 6.16.

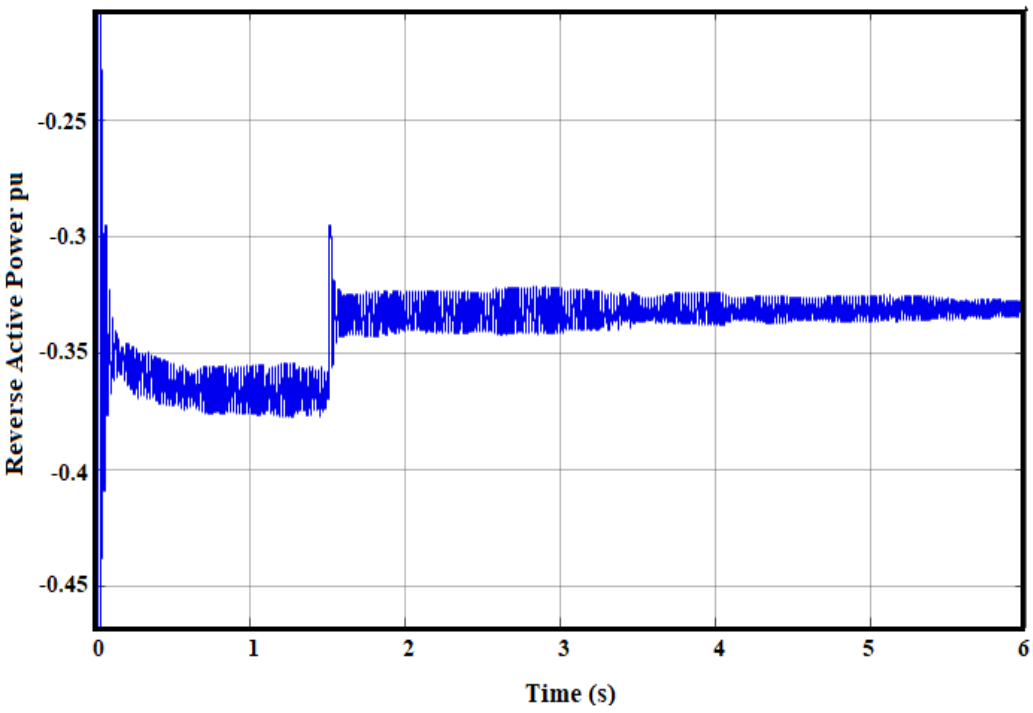

Fig. 6.15. LV Network Reverse Active Power Flow with BESS

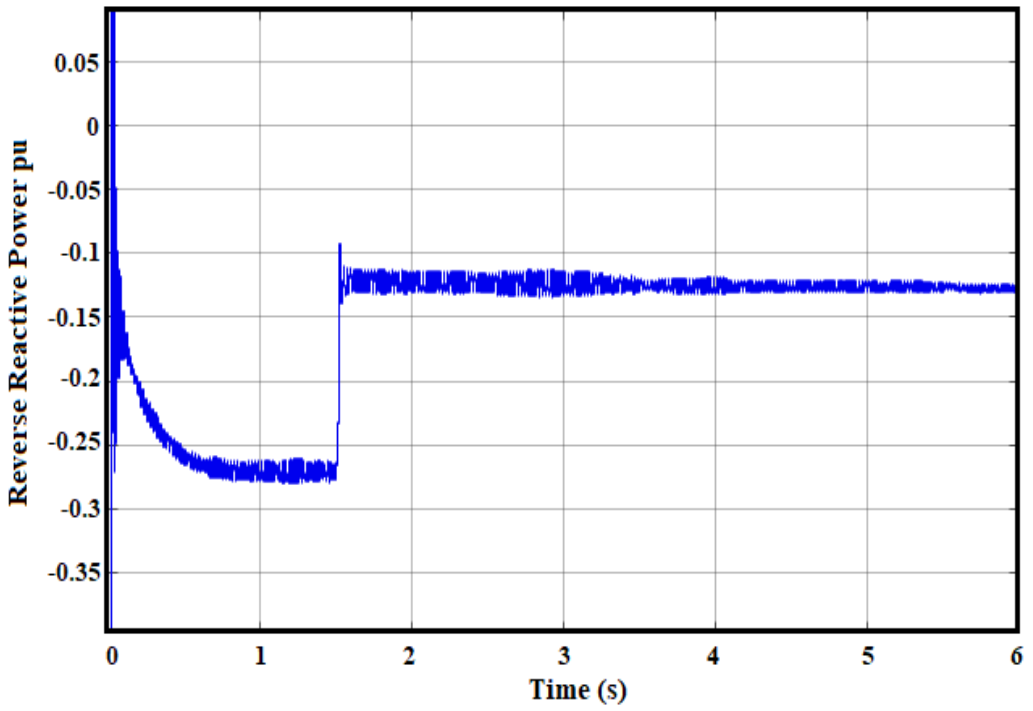

Fig. 6.16. LV Network Reverse Reactive Power Flow with BESS

6.9. Comparison between Proposed CAPR Strategy, BESS and D-STATCOM

To evaluate the effectiveness of the proposed CAPR strategy, this section of the thesis compared the performance of the proposed CAPR strategy to BESS and a central compensator device (D-STATCOM) on the scaled down radial LV distribution. From the simulation results, we observed that the proposed CAPR strategy, BESS strategy, and the D-STATCOM device were able to reduce the voltage at the PCC below the upper voltage set limit of +5% with a 60% PV penetration as shown in Fig 6.17. Voltage rise at the PCC was gradually ramp down from 1.067 pu to 1.04 pu by the CAPR strategy and it took about 6s to reduce the voltage below the upper voltage set limits. This is because the threshold algorithm perturbs and observe while changing the controlled DC link current $I^{*}c$ to ramp down the voltage at the point at the PCC. The introduction of the BESS device reduces the PV inverter input power and this action brought down the voltage at the PCC from 1.067 pu to 1.038 pu. But when the D-STATCOM device was introduced in 1.5s, the voltage rise was reduced instantly from 1.067 p.u to of 1.0 pu which is the D-STATCOM reference voltage.

In terms of power flow, the proposed CAPR ramp down the VSI output power and this action reduced the reverse active power in the distribution network by 18.9%, while the BESS and D-STATCOM scheme slightly reduces the reverse active power by 10.8% and 5.4% respectively as shown in Fig. 6.18. The reverse power flow for the D-STATCOM is smaller because it is designed to control voltage and not power.

Figs. 6.19 and 6.20 show the impact of these voltage control strategies on the LV distribution network losses. From Fig. 6.19, we observed that when the LV distribution network experience 60% PV penetration, the losses increased from 214 W to 380 W which is about 77% increase. The introduction of BESS reduces the losses from 380 W to 245 W which is

about 35% reduction. This is due to the reduction of the PV inverter input power. But when D-STATCOM was applied to the system in 1.5s, the losses increase further from 380 W to 616 which resulted in about 140% increase from the initial state of 214 W. This is because the D-STATCOM reduces the voltage in the LV distribution network without reducing power and this action increases the line current of the LV distribution network. Reactive power losses were also increased due to the increases in the LV distribution network current. However, when the proposed CAPR strategy was used, the losses on the system were slightly increased from 214 W to 216 W in 6s which is about 0.9% increase as shown in Fig 6.19. From Fig 6.20, we also observed that the BESS and D-STATCOM provide faster and better response to voltage disturbance than CAPR but with increase losses, while the CAPR strategy mitigates voltage rise with a slower response but with better network losses and reverse power (both active and reactive) as shown in Fig 6.19 and Fig 6.20.

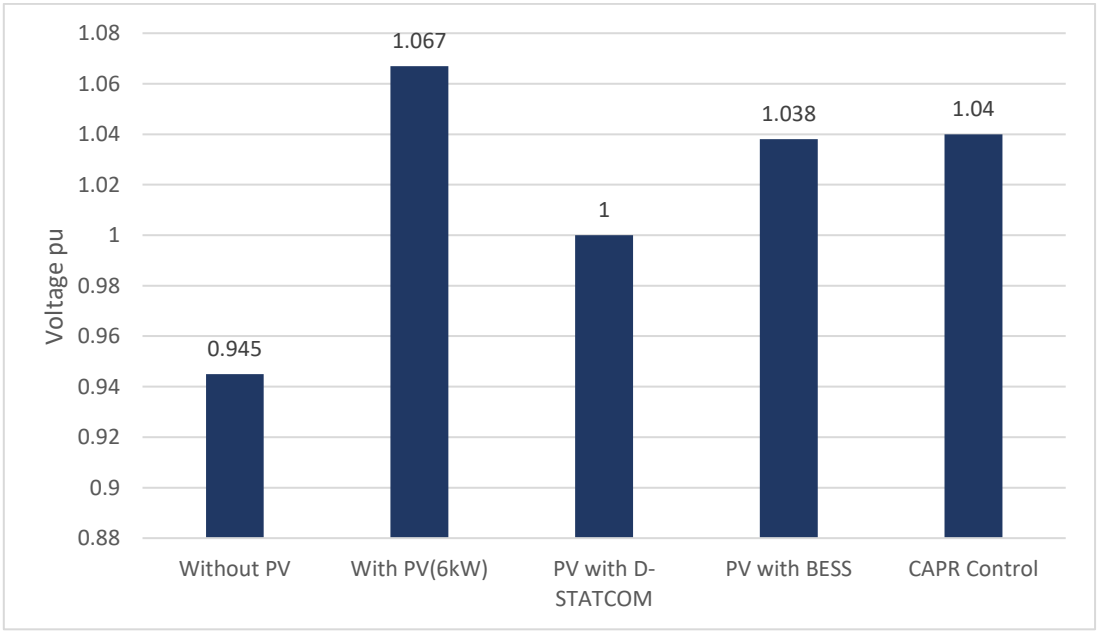

Fig. 6.17: Voltage at the PCC_A under Different Scenarios

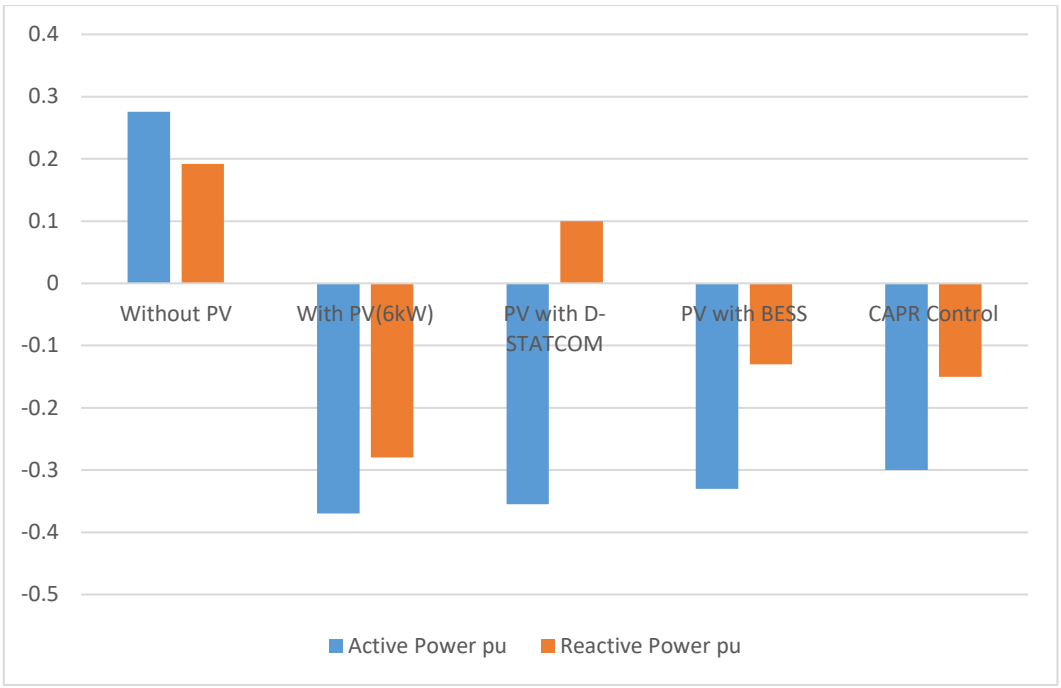

Fig. 6.18: LV Network Power Flow under Different Scenarios

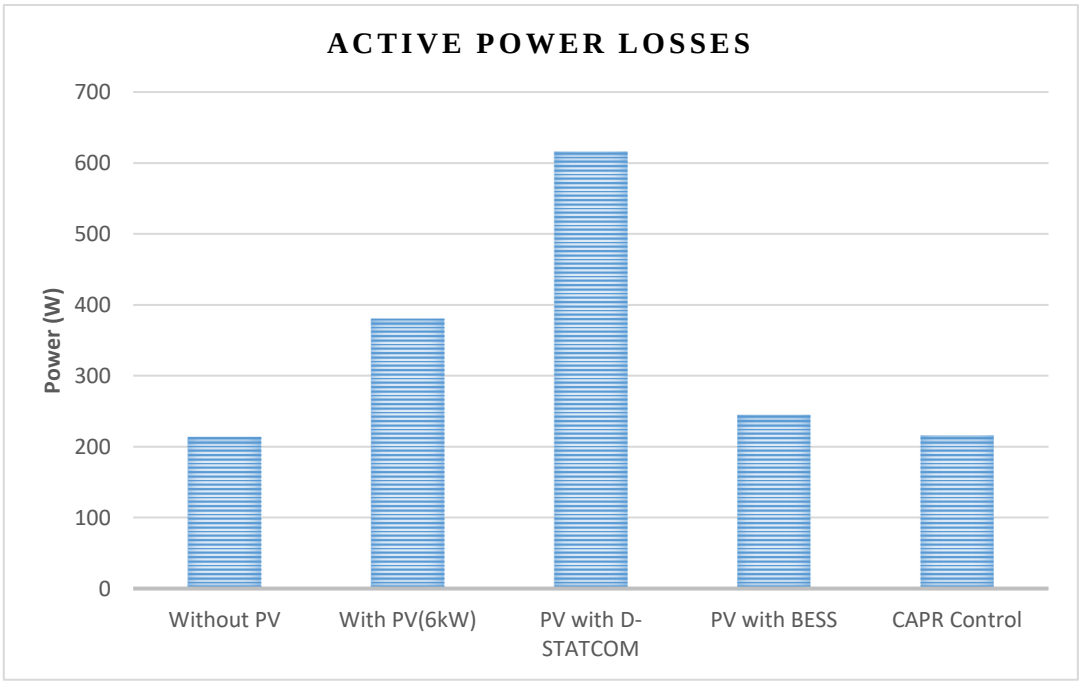

Fig. 6.19: Impact of Active Power Losses in the LV Network under Different Scenarios

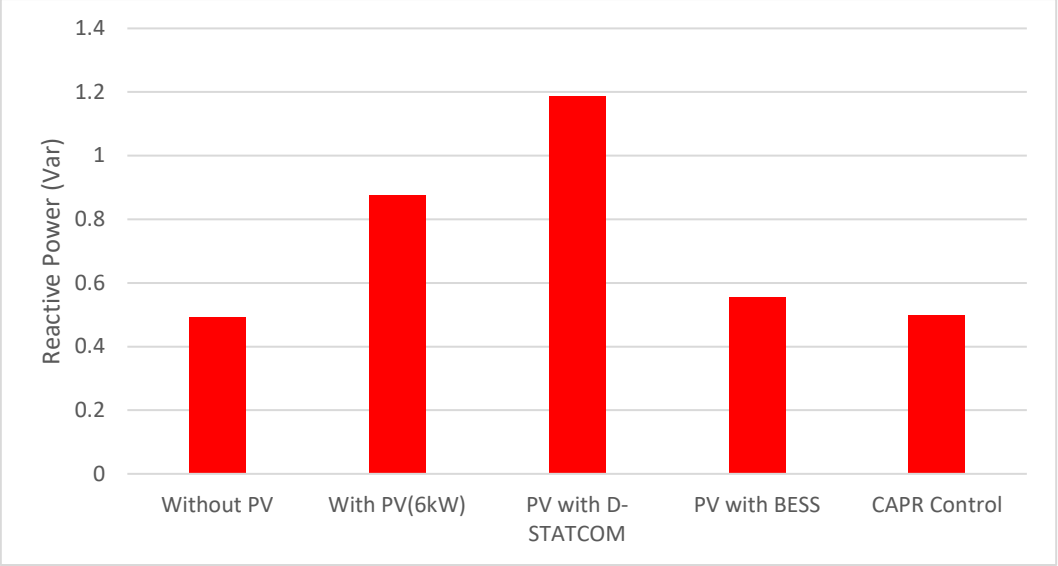

Fig 6.20: Impact of Reactive Power Losses in the LV Network under Different Scenario's

6.6 Summary

In this chapter 6, the performance of the proposed CAPR strategy was assessed by comparing it to the BESS and D-STATCOM devices. From the simulation results, it was found that the BESS and D-STATCOM were faster in terms of responding to the voltage rise issue when compared to the proposed control technique. The BESS and D-STATCOM perform very well with fast response to grid voltage disturbance and were able to regulate the voltage at the PCC within the voltage standard limit. However, the use of D-STATCOM also led to increased power losses due to increase network current. High losses can affect network conductors and may require grid reinforcement, this could be costly and a burden to DNOs. Installing D-STATCOM on every distribution network due to higher PV penetration will lead to cost burden on the DNOs considering the cost of D-STATCOM. The results demonstrated that the introduce BESS performs better than the D-STATCOM strategy in terms of losses (active and reactive) and reverse power flow according to Fig. 6.18 and Figs. 6.19 and 6.20 while the CAPR technique performs better than the BESS.

Chapter 7
Conclusion and Recommendation

7.1. Conclusion

The objective of the thesis is to investigate, analyse and develop a sudden voltage rise mitigation strategy for a radial LV distribution network with high PV system penetration. The simulations presented in chapter 4 show that by increasing the penetration of PV system on a radial LV distribution network, this may lead to some negative impacts such as sudden voltage rise, reverse power flow, increase line losses, increase voltage harmonics and transformer overloading. Based on the identified problems, DNOs favours disconnection of the PV systems from the LV network and this may cause disturbances leading to stability issues.

To address, the issue of sudden voltage rise, a CAPR was proposed. The proposed CAPR strategy which is based on the PI PWM current controller scheme proves to be effective in terms of ramping down the PV power during higher PV penetration in an LV distribution network. The CAPR strategy only kicks in when the voltage at the PCC is greater than threshold upper voltage set limit. The results obtained show that the proposed CAPR strategy was able to curtail voltage rise under higher PV penetration by ramping down the PV output power and keeping the voltage at the PCC within the standard voltage limit of ±5% on a simple scaled down radial LV distribution network as present in Chapter 5.

Finally, BESS and D-STATCOM devices were used to curtail voltage rise issues in the scaled down radial network and the results obtained in the investigation were compared with that of the proposed CAPR strategy. When comparing the devices for voltage rise mitigation, it was noticed from the simulation results that the BESS and D-STATCOM devices have a

faster response time when compared to the CAPR strategy. However, the D-STATCOM allows more PV power and this can lead to a high current and excess transformer loading which may require grid reinforcement. This could be costly for customers, DNOs, and utility. The BESS performs better than the D-STATCOM in terms of losses, and reverse power flow while the CAPR strategy performs better than both strategies in terms of losses and reverse power flow. The three voltage rise mitigation strategies reduce voltage within the acceptable voltage limit of ±5%.

7.2 Recommendation

The proposed CAPR strategy in this thesis has laid the foundation for an interesting direction to increase the effectiveness of the proposed method. An interesting research point will be further study of the control of the ramp output of the PV array so as to stabilize the ramp output voltage of the inverter when the voltage at the PCC is within standard voltage limits.

References

[1] W. Rickerson, C. Laurent, D. Jacobs, C. Dietrich and C. Hanley, "Feed-in Tariffs as a Policy Instrument for Promoting Renewable Energies and Green Economics in Developing Countries," United Nations Empowerment Programme, 2012.

[2] E. Bellini, "PV Magazine," PV magazine, 2 March 2017. [Online]. Available: www.pvmagazine.com/2017/03/02/italy-installed-369-mw-of-new-pv-systems-in-2016/. [Accessed 4 10 2017].

[3] BEIS, "GOV.UK," 27 July 2017. [Online]. Available: www.gov.uk/government/statistics/renewable-sources-of-energy-chapter-6-digest-of-united-kingdom-energy-statistic-dukes. [Accessed 4 October 2017].

[4] M. B and N. R, "Integrating high penetrations of PV into Southern California: Year 2 project update," in *38th IEEE Photovoltaic Specialists Conference*, Austin, 2012.

[5] W. Palz, Power for the world: The Emergency of Electricity from the Sun, Singapore: Pan Stanford Publishing Pte. Ltd. Penthouse Level, Suntec Tower 3, 8 Temasek Boulevard, 2011.

[6] PQRS, "PQRS," 2016. [Online]. Available: http://pqrs.co.za/eskoms-next-step-in-solar-pv/]. . [Accessed 8 August 2017].

[7] A. J. R and S. S. J., "Integration challenges of photovoltaic distributed generation on power distribution systems," in *IEEE Power and Energy Society General Meeting* , San Diego, CA, 2011.

[8] S. S. K, R. V and S. J, "Steady state analysis of high penetration PV on utility distribution feeder," in *PES T&D*, Orlando, FL, 2012.

[9] P. G, D. J, H. D, B. R and D. W, "Distribution Generation: Benefits and issues," *Energy Policy,* vol. 33, pp. 787-798, 2005.

[10] P. D and Y. L, "Impact of unbalance penetration of single phase grid connected Photovoltaic generators on distribution network," in *Proceedings of 2011 46th International Universities' Power Engineering Conference (UPEC)*, Soest, Germany, 2011.

[11] M. F, F. Y. T, B. T and B. B, "Energy storage options for voltage support in low-voltage grids with high penetration of photovoltaic," in *3rd IEEE PES Innovative Smart Grid Technologies Europe (ISGT Europe)*, Berlin, 2012.

[12] S. A, E. R, S. L, R. B. G and B. J. C, "Coordinated Active Power-Dependent Voltage Regulation in Distribution Grids With PV Systems," *IEEE Transactions on Power Delivery,* vol. 29, no. 3, pp. 1454-1464, 2014.

[13] Y. W. K, H. L, O. E and K. V, "Neural network-based active power curtailment for overvoltage prevention in low voltage feeder," *Expert system with application,* vol. 41, no. 4, pp. 1063-1070, 2014.

[14] C. S, G. A, M. N and R. S, "Local Voltage Regulation in LV Distribution Networks with PV distributed Generation," in *Power electronics, Electrical drives, Automation and Motion International Symposium*, 2006.

[15] S. e. a. A, "Role of FACTS devices in improving penetration of renewable energy," in *IEEE 7th International Power Engineering and Optimization Conference (PEOCO)*, Langkawi, 2013.

[16] J.-W. Arnulf, "Snapshot of Photovoltaics—March 2017," *Sustainability,* vol. 9, p. 783, 2017.

[17] P. K. Ainah and K. Folly, "Voltage Rise issue with high penetration of grid connected PV," in *19th World Congress, The international Federation of Automatic Control*, Cape Town, 2014.

[18] L. H, J. D. L. Le and C. A. A, "Impact of high penetration of solar photovoltaic generation on power system small signal stability," in *International Conference on Power System Technology*, Hangzhou, 2010.

[19] REI, "Renewable Energy Institute," 2017. [Online]. Available: http://www.renewable-ei.org/en/statistics/fit.php. [Accessed 2 July 2017].

[20] Q. Zhang, Q. Y. Yan, L. Yang and X. Wang, "Overall review of feed-in tariff and renewable portfolio standard policy: A perspective of China," in *International Conference on New Energy and Future Energy System*, 2016.

[21] E. B. initiative, "Feed-In Tariffs: A Brief History," initiative, Building Efficiency, Big ideas for better building and cities, 2010.

[22] W. f. Council, "Feed-In Tariffs –Boosting Energy for our Future," World Future Council, 2016.

[23] M. Miguel, Feed-in Tariffs: Accelerating the development of renewable energy, London: Earthscan, 2007.

[24] L. J. A. P, M. A. G and M. C. C. L. M, "A View of Micro-grid," *WIREs Energy Environment,* vol. 2, no. 1, pp. 86-103, 2013.

[25] James, "Callmepower," Callmepower, 3 June 2015. [Online]. Available: http://callmepower.com/faq/energy-markets/difference-between-transmission-distribution. [Accessed 4 August 2017].

[26] C. P and R. R, "An approach to quantify the technical benefits of distributed generation," *IEEE Transactions on Energy Conversion,* vol. 19, no. 4, pp. 764-773, 2004.

[27] M. M, O. T, C. D, K. T, S. J and B. P, "Advanced Grid Planning and Operations," Sandia National Laboratories, 2008.

[28] M. A. M, H. M. J and P. H. R, "Analysis of Voltage Rise Effect on Distribution Network with Distributed Generation," in *The international Federation of Automatic Control*, Milano, 2011.

[29] M. J, S. G, C. S and J. N, "Allocation of losses in distribution systems with embedded generation," *IEE Proceedings - Generation, Transmission and Distribution,* vol. 147, no. 1, pp. 7-14, 2000.

[30] C. Carter-Brown and C. T. Gaunt, "Model for apportionment of total voltage drop in combined medium and Low voltage distribution feeder," *South African institute of Electrical Engineers,* vol. 97, no. 1, 2006.

[31] H. S and O. J, "Methods and strategies for overvoltage prevention in low voltage distribution systems with PV," *IET Renewable Power Generation,* vol. 11, no. 2, pp. 205-214, 2017.

[32] G. C and R. M. A, "A review of voltage control techniques of networks with distributed generations using On-Load Tap Changer transformers," in *45th International Universities Power Engineering Conference (UPEC)*, Cardiff, 2010.

[33] E. A, Z. F, S. R, B. B and K. S, "Controlling active low voltage distribution grids with minimum efforts on costs and engineering," in *IECON 2013 - 39th Annual Conference of the IEEE Industrial Electronics Society*, Vienna, 2013.

[34] A. H, A. R. A and L. C, "Enabling Large-Scale PV integration into the Grid," in *IEEE Green Technologies Conference*, Tulsa, 2012.

[35] Y.-K. Wu, S.-H. Tsai and M.-Y. Zou, "Accommodating High PV Penetration on the Distribution System of Kinmen Island," *Energy and Power Engineering,* vol. 5, pp. 209-214, 2013.

[36] X. Liu, A. Aichhorn, L. Liu and H. LI, "Coordinated Control of Distributed Energy Storage System with Tap Changer Transformers for Voltage rise Mitigation under high Photovoltaic Penetration," *IEEE Transaction on Smart grid,* vol. 3, no. 2, pp. 897-906, 2012.

[37] W. Kramer, S. Chakraborty, B. Kroposki and H. Thomas, "Advance Power Electronic Interfaces for Distributed Energy Systems," National Renewable Energy Laboratory (NREL), 2008.

[38] H. S, R. C and A. M. E, "A Battery Based Solution to Overvoltage Problems in Low Voltage Distribution Network with Micro-Generation," *International Journal on Electrical Engineering and Informatics,* vol. 6, no. 1, 2014.

[39] T. H. Tengku Juhana, M. Azah and H. S. Hussain, "A review on Voltage Control Methods for Active Distribution Network," *PRZEGLĄD ELEKTROTECHNICZNY (Electrical Review),* vol. 88, no. 6, 2012.

[40] E. Bernal. A, Q. Li and J. Xie, "A Novel Central Voltage-Control Strategy for Smart LV Distribution Networks," *Springer International Publishing, Swizerland,* pp. 16-30, DARE, 2015.

[41] N. M, P. A. N, T. B, N. B. A and T. C. W, "Benefits of SVC and STATCOM for electric utility application," in *IEEE PES Transmission and Distribution Conference and Exposition*, 2003.

[42] O. Gagrica, P. H. Nguyen, W. L. Kling and T. Uhl, "Microinverter Curtailment Strategy for Increasing Photovoltaic Penetration in Low-Voltage Networks," *IEEE Transactions on Sustainable Energy,,* vol. 6 , no. 2, pp. 369-379, , April 2015..

[43] S. T, M. F and B. M, "Improved low voltage grid-integration of photovoltaic systems in Germany," in *IEEE Power & Energy Society General Meeting*, Vancouver, BC,, 2013.

[44] T. Reinaldo and A. C. L. Luiz, "Impact of active power curtailment on overvoltage prevention and energy production of PV inverters connected to low voltage residential feeders," *Renewable energy,* vol. 36, pp. 3566-3574, 2011.

[45] T. R, L. L. A. C and E.-F. T. H. M, "Droop-based active power curtailment for overvoltage prevention in grid connected PV inverters," in *IEEE International Symposium on Industrial Electronics*, Bari, 2010.

[46] Y. Wai Kean, H. Lisa, O. Elizabeth and K. Vishy, "Neural network-based active power curtialment for overvoltage prevention in low voltage feeders," *Expert Systems with Applications,* vol. 41, pp. 1063-1070, 2014.

[47] H. Nick, T. Hazel G and H. Jonathan, "Voltage Regulation at Sites with Distribution Generation," *IEEE Transactions on Industry Applications,* vol. 44, no. 2, pp. 445-454, 2008.

[48] M. L. S, M. J. L and J. A. A, "Analysis of bus Voltage Regulation and OLTC Performance on Mismatched Parallel-connected Transfomer," in *AFRICON* , Nairobi, 2009.

[49] A. Navarro-Espinosa and O. L. F, "Increasing the PV hosting capacity of LV networks: OLTC-fitted transformers vs. reinforcements," in *IEEE Power & Energy Society Innovative Smart Grid Technologies Conference (ISGT)*, Washington, 2015,.

[50] A. T. Procopiou and L. F. Ochoa, "Voltage Control in PV-Rich LV Networks Without Remote Monitoring," *IEEE Transactions on Power Systems,* vol. 32 , no. 2, pp. 1224-1236, March 2017.

[51] X. Qiangqiang, H. Ryoichi, K. Hiroyuki and E. Tanaka, "Coordinated Control of OLTC nad Multi-CEMSs for Overvoltage Prevention in Power Distribution System," *IEEJ Transactions on Electrical and Electronic Engineering,* 2017.

[52] S. Potjanee, W. Auttapol, P. Kritprajun and A. Nopparat, "Potential solutions to Reduce Voltage Rise in LV Distribution Network with High PV Rooftop Penetration," in *the 21st Conference of the Electric Power Industry, Energy sustainablity and security: Choices and challenges for power industry*, Bangkok, 2016.

[53] Y. Y, Blaabjerg and Z. Z, "Benchmarking of Grid Fault Modes in Single-Phase Grid-Connected Photovoltaic Systems," *IEEE Transactions on Industry Applications,* vol. 49, no. 5, pp. 2167-2176, 2013.

[54] R. Castro, M. Almeida, C. Jesus, P. Carvalho and L. Ferreira, "Voltage Control Issues in Low Voltage Networks with Microgeneration," in *1st International Conference on Smart Grids and Green IT Systems*, Porto, 2012.

[55] X. T and T. P. C, "Voltage Control Techniques for Electrical Distribution Networks including Distributed Generation," in *Proceeding of the 17th World Congress, the international federation of Automatic Control*, Seoul, 2008.

[56] Y. Guangya, M. Francesco, J. Miguel, K. S. H. Soren Baekhoj, O. Jacob, I. Hans. Henrik and K. H. B. Fredreriksen, "Voltage rise Mitigation for Solar PV integration at LV grids," *J. Mod. Power Syst. Clean Energy,* vol. 3, no. 3, pp. 411-421, 2015.

[57] S. D and S. R. K, "Adaptive control of energy storage for voltage regulation in distribution system," in *IEEE International Conference on Smart Energy Grid Engineering (SEGE)*, Oshawa, 2013.

[58] A. M. J. E, M. K. M and S. D, "Mitigation of Rooftop Solar PV Impacts and Evening Peak Support by Managing Available Capacity of Distributed Energy Storage Systems," *IEEE Transactions on Power Systems,* vol. 28, no. 4, pp. 3874-3884, 2013.

[59] C. M and C. B. H., "Impact of Smart Inverter Control with PV Systems on Voltage Regulator in Active Distribution Networks," in *11th Annual High Capacity Optical Networks and Emerging/Enabling Technologies (Photonics for Energy), 115-119*, 2014.

[60] A. M, M. K and S. D., "A Novel Approach for Ramp-rate Control of Solar PV using Energy Storage to Mitigate Output Fluctuations Caused by Cloud Passing," *IEEE Transaction on Energy Conversion,* vol. 29, no. 2, pp. 507-518, 2014.

[61] N. Tummuru Reddy, M. Mishra. K and S. S, "Integration of PV/Battery Hybrid Energy Conversion System to grid with Power quality Improvement Features," in *International Conference on Industrial Technology (ICIT)*, 2013.

[62] Sustainable.co.za, "Sustainable.co.za," Sustainable.co.za, 21 July 2017. [Online]. Available: http://www.sustainable.co.za/solar-power/solar-storage-batteries.html. [Accessed 21 July 2017].

[63] A. G and S. K. A, "Voltage Control and dynamic performance of power transmission system using STATCOM and its comparison with SVC," *International Journal of Advances in Engineering and Technology,* vol. 2, no. 1, pp. 437-442, 2012.

[64] P. L. B, L. G and G. A, "Distribution feeder voltage support and power factor control by distributed multiple inverters,," in *IEEE Electrical Power and Energy Conference*, Winnipeg, 2011.

[65] A. Saberian, P. Farzan, N. Fadaee. M, H. Hizam, C. Gomes, O. Mohammad L, M. A. Mohd Radzi and A. K. Mohd AinalAbidin, "Role of FACTS devices in improving penetration of renewable energy," in *IEEE 7th International Power Engineering and Optimization Conference (PEOCO)*, Langkawi, 2013.

[66] M. A. Tayyab, M. Vaziri, A. Yazdani and M. Zarghami, "Distributed generation effects on voltage profile of distribution grid with SVC and Smart Inverter," in *IEEE Power & Energy Society General Meeting*, Denver, 2015.

[67] C. S. Chen, L. C. H, H. W. L, H. C. T and K. T. T, "Enhancement of PV Penetration With DSTATCOM in Taipower Distribution System," *Transactions on Power Systems,* vol. 28, no. 2, pp. 1560-1567, 2013.

[68] E. N, W. T, G. C, D. R. T and D. J, "Coordinated voltage control scheme for Flemish LV distribution grids utilizing OLTC transformers and D-STATCOM's," in *12th IET International Conference on Developments in Power System Protection (DPSP 2014)*, Copenhagen, 2014.

[69] Alibaba.com, "Alibaba.com," Alibaba.com, 21 July 2017. [Online]. Available: https://www.alibaba.com/trade/search?fsb=y&IndexArea=product_en&CatId=14191107&SearchText=statcom&isGalleryList=G. [Accessed 21 July 2017].

[70] Indiamart, "Indiamart," Indiamart, 21 July 2017. [Online]. Available: https://www.indiamart.com/proddetail/static-var-generator-2000-14715094733.html. [Accessed 21 July 2017].

[71] R. Passey, T. Spooner, L. Margill, M. Watt and K. Syngellakis, "The Potential Impacts of grid-connected distribution and how to address them: A Review of Technical and non-technical factors," *Energy Policy,* vol. 39, pp. 6280-6290, 2011.

[72] V. Scaini, "Grid Support Stability for reliable, renewable power," EATON CORPORATION, December 2012.

[73] L. F. Casey, C. Schauder, J. Cleary and M. Ropp, "Advanced inverters facilitate high penetration of renewable generation on medium voltage feeders - impact and benefits for the utility," in *IEEE Conference on Innovative Technologies for an Efficient and Reliable Electricity Supply*, Waltham, MA, 2010.

[74] V. T. L, D. K. J. D. M, M. B and V. L, "Improvement of active power sharing ratio of P/V droop controllers in low-voltage islanded microgrids," in *IEEE Power & Energy Society General Meeting*, Vancouver, 2013.

[75] K. Lemkens, F. Geth, P. Vingerhoets and Deconinck, "Reducing overvoltage problems with active power curtailment - Simulation results," in *IEEE PES Innovative smart grid technologies Europe*, Copenhagen, 2013.

[76] S. J. J, L. H. J, J. W. W and W. D. J, "Voltage control method using modified voltage droop control in LV distribution system," in *Transmission & Distribution Conference & Exposition: Asia and Pacific*, Seoul, 2009.

[77] C. B. I, S. D, M. E. A, K. T, M. V. A and T. R, "Improved voltage regulation strategies by PV inverters in LV rural networks," in *3rd IEEE International Symposium on Power Electronics for Distributed Generation Systems (PEDG)*, Aalborg, 2012.

[78] M. Hojo, H. Hatano and Y. Fuwa, "Voltage rise Suppression by Reactive Power Control with Cooperating Photovoltaic generation Systems," in *20th International Conference on Electricity Distribution systems*, Praque, 2009.

[79] M. Farivar, R. Neal, C. Clarke and S. Low, "Optimal Inverter VAR Control in Distribution System with High PV penetration," in *IEEE Power and Energy Society General Meeting*, San Diego, 2012.

[80] S. Ghosh, S. Rahman and M. Pipattanasomporn, "Local distribution voltage control by reactive power injection from PV inverters enhanced with active power curtailment," in *IEEE PES General Meeting | Conference & Exposition*, National Harbor, MD, 2014.

[81] T. R, L. L. A. C and E.-F. T. H. M, "Coordinated Active Power Curtailment of Grid Connected PV Inverters for Overvoltage Prevention," *IEEE Transactions on Sustainable Energy,* vol. 2, no. 2, pp. 139-147, April 2011.

[82] T. R and L. L. A. C., "Voltage Regulation in Radial Distribution Feeders with High Penetration of Photovoltaic," in *IEEE Energy 2030 Conference*, Atlanta, GA, 2008.

[83] V. A. K. Pappu, B. Chowdhury and R. Bhatt, "Implementing frequency regulation capability in a solar photovoltaic power plant," in *North American Power Symposium 2010*, Arlington, TX,, 2010.

[84] F. A. P. Olivier, D. Ernst and T. Van Cutsem, "Active Management of Low-Voltage Networks for Mitigating Overvoltages Due to Photovoltaic Units," *IEEE Transactions on Smart Grid,* vol. 7, no. 2, pp. 926-936, 2016.

[85] G. Mokhtari, G. Nourbakhsh, G. Ledwich and A. Ghosh, "Overvoltage and overloading prevention using coordinated PV inverters in distribution network," in *IECON 2014 - 40th Annual Conference of the IEEE Industrial Electronics Society*, Dallas, 2014.

[86] V. K. M, "Smart Grid as a desideratum in the energy landscape: Key aspects and challenges," in *EEE International Conference on Engineering Education: Innovative Practices and Future Trends (AICERA)*, Kottayam, 2012.

[87] H. M, H. S and M. K, "Survey of smart grid concepts, architectures, and technological demonstrations worldwide," in *IEEE PES CONFERENCE ON INNOVATIVE SMART GRID TECHNOLOGIES LATIN AMERICA (ISGT)*, Medellin, 2011.

[88] SGEM, "SGEM," [Online]. Available: http://sgemfinalreport.fi. [Accessed 27 August 2017].

[89] H. Gharavi and G. Reza, "Smart Grid: The Electric Energy System of the Future," *Proceeding of the IEEE,* vol. 99, no. 6, pp. 917-921, 2011.

[90] S. A, N. S, L. R. N, C. S, C. S. P and C. N, "Smart grid initiative for power distribution utility in India," in *IEEE Power and Energy Society General Meeting*, San Diego, 2011.

[91] IEC, "IEC," Internation Electrotechnical Commission, 2017. [Online]. Available: www.iec.ch/smartgrid/background/explained.htm. [Accessed 10 May 2017].

[92] E. Aernal. A, Q. Li and J. Xie, "A Novel Central Voltage-Control Strategy for Smart LV Distribution Networks," *Springer International Publishing, Swizerland,* pp. 16-30, DARE, 2015.

[93] B. Nasiri, A. Ahsan, D. M. Gonzalez, C. Wagner, U. Häger and C. Rehtanz, "Integration of smart grid technologies for voltage regulation in low voltage distribution grids," in *IEEE Innovative Smart Grid Technologies - Asia (ISGT-Asia)*, Melbourne, VIC., 2016.

[94] E. Bernal Alzate and J. Xie, "Smart LV distribution networks: An approach for power flow formulation with smart home models," in *6th International Symposium on Power Electronics for Distributed Generation Systems (PEDG)*, Aachen, 2015.

[95] G. Mokhtari, G. Nourbakhsh, F. Zare and A. Ghosh, "Overvoltage Prevention in LV smart grid using customer resources coordination," *Energy and buildings,* vol. 61, pp. 387-395, 2013.

[96] K. U. N, "Distributed Generation and Power quality," in *International Conference on Evironmental Engineering* , Karpacz, Poland, 2009.

[97] G.-l. F and F. C, "Review of Distributed Generation Concept: Attempt of Unification," in *International Conference on Reneable Energies and Power Quality*, Espana, March 2005.

[98] Gas.Research.Institute, "Distributed Power Generation: A strategy for Comparative energy industry," Gas Research Institute, Chicago, 1998.

[99] A. Thomas, A. Goran and S. Lennart, "Distribution Generation: A Definition," *Electrical Power System Research,* vol. 57, no. 3, pp. 195-204, 2001.

[100] G. S. W, "Vannishing Power Lines and Emerging Distributed Generation," *Wake Forest Journal of Law and Policy,* vol. 4, no. 2, pp. 347-396, 2014.

[101] GRI, "The Role of Distributed Generation in Competitive Energy Markets," Gas Research Institute, Chicago, 1999.

[102] M. J. A, X. Y and B. G. D, "An approach to determine Distributed Generation (DG) benefits in power networks," in *40th North American Power Symposium*, Calgary, 2008.

[103] A. P. K and F. K. A, "Development of Micro-Grid in Sub-Saharan Africa: An Overview," *International Review of Electrical Engineering (IREE),* vol. 10, no. 5, pp. 633 - 645, 2015.

[104] I. Std-547.3, "IEEE Guide for monitoring, information exchange and control of distribution resources interconnected with electri power systems," IEEE, 2007.

[105] I. Std-1547.3, "IEEE Guide for Design, operation, and integration of distributed resources Island systems with power systems," IEEE, 2011.

[106] I. Std-1547.7, "IEEE Guide for conducting distribution impact studies for distributed resources interconnection," IEEE, 2013.

[107] C.-M. E, L. H, J. M, E. T, T. J, D. M. H, C. S, S. D and G. B, "Interaction Between PhotovoltaicDistributed Generation andElectricity Networks," *PROGRESS IN PHOTOVOLTAICS: RESEARCH AND APPLICATIONS,* vol. 16, p. 629–643, 2008.

[108] C. Fabio, "Building Integrated Photovoltaic Systems: specific non-idealities from solar cell to grid," Politecnico di Torino, Torino, 2014.

[109] H. A, E. C. S and B. T, "Comprehensive study of power quality criteria generated by PV converters and their impacts on distribution transformers," in *38th Annual Conference on IEEE Industrial Electronics Society*, Montreal, 2012.

[110] I. Std-519, "IEEE Recommended Practice and and requirement for harmonic control in power system," IEEE Power and Energy Society, New York, 2014.

[111] H. R. Muhammad, Power Electronics Handbook: Devices, Circuit and Applications, Elsevier, 2011.

[112] V. Valery, Introduction to Power electronic, Valery Vodovozov and Ventus Publishing Aps, 2010.

[113] S. Colin, "Advance Inverter Technology for High Penetration Levels of PV Generation in Distribution Systems," National Renewable Energy Laboratory (NREL), Massachusetts, USA, 2014.

[114] L. M and H. S, "Decoupled Control of grid connected Photovoltaic System using Fractional order Controller," *Ain Shams Engineering Journal,* 2016.

[115] N. Mohan, U. Tore M. and R. William P., Power Electronics, Converters, Applications and Design, John Wiley and Sons, Inc. Second Edition, 1995.

[116] M. K. Mishra and K. Karthikeyan, "Design and analysis of voltage source inverter for active compensators to compensate unbalanced and non-linear loads," in *International Power Engineering Conference (IPEC)*, Singapore, 2007.

[117] I. P. M. D. M. Mitsubishi, "Using Intelligent Power Modules," Mitsubishi, 1998.

[118] M. Milosevic, "Decoupling Control of d and q Current Compnonent in three phase Voltage Source Inverter," ETH Zurich, PhD disertation, Zurich, 2007.

[119] B. N, R. A, A. A, R. A and B. H, "Determination methods for controller parameters of back-to-back converters in electric power grids," in *Electric Power Quality and Supply Reliability (PQ)*, Tallinn, 2016.

[120] S. Chandra, M. Bhalekar, S. Umashankar and D. P. Kothari, "Testing and Hardware Implementation of SPWM Inverter using TMSF28335eZDSP," in *International Conference on Circuit, Power and Computing Technologies (ICCPCT)*, Nagercoil, 2013.

[121] S. Umashankar, B. Mandar, S. Chandra, D. Vijayakumar and D. Kothari, "DSP Based Real Time Implementation of AC-DC-AC Converter Using SPWM Technique," *International Journal of Electronic Communication and Electrical Engineering,* vol. 3, no. 1, 2013.

[122] G. H. Narain and G. Laszlo, Understanding FACTS:Concepts and Technology of Flexible AC Transmission Systems, Wiley-IEEE Press, 2000.

[123] F. Jawad and S. Ghazanfar, "Modeling and Simulation of three phase with rectifer-type nonlinear Loads," *Armenian Journal of Physics,* vol. 2, no. 4, pp. 307-316, 2009.

[124] A. Abdalrahman, Z. Abdalhalim and A. Ahmed, "Simulation and Implementation of Grid-connected inverters," *International Journal of Computer Applications,* vol. 60, no. 4, 2012.

[125] I. P. M, R. M. J, T. D. W. P and S. M, "Power quality of a voltage source converter in a smart grid," in *IEEE Grenoble Conference*, Grenoble, 2013.

[126] B. C and M. M, "Understanding of Tuning techniques of Converter Controllers for VSC-HVDC," in *Nordic Workshop on Power and Industrial Electronics*, 2008.

[127] X. Ling, "Modeling, Analysis and Control of Voltage-Source Converter in Microgrids and HVDC," University of South Florida, PhD Disertation, California, 2013.

[128] Y. Amirnaser and I. Reza, "Three-Level, Three-Phase, Neutral-Point Clamped, Voltage-Sourced Converter," in *Voltage-Sourced Converters in Power Systems:Modeling, Control, and Applications* , Wiley-IEEE Press,, 2010, p. 541.

[129] K. Oskars, S. Ingars and R. Leonids, "A PLL Scheme for Synchronization with Grid Voltage Phasor in Active Power Filter Systems," *Scientific Journal of Riga Technical University, Power and Electrical Engineering,* vol. 27, pp. 133-136, 2010.

[130] X.-Q. Guo, W.-Y. Wu and H.-R. Gu, "Phase Locked Loop and Synchronization methods for grid-interfaced Converters: a review," *PRZEGLĄD ELEKTROTECHNICZNY (Electrical Review),* 2011.

[131] O. Jim, "PLL design for inverter grid connection, simulation for ideal and non-ideal grid conditions," UPPSALA UNIVERSITET, 2011.

[132] E. Adzic, V. Porobic, B. Dumnic, N. Celanovic and V. Katic, "PLL Synchronization in Grid-connected Converters," in *The 6th PSU-UNS International Conference on Engineering and Technology (ICET)*, Serbia, 2013.

[133] S. Nandurkar. R and M. Rajeev, "Design and Simulation of Three Phase inverter for grid connected Photovoltaic systems," in *Third Biennial National Conference (NCNTE)*, 2012.

[134] K. V and B. V, "Operation of a phase locked loop system under distorted utility conditions," in *Applied Power Electronics Conference and Exposition*, San Jose, 1996.

[135] L. Andrey, K. Tero and P. Jarmo, "Investigation into harmonics of LVDC power distribution network using EMTDC/PSCAD Software," in *International Conference on Renewable energies and Power quality ('ICREPQ' II)*, Las Palmas de Gran Canaria, April 2010.

[136] k. Vikas, N. Savita and b. Prashant, "Power Quality Disturbances in Grid Connected Solar System and its Prevention," *International Journal of engineering and Innovative Technology (IJEIT),* vol. 1, no. 5, 2012.

[137] I. Preye. M, R. M. J and T. D. W. P, "Factors affecting harmonic generated by a generic voltage source converter within Micro-grid," in *Saudi Arabia Smart grid Conference*, Jeddah, 2012.

[138] A. Khaled H., F. Stephen J. and W. Barry W., "Passive Filter Design for Three-Phase Inverter Interfacing in Distributed Generation," *Electrical Power Quality and Utilisation, Journal,* vol. 13, no. 2, pp. 49-58, 2007.

[139] M. Y. Park, M.-H. Chi, J.-H. Park, H.-G. Kim, T.-W. Chun and E.-C. Nho, "LCL-filter design for grid-connected PCS using total harmonic distortion and ripple attenuation factor," in *International Power Electronics Conference*, ECCE , 2010 .

[140] R. A., S. M. G, A.-D. A and M. S. M., "LCL Filter Design and Performance Analysis for Grid-Interconnected Systems," *IEEE Transactions on Industry Applications,* vol. 50, no. 2, pp. 1225-1232, 2014.

[141] X. Z, S. L and Y. X, "Parameters Design and control strategy of cascade STATCOM Based on LCL Filter," *International Journal of Control and Automation,* vol. 7, no. 1, p. 307 320, 2014.

[142] H. H, D. N, T. O, T. T and Y. K, "A Fast and Robust Load Flow Method for Distribution System with Distributed Generations," in *ICSGCE*, Chengdu, China, 2011.

[143] R. T. B, M. V.V.S.N and A. K, "An Efficient and Simple Load Flow Approach For Radial and Mesh Distribution Networks," *International Journal of Grid and Distributed Computing,* vol. 9, no. 2, pp. 85-102, 2016.

[144] D. I and J. C, "Rotational Load Flow Method for Radial Distribution Systems," *International Journal of Electrical and Computer Engineering,* vol. 6, no. 3, pp. 1344-1352, 2016.

[145] M. R. J. A and G. S, "Power Flow Analysis for Radial Distribution System Using Backward/ForwardSweep Method," *International Journal of Electrical and Computing Engineering,* vol. 8, no. 10, pp. 1628-1632, 2014.

[146] M. E. Baran, H. Hooshyar, Z. Shen and A. Huang, "Accommodating High PV Penetration on Distribution Feeders," *IEEE Transactions on Smart Grid,* vol. 3, no. 2, pp. 1039-1046, 2012.

[147] A. Guinane, G. M. Shafiullah, A. M. T. Oo and B. E. Harvey, "Voltage fluctuations in PV penetration on SWER networks — A case study for regional Australia," in *IEEE Power and Energy Society General Meeting*, San Diego, CA, 2012.

[148] C. A, D. T. E, D. M, F. G and T. M, "PV plants for voltage regulation in distribution networks," in *47th International Universities Power Engineering Conference (UPEC)*, London, 2012.

[149] R. S and N. I., "Energy impacts of the smart home - Conflicting Visions," in *ECEEE SUMMER STUDY • Energy efficiency first: The foundation of a low-carbon socie*, Lyngby, 2011.

[150] Z. Q, Y. Q. Y, Y. L and W. X, "Overall review of feed-in tarrif and renewable potfolio standard policy: A perspective of China," in *International conference on new energy and future energy system*, 2016.

[151] D. P. V. 13.2, "Volume I, Handling of PowerFactory," DigSilent Powerfactory, 2013.

[152] K. G and W. R, "Loading Capacity of standard oil transformers on photovoltaic load profiles," in *World Renewable Energy Congress (WRECX)*, 2008.

[153] Mathwork, Simulink, Getting started Guide, Natick: The MathWork.Inc, 3 Apple Hill Drive, Natick, MA 01760-2098, 2017.

[154] F. L. A, A. J. M and G. C. G, "Photovoltaic solar system connected to the electric power grid operating as active power generator and reactive power compensator," *Solar Energy,* vol. 84, no. 7, pp. 1310 - 1317, 2010.

[155] T. M, M. J, d. S.W.H and M. P, "Improved and extended DG capability in voltage regulation by reactive and active power," in *International Conference on Power Engineering, Energy and Electrical Drives*, Setubal, 2007.

[156] B. A, B. K. S and S. B, "DSTATCOM control Algorithm: A review," *International Journal of Power Electronics and Drive System (IJPEDS),* vol. 2, no. 3, pp. 285-296, 2012.

[157] R. G. F, T. M and I. I, "Improved power quality solutions using advanced solid-state switching and static compensation technologies," in *IEEE Power Engineering Society. 1999 Winter Meeting*, 1999.

[158] T. G. A, "Power quality hardware solutions for distribution systems: Custom Power," in *IEE North Eastern Centre Power Section Symposium on the Reliability, Security and Power Quality of Distribution Systems*, Durham, 1995.

[159] M. A, G. F. Z, M. C, K. K. D. E and A. A. F, "Study, analysis and simulation of a static compensator D-STATCOM for distribution systems of electri power," *Leonardo Journal of sciences,* no. 25, pp. 117-130, 2014.

[160] G. R and G. A., "Frequency-domain characterization of sliding mode control of an inverter used in DSTATCOM application," *IEEE Transactions on Circuits and Systems I: Regular Papers,* vol. 53, no. 3, pp. 662-676,, March 2006..

[161] S. B, A. A, M. A. P, G. J. R. P and S. B. N, "Application of DSTATCOM for Mitigation of Voltage Sag for Motor Loads in Isolated Distribution Systems," in *IEEE International Symposium on Industrial Electronics,* , Montreal, Que, 2006.

[162] L. P. W, "A benchmark system for simulation of the D-STATCOM," *IEEE Power Engineering Society Winter Meeting. Conference Proceedings,* vol. 1, pp. 496-498, 2002.

[163] H. M. A, M. A and H. A, "Modeling and power quality analysis of STATCOM using phasor dynamics," in *EEE International Conference on Sustainable Energy Technologies*, Singapore, 2008.

[164] D. H. Shukla and N. B. Panchal, "New Contol Approach for D-STATCOM," *International Journal of Engineering Development and Research,* vol. 2, no. 1, pp. 135-143, 2014.

[165] M. Hendri, M. Norman, M. Scnan, M. Azah and Y. Sallehhudin, "Design of a Prototype D-STATCOM for Voltage sag Mitigation," in *National Power and Energy Conference (PECon)*, Kuala Lumpur, Malaysia, 2004.

[166] R. Ravathi and J. Ramprabu, "A ZigZag-Delta Phase-shifting Transformer and Three-leg VSC based DSTATCOM for Power Quality Improvement," *International Journal of Advances in Engineering and Technology,* vol. 2, no. 1, pp. 552-563, 2012.

[167] S. K, "Control design and application of D-STATCOM for load voltage control," Surananee University of Technology, PhD thesis, 2012.

[168] IEA, "World energy outlook 2011," International energy agency, 2011.

Appendix A.

A1: Derivation of the close loop transfer function of the dq-SRF PLL

$$G_{oL} = \frac{K_p V_m}{aT_s} \frac{(as+\frac{a}{\tau})}{s^2(s+\frac{1}{T_s})} \quad \text{(A.1)}$$

$$\mathrm{G_{OL}} = \frac{6.293*10^5\ \mathrm{s} + 3.107*10^7}{\mathrm{s^3} + 2000\ \mathrm{s^2}} \quad \text{(A.2)}$$

$$\mathrm{G_{CL}} = \frac{\mathrm{G_{oL}}}{1+\mathrm{G_{oL}}} \quad \text{(A.3)}$$

$$\mathrm{G_{CL}} = \frac{\frac{6.293*10^5\ \mathrm{s} + 3.107*10^7}{\mathrm{s^3} + 2000\ \mathrm{s^2}}}{1+\frac{6.293*10^5\ \mathrm{s} + 3.107*10^7}{\mathrm{s^3} + 2000\ \mathrm{s^2}}} \quad \text{(A.4)}$$

$$\mathrm{G_{CL}} = \frac{\frac{6.293*10^5\ \mathrm{s} + 3.107*10^7}{\mathrm{s^3} + 2000\ \mathrm{s^2}}}{\frac{s^3+2000s^2+6.293*10^5\ \mathrm{s} + 3.107*10^7}{\mathrm{s^3} + 2000\ \mathrm{s^2}}} \quad \text{(A.5)}$$

$$\mathrm{G_{CL}} = \frac{6.293*10^5\ \mathrm{s} + 3.107*10^7}{\mathrm{s^3} + 2000\ \mathrm{s^2}+6.293*10^5\ \mathrm{s} + 3.107*10^7} \quad \text{(A.6)}$$

Appendix B

B.1: Clarke and Parks transformations for dq transformations used for the VSI PI controllers

V_{abc} = Three-Phase Sinusoidal Voltage

$$V_a = V_m \sin(\omega t) \tag{B.1}$$

$$V_b = V_m \sin(\omega t - \tfrac{2\pi}{3}) \tag{B.2}$$

$$V_c = V_m \sin(\omega t + \tfrac{2\pi}{3})\pi r^2 \tag{B.3}$$

V_{abc} - $V_{\alpha\beta} - V_{dq}$

$$V_a + V_b + V_c = 0 \tag{B.4}$$

$$\begin{vmatrix} V_\alpha \\ V_\beta \end{vmatrix} = \frac{2}{3} \begin{vmatrix} 1 & \frac{-1}{2} & \frac{-1}{2} \\ 0 & \frac{\sqrt{3}}{2} & \frac{-\sqrt{3}}{2} \end{vmatrix} \begin{vmatrix} V_a \\ V_b \\ V_c \end{vmatrix} \tag{B.5}$$

$$\begin{vmatrix} V_d \\ V_q \end{vmatrix} = \frac{2}{3} \begin{vmatrix} \cos\omega t & \cos(\omega t - \frac{2\pi}{3}) & \cos(\omega t + \frac{2\pi}{3}) \\ -\sin\omega t & -\sin(\omega t - \frac{2\pi}{3}) & -\sin(\omega t + \frac{2\pi}{3}) \end{vmatrix} \begin{vmatrix} V_a \\ V_b \\ V_c \end{vmatrix} \tag{B.6}$$

V_{dq} - $V_{\alpha\beta} - V_{abc}$

$$\begin{vmatrix} V_\alpha \\ V_\beta \end{vmatrix} = \begin{vmatrix} \cos\omega t & -\sin\omega t \\ \sin\omega t & \cos\omega t \end{vmatrix} \begin{vmatrix} V_d \\ V_q \end{vmatrix} \tag{B.7}$$

$$\begin{vmatrix} V_a \\ V_b \\ V_c \end{vmatrix} = \begin{vmatrix} 1 & 0 \\ \frac{-1}{2} & \frac{\sqrt{3}}{2} \\ \frac{-1}{2} & \frac{\sqrt{3}}{2} \end{vmatrix} \begin{vmatrix} V_\alpha \\ V_\beta \end{vmatrix} \tag{B.8}$$

$$\begin{vmatrix} V_a \\ V_b \\ V_c \end{vmatrix} = \begin{vmatrix} \cos\omega t & \sin\omega t \\ \cos(\omega t - \frac{2\pi}{3}) & \sin(\omega t - \frac{2\pi}{3}) \\ \cos(\omega t + \frac{2\pi}{3}) & \sin(\omega t + \frac{2\pi}{3}) \end{vmatrix} \begin{vmatrix} V_d \\ V_q \end{vmatrix} \tag{B.9}$$

where ω = the angle between dq and αβ reference frames

Appendix C

C.1: Equivalent Model of a Photovoltaic Solar Cell

A simple PV solar cell is described as a current source in parallel with a diode. The output power of the solar cell depend on the intensity of the irradiation falling on the cell.

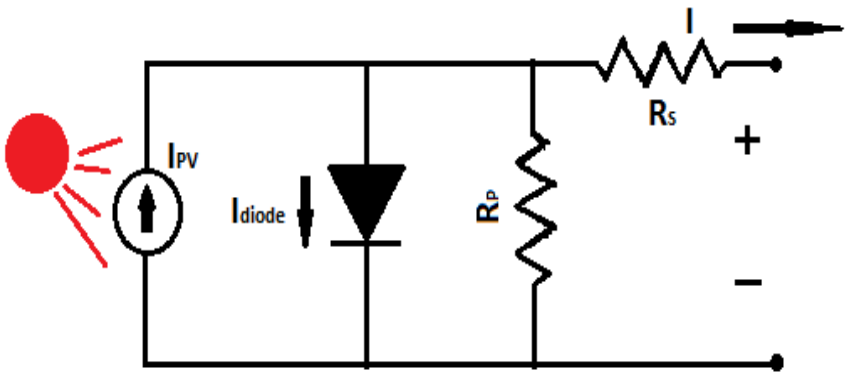

$$I = I_{PV} + I_{diode} = I_{PV} - I_O \ [\exp(\frac{q*V}{\propto *k*T} - 1)] \qquad \text{(C.1)}$$

where:

- ✓ I_{PV} = current generated by solar radiation
- ✓ I_O = diode leakage current
- ✓ I_{diode} = diode current
- ✓ K = Boltzmann constant [$1.3806*10^{-23}$ J/K]
- ✓ q = electron charge [$1.6021*10^{-19}$ C]
- ✓ $T*K$ = temperature of the p-n junction
- ✓ α = diode identity constant

C.2: Different model PV solar cell available in MATLAB®/Simulink®

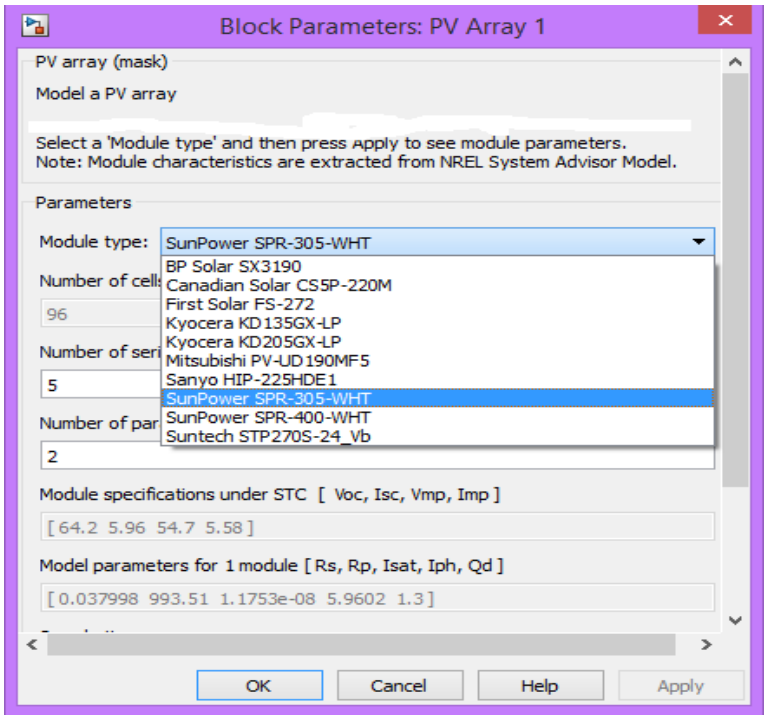

C.3: IV and PV characteristic curve of selected 3Kw PV array available in MATLAB®/Simulink®

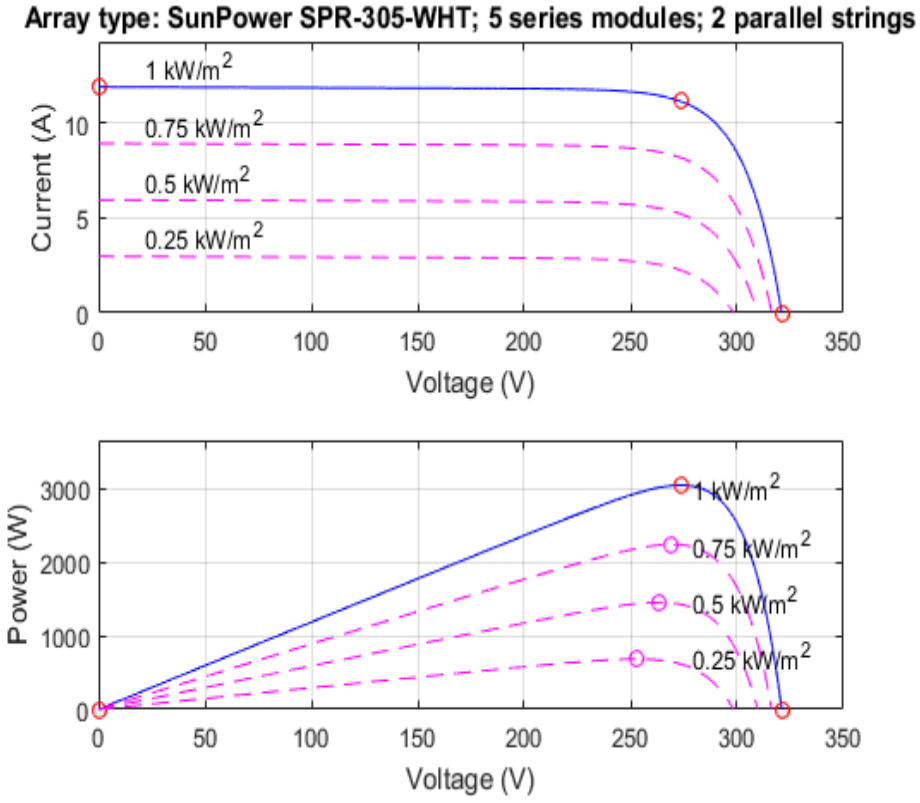

C.4: Inverter DC side Parameters (a) PV Output Voltage (b) PV Output Current (c) PV Output Power used in our investigation from Simulink

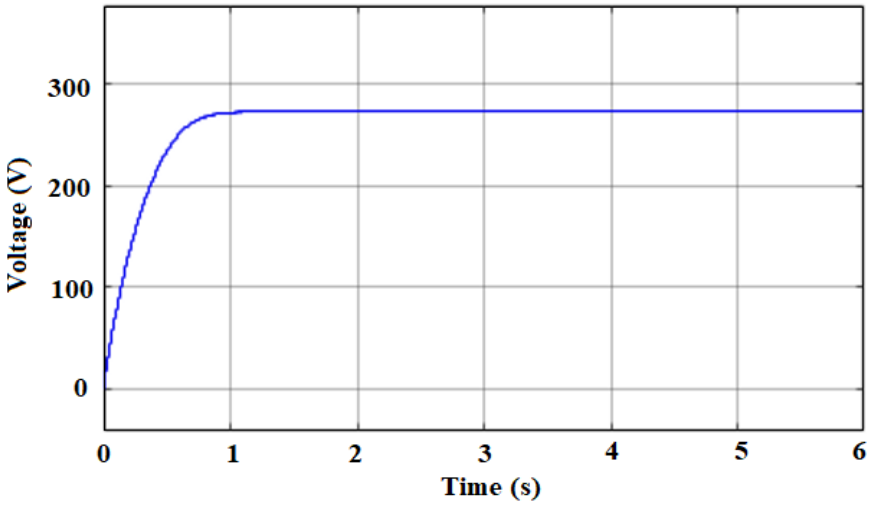

(a)

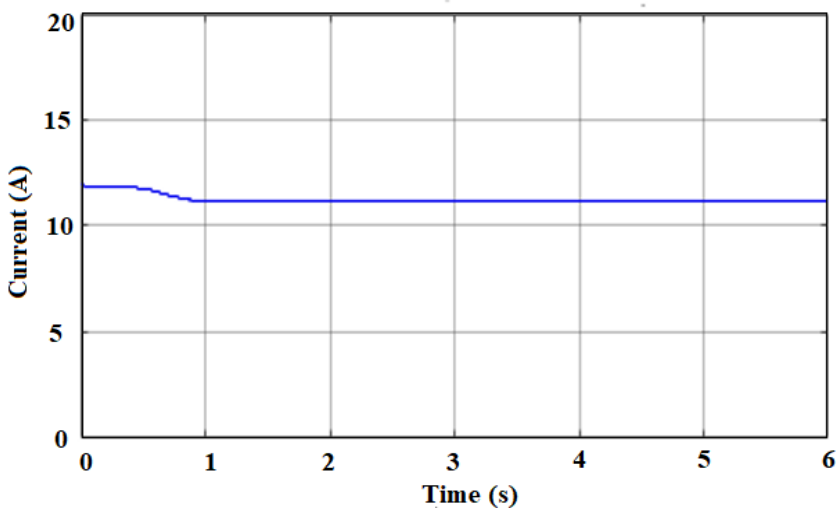

(b)

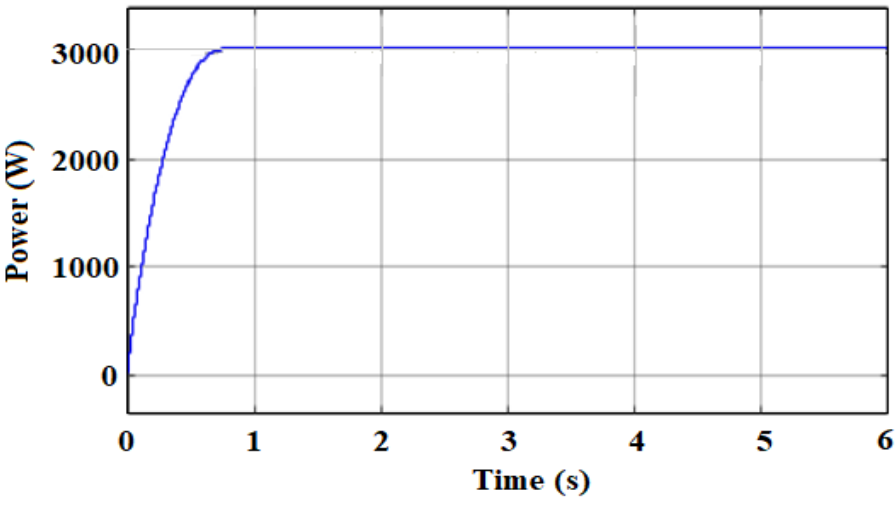

(c)

Appendix D

D.1: Proposed Simulink block Proposed CAPR Control Strategy

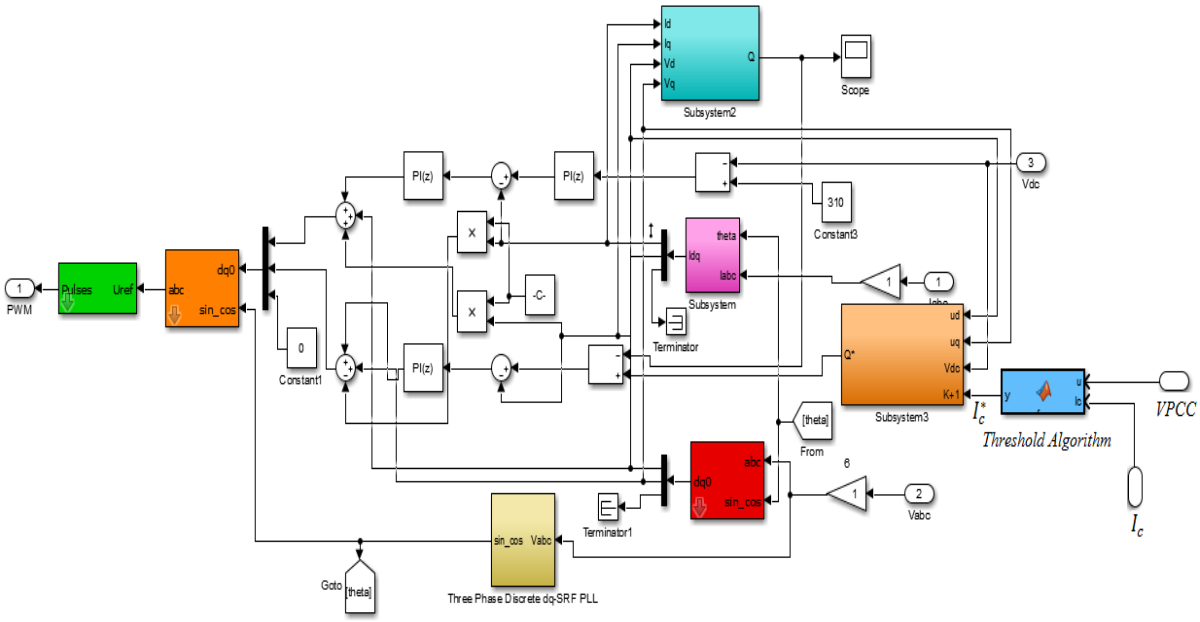

D.2: Overall system with propose active power control technique

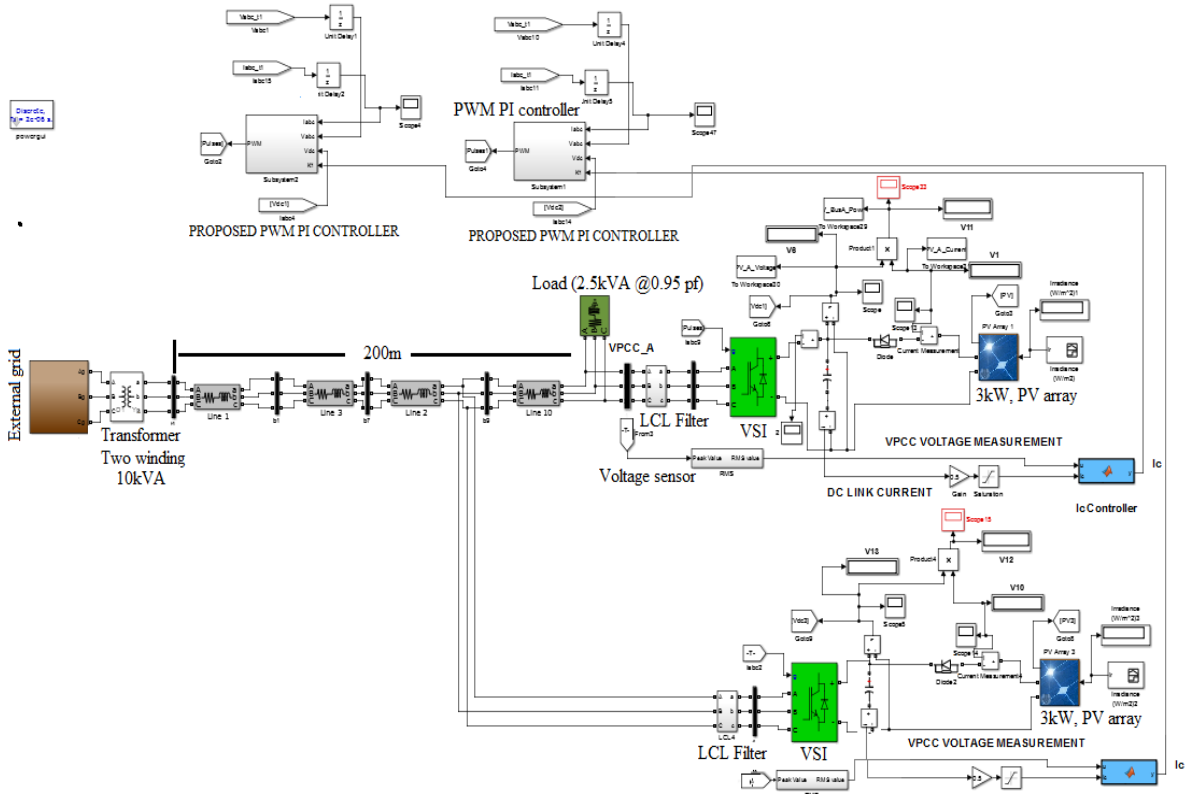

Appendix E

E.1: Simulink Configuration and control of D-STATCOM

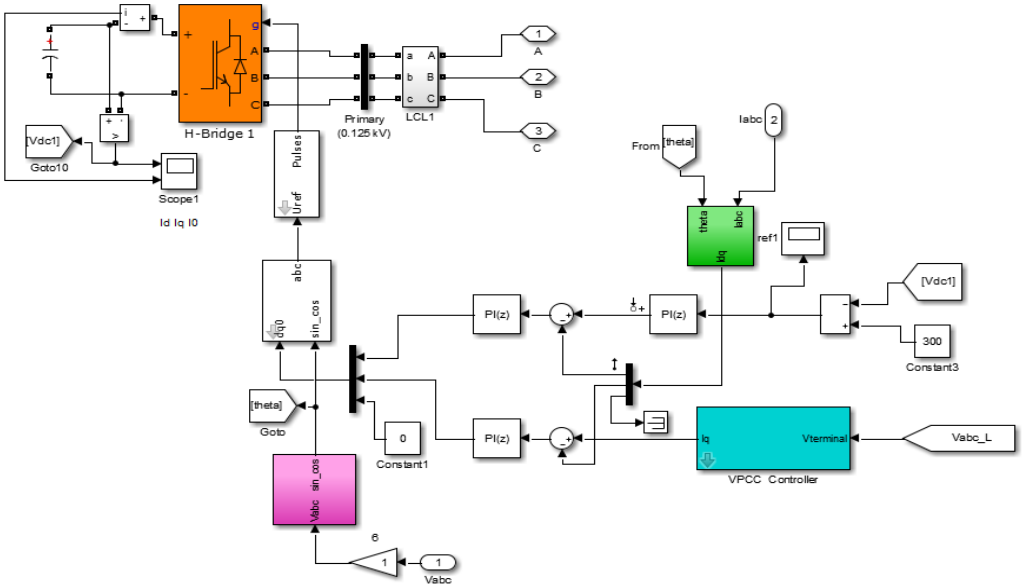

E.2: Simulink Overall system with the application of D-STATCOM

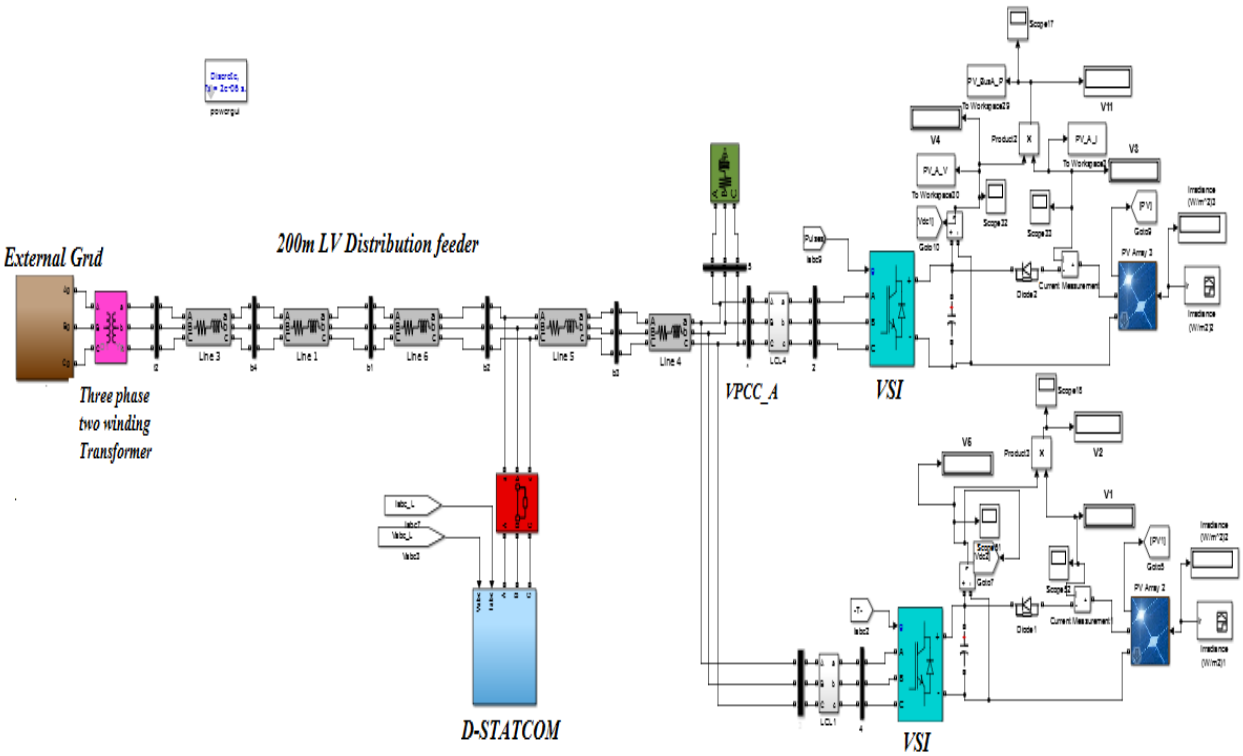

E.3: D-STATCOM Voltage PI Regulator

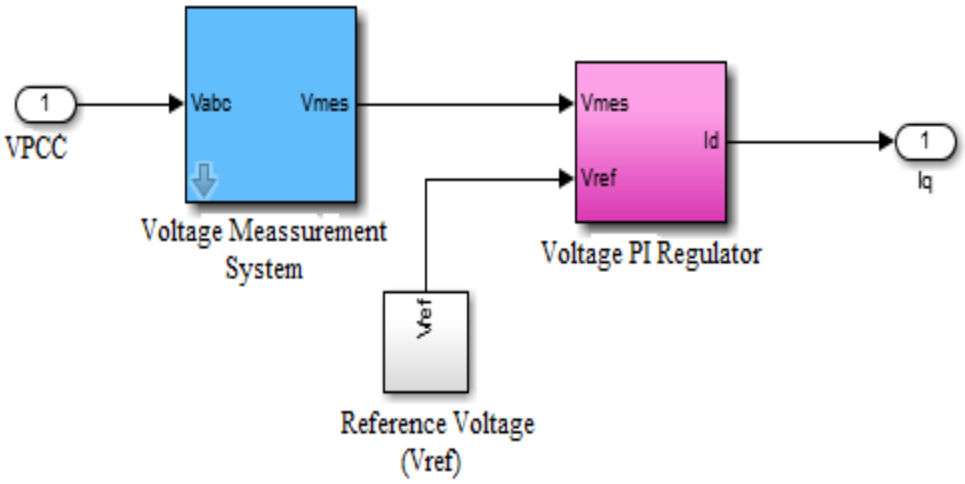

E.4: DC Capacitor Voltage Control

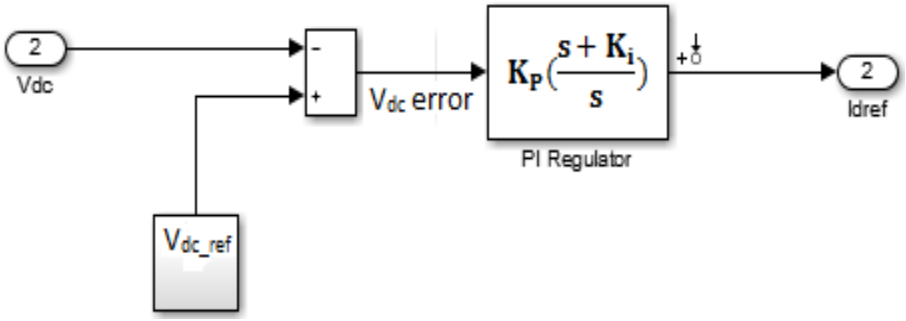

Appendix F

F1: Equivalent Model of Battery without Temperature Effect

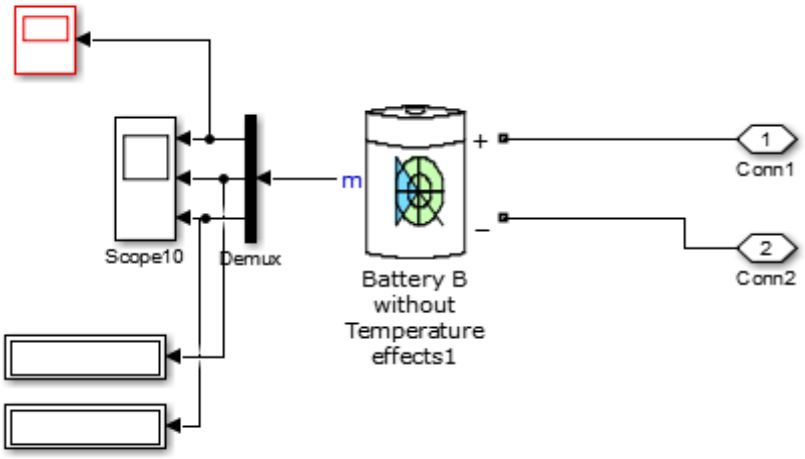

F2: Different Modelled Battery Devices available in MATLAB®/Simulink®

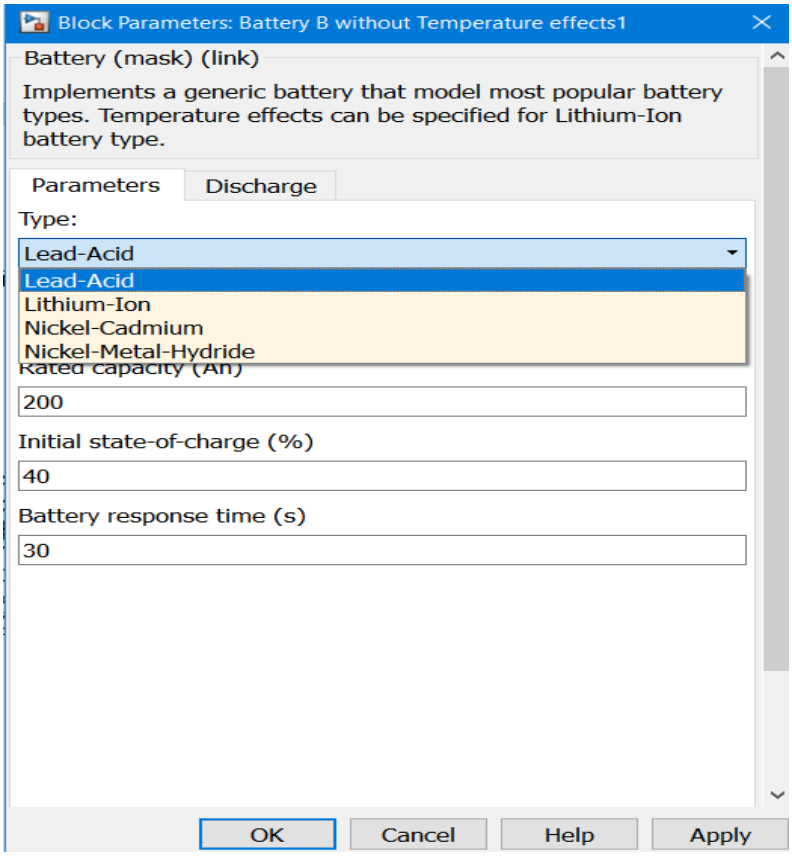

F3: Simulink Overall System with BESS